

# Seismic Evaluation of Hazard-Resistant Lifelines: Fusible PVC Pipe and Fittings

Program Report

Submitted to:

Tom Marti

Aegion Corporation  
Underground Solutions Inc.

Prepared by:

B. P. Wham

C. R. Ihnotic

D. K. Anderson

J. L. Ramos

D. Balcells



Center for Infrastructure, Energy, and Space Testing  
Civil, Environmental, and Architectural Engineering  
University of Colorado Boulder  
Boulder, CO 80309

July 2021



## Table of Contents

Table of Contents .....	2
List of Figures .....	4
List of Tables .....	7
1. Introduction.....	9
1.1 Test Specimens .....	9
1.2 Test Overview .....	10
1.3 Tensile Coupon Tests .....	11
1.3.1 University of Colorado, Boulder .....	11
1.3.2 PSI Laboratory .....	13
2. Axial Testing.....	15
2.1 Axial Test Setup .....	15
2.1.1 Specimen Installation Procedure .....	16
2.1.2 Instrumentation .....	18
2.2 Axial Test Procedure .....	19
2.2.1 Pretest.....	19
2.2.2 Test Sequence.....	20
2.2.3 Stop or Pause Criteria.....	20
3. Axial Tension Test Results .....	21
3.1 Tension Test (PT04)- fPVC w/ Megalug Coupling.....	21
3.2 Tension Test (PT07)- fPVC w/ Fused Connection.....	23
3.3 Tension Test (PT08)- fPVC w/ Megalug Coupling.....	27
3.4 Tension Test (PT14)- fPVC w/ Fused Connection.....	29
3.5 Tension Test (PT15)- fPVC w/ Megalug Coupling.....	32
3.6 Tension Test (PT16)- fPVC w/ Megalug Coupling and Stiffeners .....	35
3.7 Tension Test (PT34) – fPVC w/ Lokx Coupling.....	39
3.8 Tension Test Overview.....	42
4. Axial Compression Test Results .....	47
4.1 Compression Test (PC10)- fPVC w/ Megalug Coupling .....	48
4.2 Compression Test (PC13)- fPVC w/ Fused Connection .....	52
4.3 Compression Test Summary.....	56
5. Axial Tests Discussion and Conclusion.....	59
6. Four-point Bending Tests.....	62



6.1	Bending Test Experimental Setup .....	62
6.1.1	Bending Test Instrumentation .....	64
6.2	Experimental Measures of Pipeline System Response .....	64
6.2.1	Crosshead Displacement .....	65
6.2.2	Applied Moment .....	65
6.2.3	Radius of Curvature .....	66
6.2.4	Internal Pressure.....	66
6.3	Bending Test Procedure.....	66
6.3.1	Pretest.....	66
6.3.2	Test Sequence.....	67
6.3.3	Stop or Pause Criteria.....	67
7.	Bending Test Results .....	68
7.1	PB03 – fPVC w/ Megalug Coupling .....	68
7.2	PB04 – fPVC w/ Fused Connection .....	75
7.3	PB05– Fused Pipe with Fused Connection.....	82
7.4	Summary of Bending Tests Results.....	88
7.5	Bending Test Classification.....	92
8.	Conclusions.....	94
	Acknowledgements.....	95
	References.....	95
	Appendix A: Cyclic Tension Test (PS11) Results.....	96
	Appendix B: Field Cut Procedures .....	101
	Appendix C: Strain Gauge Application Procedure .....	107
	Appendix D: Megalug Restraint Assembly .....	108
	Appendix E: Applied Moment Verification.....	109
	Appendix F: Radius of Curvature (RoC) Calculation.....	113



## List of Figures

Figure 1.1. Examples of the (a) fused connection, (b) Megalug coupling, and (c) Lokx coupling .....	10
Figure 1.2. Fusible Coupon Tests, Stress vs. Extensometer .....	11
Figure 1.3. Coupon Tests (a) Stress vs. Extensometer Strain and (b) Stress vs. Local Axial Strain .....	13
Figure 1.4. Fusible Failed Coupon.....	13
Figure 1.5. Summary of PSI Lab coupon tests .....	14
Figure 2.1. Pipe specimen in axial test frame .....	15
Figure 2.2. Dimensioned drawing of axial test setup.....	16
Figure 2.3. Marked measurements on non-cut ends of the pipe. ....	16
Figure 2.4. Identifying the pipe coordinates (crown, invert, and spring lines) .....	16
Figure 2.5. Pipe connections to loading frame on (a) east and (b) west ends .....	17
Figure 2.6. Megalug restraints on “cut” ends of pipe .....	17
Figure 2.7. Fixed end (west) with water intake and pressure valve.....	17
Figure 2.8. Specimen instrumentation .....	19
Figure 2.9. Image of PT04 (a) before the start of testing and (b) after failure.....	21
Figure 2.10. PT04 results for internal pressure, actuator displacement and axial force vs time.....	22
Figure 2.11. PT04 force vs actuator displacement.....	22
Figure 2.12. PT04 force vs joint displacement .....	22
Figure 2.13. PT04 average axial and circumferential strains.....	23
Figure 2.14. PT04 stress vs strain .....	23
Figure 2.15. Specimen PT07 results for pressure, axial force, and actuator displacement vs time .....	24
Figure 2.16. PT07 force vs actuator displacement.....	25
Figure 2.17. PT07 force vs joint displacements.....	25
Figure 2.18. LVDT locations for PT07.....	25
Figure 2.19. Failure at east end for PT07.....	25
Figure 2.20. PT07 axial and circumferential strains vs time.....	26
Figure 2.21. PT07 average axial and circumferential strains vs time .....	26
Figure 2.22. PT07 stress vs strain .....	26
Figure 2.23. Specimen PT08 results for pressure, axial force, and actuator displacement vs time .....	27
Figure 2.24. PT08 force vs actuator displacement.....	28
Figure 2.25. PT08 force vs joint displacements.....	28
Figure 2.26. LVDT locations for PT08.....	28
Figure 2.27. Failure at west joint for PT08 .....	28
Figure 2.28. PT08 average axial and circumferential strains vs time .....	29
Figure 2.29. PT08 stress vs strain .....	29
Figure 2.30. Specimen PT14 results for pressure, axial force, and actuator displacement vs time .....	30
Figure 2.31. PT14 force vs actuator displacement.....	30
Figure 2.32. PT14 Force vs joint displacements .....	30
Figure 2.33. LVDT locations for PT14.....	31
Figure 2.34. Failure at joint for PT14 .....	31
Figure 2.35. PT14 average axial and circumferential strains vs time .....	31
Figure 2.36. PT14 stress vs strain .....	31
Figure 2.37. Specimen PT15 results for pressure, axial force, and actuator displacement vs time .....	32



Figure 2.38. PT15 force vs actuator displacement.....	33
Figure 2.39. PT15 force vs joint displacements.....	33
Figure 2.40. LVDT locations for PT15.....	33
Figure 2.41. Failure at coupling for PT15.....	33
Figure 2.42. PT15 average axial and circumferential strains vs time .....	34
Figure 2.43. PT15 stress vs strain .....	34
Figure 2.44. Typical installation of stiffener insert.....	36
Figure 2.45. Typical LVDT attachment for PT16.....	36
Figure 2.46. Specimen PT16 results for pressure, axial force, and actuator displacement vs time .....	37
Figure 2.47. PT16 force vs actuator displacement.....	37
Figure 2.48. PT16 force vs joint displacements.....	37
Figure 2.49. PT16 failure at joint.....	38
Figure 2.50. PT16 average axial and circumferential strains vs time .....	38
Figure 2.51. PT16 stress vs strain .....	38
Figure 2.52. Sting pot attachment for PT34.....	39
Figure 2.53. PT34 – Pressure, Act. Disp., and Act. Force vs. Time .....	40
Figure 2.54. PT34 force vs actuator displacement.....	40
Figure 2.55. PT34 force vs joint displacements.....	40
Figure 2.56. PT34 failure at joint.....	41
Figure 2.57. PT34 average axial and circumferential strains vs time .....	41
Figure 2.58. PT34 stress vs strain .....	41
Figure 2.59. Fused pipe axial force vs actuator displacement .....	43
Figure 2.60. Fused pipe axial force vs joint displacement.....	43
Figure 2.61. Fused pipe axial force vs axial strain.....	44
Figure 2.62. Fused pipe axial force vs circumferential strain.....	44
Figure 2.63. Megalug coupling axial force vs actuator displacement.....	45
Figure 2.64. Megalug coupling axial force vs joint displacement .....	45
Figure 2.65. Megalug coupling axial force vs axial strain.....	45
Figure 2.66. Megalug coupling axial force vs circumferential strain .....	45
Figure 2.67. Axial Force vs. Act. Disp. for all fusible PVC tension tests.....	46
Figure 3.1. Compression test setup.....	47
Figure 3.2. Megalug end restrain orientation for compression .....	47
Figure 3.3. Specimen PC10 results for pressure, axial force, and actuator displacement vs time .....	48
Figure 3.4. PC10 force vs actuator displacement.....	49
Figure 3.5. PC10 force vs joint displacements.....	49
Figure 3.6. LVDT locations for PC10.....	49
Figure 3.7. Failure at west end for PC10 .....	49
Figure 3.8. PC10 axial and circumferential strains vs time .....	50
Figure 3.9. PC10 average axial and circumferential strains vs time .....	50
Figure 3.10. PC10 stress vs strain.....	50
Figure 3.11. Compression test progression.....	51
Figure 3.12. Specimen PC13 results for pressure, axial force, and actuator displacement vs time .....	52
Figure 3.13. PC13 Force vs actuator displacement.....	53
Figure 3.14. PC13 force vs joint displacements.....	53



Figure 3.15. String potentiometer locations for PC13 .....	53
Figure 3.16. PC13 axial and circumferential strains vs time .....	54
Figure 3.17. PC13 average axial and circumferential strains vs time .....	54
Figure 3.18. PC13 Stress vs strain .....	54
Figure 3.19. Compression test (PC13-Fuse) progression.....	55
Figure 3.20. Axial force vs Act. Disp. for fPVC pipe with Megalug coupling & fused connection .....	57
Figure 3.21. Axial force vs Joint Disp. comparison for fPVC pipe with coupling & fused connection.....	57
Figure 3.22. Axial compression force vs Axial strain for fusible pipe with Megalug & fused connection	58
Figure 3.23. Axial compression force vs Circumferential strain for fusible pipe with Megalug & fused connection .....	58
Figure 5.1. Test frame with 6-in. diameter PVC.....	63
Figure 5.2. Pipe loading saddles with high-capacity bearings .....	63
Figure 5.3. PB03 with Megalug connection .....	69
Figure 5.4. Images of PB03 during the test progression .....	70
Figure 5.5. PB03 Time history of crosshead displacement, applied force, and pressure.....	71
Figure 5.6. PB03 axial strains and circumferential strains vs. time and imposed crosshead displacement	72
Figure 5.7. PB03 results for (a) applied displacement & resisting moment and (b) curvature & internal pressure .....	73
Figure 5.8. PB03: (a) crosshead displacement vs. curvature and (b) moment vs. curvature .....	74
Figure 5.9. PB03 curvature history of axial strain .....	74
Figure 5.10. PB04 6-in. (150 mm) diameter fusible PVC with fused connection .....	76
Figure 5.11. Images of PB04 during the test progression .....	76
Figure 5.12. PB04 test results for (a) crosshead displacement, applied force, & pressure vs. time and (b) calculated curvature & applied moment .....	77
Figure 5.13. PB04: (a) crosshead displacement vs. curvature and (b) moment vs. curvature .....	78
Figure 5.14. PB04 strain evolution for (a)(c) axial and (b)(d) circumferential strains vs. time and applied crosshead displacement.....	80
Figure 5.15. PB04 curvature history of axial strain .....	81
Figure 5.16. Images of PB05 during the test progression .....	84
Figure 5.17. PB05 (a) applied displacement & moment and (b) curvature & internal pressure vs. time ..	85
Figure 5.18. PB05: (a) crosshead displacement vs. curvature and (b) moment vs. curvature .....	86
Figure 5.19. Time history of PB05 (a) axial and (b) circumferential strains .....	87
Figure 5.20. Axial strains at SG-60 (a) crown and (b) invert as a function of applied curvature .....	89
Figure 5.21. Axial strains at SG-20 (a) crown and (b) invert as a function of applied curvature .....	89
Figure 5.22. Comparison of bending test moment vs. curvature .....	90
Figure 5.23. Comparison of applied moment vs (a) crown and (b) invert axial strains located at SG-60..	91
Figure 5.24 Applied moment vs. (a) crown and (b) invert strains within constant moment region .....	91
Figure 6.1. Specimen PS11 (a) before and (b) after axial tension test.....	96
Figure 6.2. PS11 results for internal pressure, actuator displacement and axial force vs time .....	97
Figure 6.3. Specimen PS11 actuator force vs (a) actuator displacement for cyclic displacements and (b) actuator displacement for entire test .....	97
Figure 6.4. Specimen PS11 measured (a) average strains, and (b) joint displacement.....	98
Figure 6.5. Progression of cyclic test PS11 .....	99
Figure 6.6. Specimen PS11 after failure: (a) circumferential fracture and (b) test overview .....	100



Figure 7.1. Load path of applied force, P..... 109  
 Figure 7.2. Comparison of BT03 Bending Stress ..... 112  
 Figure 7.3. Circles of curvature shown for imposed displacement in red and region of maximum moment in green..... 113  
 Figure 7.4. RoC coordinate locations for representative deflected shape..... 114  
 Figure 7.5. Image showing the theurgical circle from which the radius of curvature is determined ..... 115  
 Figure 7.6. Strain-Curvature relationship ..... 116  
 Figure 7.7. Comparison of calculated strain versus measured strain at pipe invert ..... 117  
 Figure 7.8. Comparison of Radius of Curvature and Curvature calculations as a function of time ..... 118  
 Figure 7.9. Comparison of Radius of Curvature and Curvature calculations as a function of crosshead displacement..... 119

**List of Tables**

Table 1.1. Summary of Axial Tests and Specimens ..... 10  
 Table 1.2. Summary of Bending Tests and Specimens..... 11  
 Table 1.3. Summary of Tensile Coupon Tests..... 12  
 Table 2.1. Summary of Tension Test Results ..... 42  
 Table 2.2. Summary of Apparent Moduli of Elasticities for Tension Tests ..... 42  
 Table 3.1. Summary of Compression Test Results ..... 56  
 Table 3.2. Summary of Apparent Moduli of Elasticity for Compression Tests..... 56  
 Table 4.1. Summary of All Axial Test Results ..... 60  
 Table 4.2. Summary of All Apparent Moduli of Elasticities ..... 60  
 Table 5.1. Instrumentation Naming Convention..... 64  
 Table 5.2. Overview of Bending Tests ..... 68  
 Table 5.3. Instrumentation of PB03 ..... 69  
 Table 5.4. Maximum Strain Values at Rupture for PB03 ..... 71  
 Table 5.5. Maximum Parameter Values of PB03 ..... 73  
 Table 5.6. Instrumentation of PB04 ..... 75  
 Table 5.7. Maximum Parameter Values of PB04 ..... 78  
 Table 5.8. Maximum Strain Values Recorded in PB04..... 79  
 Table 5.9. Instrumentation of PB05 ..... 82  
 Table 5.10. Maximum Parameter Values of PB05 ..... 85  
 Table 5.11. Extreme Axial Strain Values Recorded in PB05 ..... 86  
 Table 5.12. Overview of Fused Bending Test Results..... 88  
 Table 5.13. Seismic Ground Strain Demand Levels for Buried Pipes (Davis et al. 2019) ..... 92  
 Table 5.14. Seismic Classification of Pipeline Systems Tested (all 6-in. diameter)..... 92  
 Table 7.1. Distributed Load Moment Contributions..... 110  
 Table 7.2. Point Load Moment Contributions ..... 110  
 Table 7.3. Cross Section Properties of 6 in. Diameter PVC Pipe ..... 111  
 Table 7.4. Coordinates of Radius of Curvature Locations..... 114  
 Table 7.5. Relationship Between Crosshead Displacement and Global Applied Curvature ..... 117



University of Colorado  
Boulder

Center for Infrastructure, Energy, & Space Testing

Dept. of Civil, Environmental & Architectural Engineering

College of Engineering and Applied Science  
428 UCB

Boulder, Colorado 80309-0428

t: 303.492.8221

[CIEST@colorado.edu](mailto:CIEST@colorado.edu)

website: [www.colorado.edu/center/ciest](http://www.colorado.edu/center/ciest)



## 1. Introduction

This report is submitted to Underground Solutions Inc. (herein referred to as UGS). It presents test results from a program to investigate the axial performance of nominal 6-in. (150-mm) diameter fusible pipe with fused connections, Megalug couplings, and Lokx couplings. The work was undertaken in the Center for Infrastructure, Energy, and Space Testing (CIEST) which is affiliated with the Civil, Architectural, and Environmental Engineering Department at the University of Colorado Boulder.

The intention of this study is to impose external loading conditions to test specimens that are representative of the significant deformations possible during earthquake-induced ground motions such as landsliding, fault rupture, and liquefaction-induced lateral spreading, thus characterizing the pipeline system capacity. All tests were designed and performed in accordance with procedures and recommendations provided by Wham et al. (2018 & 2019).

This report is organized into six sections. Section 1 provides introductory remarks, including discussion of the test specimens, experimental overview, and tensile coupon testing. Sections 2, 3, and Appendix A discuss axial tension, axial compression, and axial cyclic tests respectively. Section 4 concludes axial results. Section 5 covers the bending tests performed, including test setup, results, and conclusions. Concluding remarks are presented in Section 6. Appendices A-F provide detailed information on key procedures, practices, assumptions, and calculations.

### 1.1 Test Specimens

Pipe specimens consist of fusible C900 polyvinyl chloride (fusible PVC), Pressure Class 235, DR18. The connections under investigation are the PVC pipe fuse (Figure 1.1a), fused PVC pipe with Series 3800 Mega-coupling (referred to as Megalug) with Series 2000PV Mechanical Joint Restraints (Figure 1.1b) and fused PVC with Lokx coupling (Figure 1.1c). Megalug fittings are pressure rated to 305 psi (2,100 kPa) for DR18 6 in (150 mm) nominal pipe. This testing program examines the straight coupling, and the results are intended to be representative of the connection between pipe and Megalug restraint connection for any 6-in. (150-mm) diameter fitting configuration (e.g., valves, tees, bends). Pipe stiffeners were added for one axial tension test, which consisted of inserting a metal sleeve on the inner portion of the pipe that interacts with the Megalug restraint. These stiffeners are discussed in more detail in Section 2.3.6.

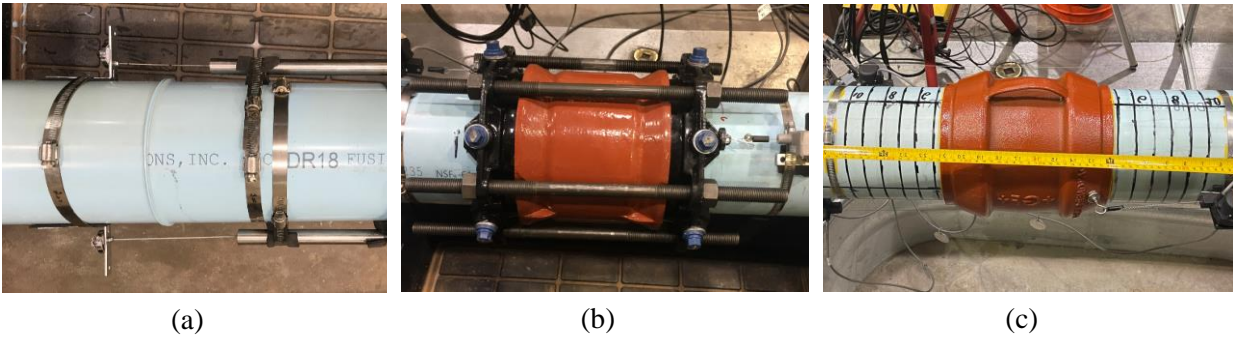


Figure 1.1. Examples of the (a) fused connection, (b) Megalug coupling, and (c) Lokx coupling

## 1.2 Test Overview

All specimens tested herein are 6-in (150-mm) diameter pipe, commercially available and conforming to C900 (PVC) standards. A 235 Pressure Class (DR18) specimen is used for each fusible PVC test. Table 1.1 provides an overview of the axial test specimens and experiments performed while Table 1.2 provides an overview of four-point bending tests. The Test ID represents the test type and a unique numerical value specific to the testing performed at CIEST. Joint Type identifies the pipe material connection type while Internal Pressure classifies the approximate internal water pressure at which each test is conducted.

Table 1.1. Summary of Axial Tests and Specimens

Test ID	Test Type	Joint Type (Company)	Internal Pressure (psi) [kPa]
PT04	Axial Tension	Megalug (EBAA)	65 [448]
PT07	Axial Tension	Fused (UGS)	65 [448]
PT08	Axial Tension	Megalug (EBAA)	65 [448]
PC10	Axial Compression	Megalug (EBAA)	63 [434]
PS11	Axial Cyclic	Megalug (EBAA)	0 [0]
PC13	Axial Compression	Fused (UGS)	7.5 [52]
PT14	Axial Tension	Fused (UGS)	7.5 [52]
PT15	Axial Tension	Megalug (EBAA)	5 [34]
PT16	Axial Tension	Megalug with stiffener	64 [441]
PT34	Axial Tension	Lokx (GF)	65 [448]

Table 1.2. Summary of Bending Tests and Specimens

Test ID	Test Type	Joint Type (Company)	Internal Pressure (psi) [kPa]
PB03	Four- Point Bending	Megalug (EBAA)	62 [427]
PB04	Four-Point Bending	Fused (UGS)	62 [427]
PB05	Four-Point Bending	Fused (UGS)	16-20 [110-138]

### 1.3 Tensile Coupon Tests

#### 1.3.1 University of Colorado, Boulder

Three test trials were conducted for the fusible coupons at the University of Colorado’s CIEST Laboratory in Boulder. Values for extensometer strain, local strain, and axial/circumferential strains and stresses were obtained. The stress strain curve for all three trials was consistent across each test. All tests exhibited an initial linear elastic response, followed by yielding. Beyond the yield point, the stress begins to decline significantly, the material exhibits necking and finally rupture. One specimen exhibited an increased period of necking before rupture when compared to the other two trials. This resulted in higher extensometer strains for this trial. The stress-strain curves for the three trials can be seen below in Figure 1.2.

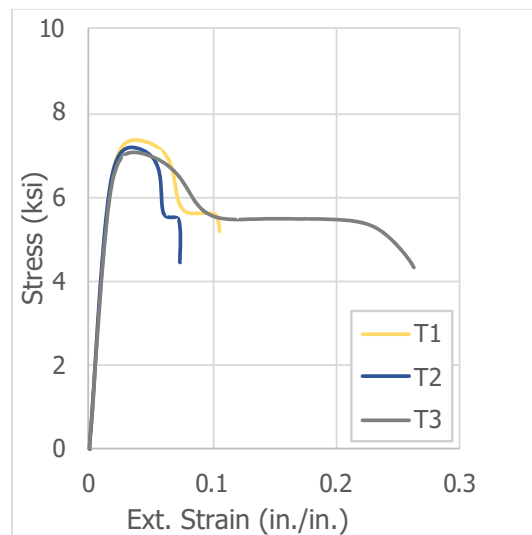


Figure 1.2. Fusible Coupon Tests, Stress vs. Extensometer



Key properties for each of the Fusible Test trials are organized in the table below (Table 1.3). The values for stress and extensometer strain for the first two trials are similar, while results from trial 3 are slightly different. The strain gage bonded to the coupon slipped early in trial 3, resulting in inaccurate readings from the strain gage, so data from this gage is disregarded. The Young’s Modulus was determined from both extensometer strain and strain gage values. Initial strain values in the linear elastic region for the stress vs. extensometer strain are consistent among all three trials.

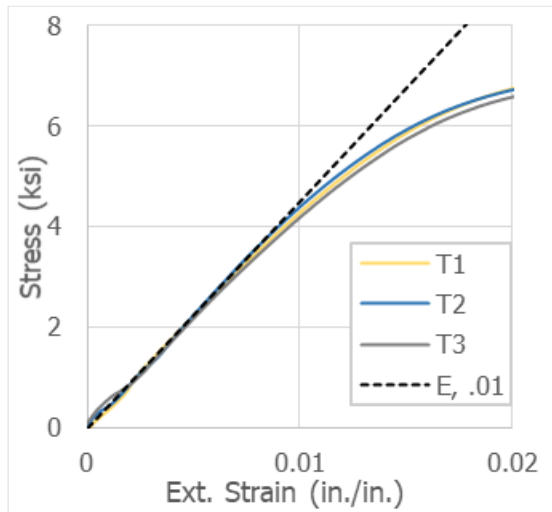
Table 1.3. Summary of Tensile Coupon Tests

Test Number	Cross Section Area (in <sup>2</sup> )	Max Stress	Max Ext. Strain	Max. Local Axial Strain	Max. Circumferential Strain
		(ksi)	(in/in)	(in/in)	(in/in)
<b>Trial 1</b>	0.209	7.36	0.105	0.0148	0.0037
<b>Trial 2</b>	0.205	7.18	0.073	0.0469	0.0053
<b>Trial 3</b>	0.215	7.09	0.262	0.0003	0.0001
<b>Mean</b>	0.210	7.21	0.146	0.0308	0.0045

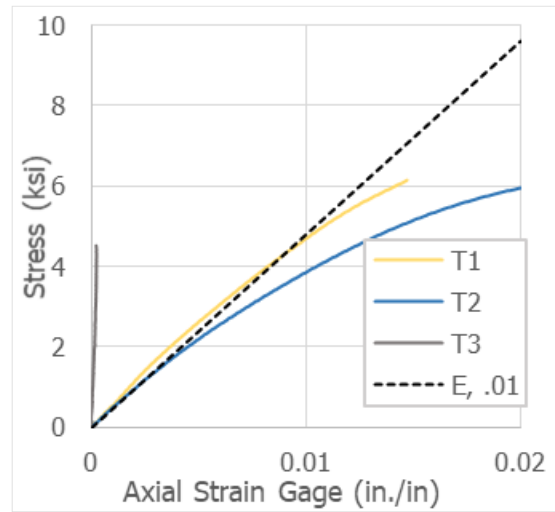
The Young’s Modulus was determined from the strain gage data at an initial value of 0.01 strain and a global value determined based on the linear portion of the curve. The Young’s Modulus was also determined from extensometer strain data at a strain value of 0.01. Although the strain gauge data for trial 3 was disregarded, the strain gage does not affect the extensometer data. Therefore, extensometer data is still consistent for all three trials and is used to determine the Young’s Modulus at 0.01 strain for all three trials. Data analysis determined Young’s Modulus based on all three trials for the extensometer strain to be approximately 450 ksi (3102 MPa). The values for Young’s Modulus based on local axial strain gage data are determined to be most representative of the actual material strain. Comparison between the Young’s Modulus determined at an initial strain of 0.01 and a global strain measured at the linear elastic region are demonstrated in Figure 1.3.



This shows that the comparison between extensometer strain and local axial strain gave a slight difference in the Young's Modulus values. Although data from the third strain gage is not usable, the Young's Modulus calculated from strain gage values are most representative of the material strain. Figure 1.4 shows a fractured specimen after failure.



(a)  $E = 450 \text{ ksi}$  (3102 MPa)



(b)  $E = 470 \text{ ksi}$  (3240 MPa)

Figure 1.3. Coupon Tests (a) Stress vs. Extensometer Strain and (b) Stress vs. Local Axial Strain



Figure 1.4. Fusible Failed Coupon

### 1.3.2 PSI Laboratory

Four test trials were conducted for the fusible coupons at PSI Laboratory. The stress strain curve for all four trials was very consistent for each test. Figure 1.5 shows the stress strain relationship for each test performed. From these tests, a representative modulus of elasticity was obtained and measured at 446 ksi (3074 MPa).

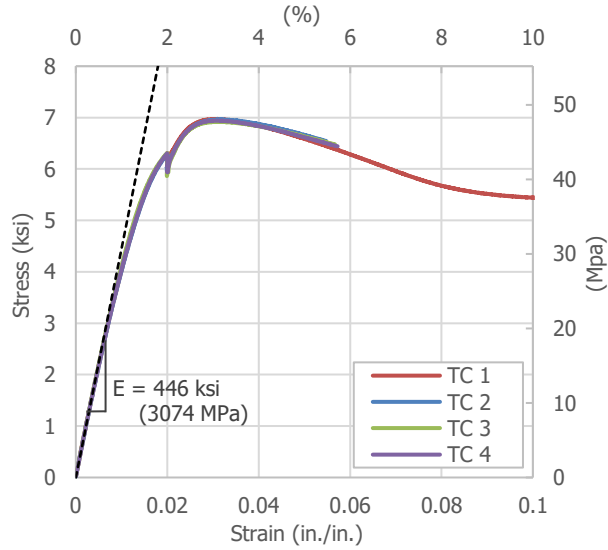


Figure 1.5. Summary of PSI Lab coupon tests

From each coupon test performed, including CIEST Lab and PSI Lab tests, the average modulus of elasticity for Fusible PVC was 455 ksi (3137 MPa), which is used for further material characteristics throughout the remainder of this report.

## 2. Axial Testing

This section provides a detailed overview of the test setup procedure and key experimental constraints associated with application of axial load to water distribution pipelines. The objective is to expose the system to external loading conditions, parallel to the axis of the pipeline representative of the significant deformations caused during earthquake-induced ground motions to characterize the pipeline system capacity. All tests are designed and performed in accordance with procedures and recommendations provided by Wham et al. (2018 & 2019) and additional details about the setup are provided by Ihnotic (2019).

### 2.1 Axial Test Setup



(a) Fused tension setup



(b) Mega-coupling tension setup

Figure 2.1. Pipe specimen in axial test frame

This section outlines the test setup procedure for axial loading of a given pipe specimen. Figure 2.1 shows an image of the axial tension test setup and equipment. A 255.17 MTS actuator, 110-kip [490-kN] load cell, and structural load frame are used to apply tensile and compressive load to the test specimen (Figure 2.2). The test specimens consist of nominal 6-in (150-mm) diameter pipe with couplings and fused connections.

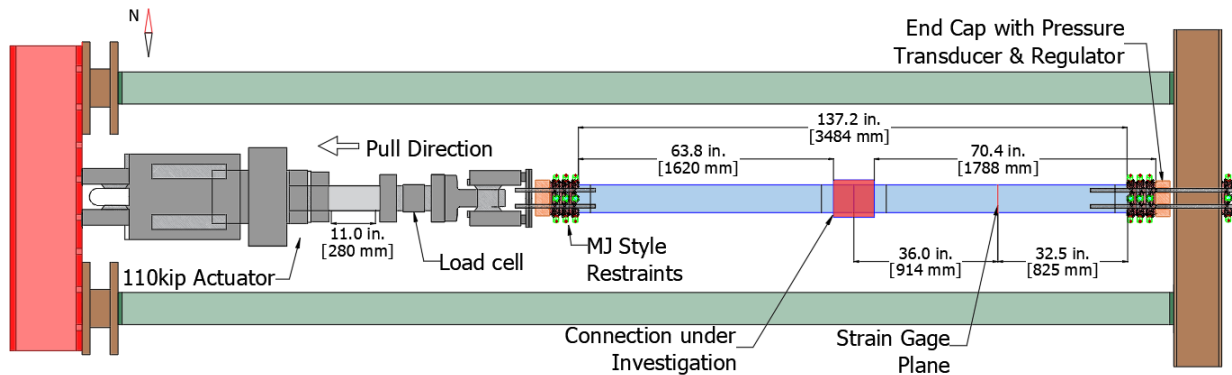


Figure 2.2. Dimensioned drawing of axial test setup

### 2.1.1 Specimen Installation Procedure

The pipe specimen is prepared at a length of approximately 13 ft (4 m) for tensile testing and 14 ft (4.25 m) for compression testing. For tension tests, the specimens typically consist of two 78-in. (1950-mm) segments. The length varies depending on the loading direction (tension or compression) and connection under investigation. The pipe is cut using standard field installation practices outlined in Appendix B. Measurements are provided at 0.5 in (13 mm) increments on the factory prepared pipe ends are inserted into the coupling or joint, as shown in Figure 2.3. A level and crowning tool are used to identify the crown, invert, and spring lines of the pipe (Figure 2.4). Strain gage planes are marked 36 in (900 mm) from either side of the specimen center line, as shown in Figure 2.2.



Figure 2.3. Marked measurements on non-cut ends of the pipe.

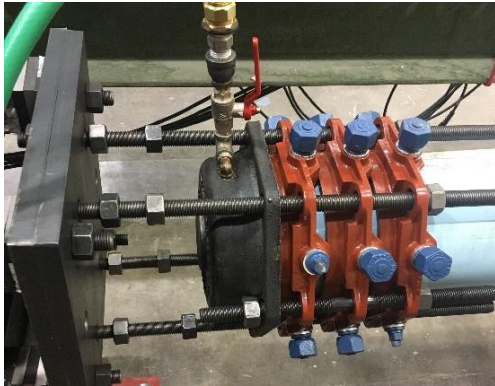


Figure 2.4. Identifying the pipe coordinates (crown, invert, and spring lines)

Three 2006PV Megalug external restraints are used at either end of the specimen to transfer externally applied axial load. Figure 2.5 shows the restraints positioned at the loading end (east) and fixed end (west) of the specimen. The outer most restraint for each end is aligned 2 in. (50 mm) from the end



pipe and hand tightened into place. Each set of restraints are aligned with their perspective end loading arrangements. The east side, fixed to the load frame, is positioned with a threaded rod located at the crown of the specimen, and the west side (actuator or loading side) is aligned with restraint nuts located at the crown. Two short threaded rods are used to pull the remaining two restraints into contact with the first, as shown in Figure 2.6, two provide a composite 3-restraint end condition. The clamping nuts of the remaining



(a) Loading end (east)



(b) Fixed end (west)

Figure 2.5. Pipe connections to loading frame on (a) east and (b) west ends



Figure 2.6. Megalug restraints on “cut” ends of pipe



Figure 2.7. Fixed end (west) with water intake and pressure valve

Megalugs are hand tightened into place.



The nuts on each end restraint are tightened in a star pattern using a torque wrench set to 30 ft-lbs (40.7 N-m). The torque wrench is increased to 60 ft-lbs (81 N-m) and the process is repeated until all restraints are secured to the pipe. While the Megalug restraint is equipped with self-torquing, twist off clamping nuts for typical field installation, prior experience suggests the incrementally increasing torque wrench provides a uniformly distributed clamping force that ensures symmetric circumferential contact and deters failure at the ends of the specimen.

Strain Gauges are installed at designated locations following the procedure outlined in “Strain Gauge Application Procedure” (Appendix C) and additional details are included in the following section.

The specimen is placed in the loading frame and the east and west connections are appropriately aligned with the actuator in its full extended position (tension test) or fully retracted position (compression test). Lubrication (necessary for the gasket) is applied to the endcap gaskets and the inner diameter of the endcaps, the gasket is positioned against the outermost end restraint (as shown in Figure 2.6), and the endcaps tightened in place with threaded rods (Figure 2.5). The east end cap is equipped with pressurization equipment and water inlet (Figure 2.7) while the west endcap includes a bleeder valve at the crown to remove air during filling of the pipe. The elbow for the water intake on the east endcap and the air release valve on the west endcap are positioned vertically. Two short threaded rods on the crown and the invert (east) and on each spring line (west) are installed to secure the endcap to the pipe. On the east end, four 36-in (900 mm) long, 0.75-in (19 mm) diameter high-strength 120 ksi (827 mPa) threaded rods are installed to secure the pipe to the frame. Two nuts per rod are threaded during placement such that their final position is between the testing frame and the endcaps, as shown in Figure 2.5. A restraint is set into place over the four rods on the outer flange of the frame (Figure 2.7). Nuts and washers are then applied to each end to secure the pipe to the testing frame. A similar procedure is followed on the east end. Four 24-in (600 mm) long threaded rods are used to fix the specimen to a transfer plate machined with a hole pattern matching the restraints. The steel nuts and threaded rod connections are arranged such that axial force from pressurization is resisted by the actuator, and thus recorded by the actuator load cell.

### **2.1.2 Instrumentation**

Figure 2.8 shows a plan view of the tension test setup and key instrumentation. Four string potentiometers (string pots) or linearly varying differential transducers (LVDT) are attached to the specimen at several locations to measure axial displacements. A string pot/LVDT is used at each end of the specimen to measure relative movement between the pipe specimen and end restraints. Two additional string pots/LVDTs are installed at the center of the specimen to measure localized relative displacement between the pipe and

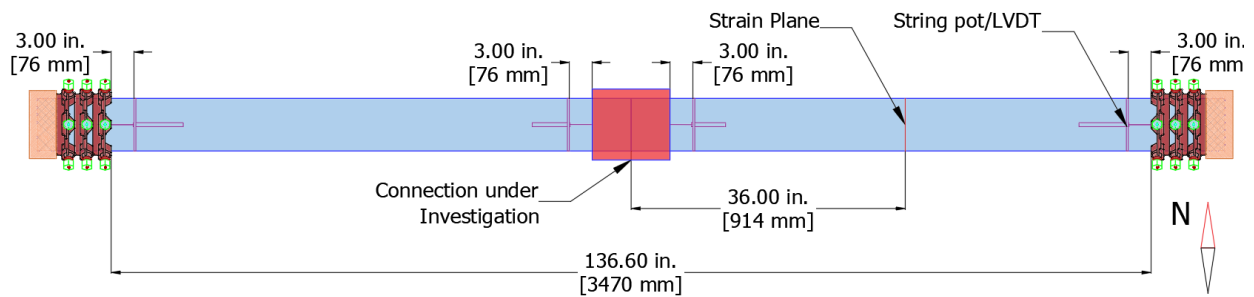


Figure 2.8. Specimen instrumentation

connection under investigation. An electronic pressure transducer (EPT) is installed on the east end to measure internal water pressure during testing.

A total of eight strain gauges are fixed to the exterior of the specimen at two plane locations (one on each segment of the specimen), designated as SG+36 and SG-36, as shown in Figure 2.8. The plane locations are positioned approximately halfway between the joint restraint (specimen centerline) and gripping restraints. At both strain planes, the strain gauges are placed at the crown, east spring line, invert, and west spring line. Gauge plane SG+36 is positioned 36 in. (900 mm) east of the specimen centerline and includes four x-y gauges, oriented in the axial and circumferential direction. Plane SG-36 is positioned 36 in. (900 mm) west of the specimen centerline and includes two x-y pairs located the specimen spring lines.

## 2.2 Axial Test Procedure

The following section provides details of the overall test sequence separated into three parts: pretest, test sequence, and discussion of pause or stop criteria.

### 2.2.1 Pretest

Once the specimen is secured in the loading frame and the calibrated instrumentation is installed, the measuring systems are verified. The pipe is filled with water with the air bleeder valve in the open position. The air bleeder valve is closed once water has streamed from it, and the system is pressurized to the laboratory pressure of approximately 65 psi (450 kPa) to check for leaks. Water is introduced into the specimen more than five hours before testing to ensure thermal acclimation to ambient laboratory conditions. Temperature readings of the external wall of the pipe are taken at several locations. Multiple pressurization sequences are completed to seat gaskets, verify readings of strain gauges, and check axial force measured by the load cell. In each of the cycles the air bleed valve is opened to release any accumulating air. Prior to a pressurization sequence, the nuts between the loading frame and the endcaps



are tightened, such that when the pipe is pressurized, the axial pressurization force can be measured by the load cell. During the pressurization sequences, the pipe is pressurized to approximately 65 psi (450 kPa) and back down to 0 psi several times. After each sequence, data was collected, stored, and analyzed to ensure proper function of all measuring systems. The area surrounding the testing frame is cleared of all tools and other objects. Once ready for the test, a pretest meeting is conducted to review installation conditions, walk through instrumentation locations and expectations, and discuss safety equipment and concerns.

### ***2.2.2 Test Sequence***

After the pretest meeting is conducted and roles assigned, the test sequence is initiated by starting the data acquisition system and laboratory hydraulic systems. A data sampling rate of 4 Hz is used for all reported tests. The loading nuts at either end of the specimen are tightened to avoid any end movement due to pressurization. The appropriate water pressure applied depends on the specific test. The test is performed under displacement control at a rate of 1 in. per minute. Displacement is applied until the specimen is no longer capable of holding internal water pressure or until the maximum stroke of the actuator, 11 in. (275 mm), is reached. Once the test is completed, the data acquisition system is turned off, laboratory hydraulic systems set to low pressure, and data is backed up.

### ***2.2.3 Stop or Pause Criteria***

Several potential causes for interruption to the test sequence are identified prior to testing. The test is paused if the specimen loses water pressure during the test. If undesirable leakage occurs at the end caps they are tightened, and the test is resumed. If any leakage is observed at the coupling or center of the specimen (serviceability limit state), the test is paused briefly, leakage rate assessed, and the test resumed until ultimate failure. The test is paused if any fundamental instrumentation malfunctions during the test, or if power is lost in any part of the testing laboratory. The test is terminated when the specimen is unable to hold internal water pressure, which typically occurs as a result of structural failure of the pipe body or connection.



### 3. Axial Tension Test Results

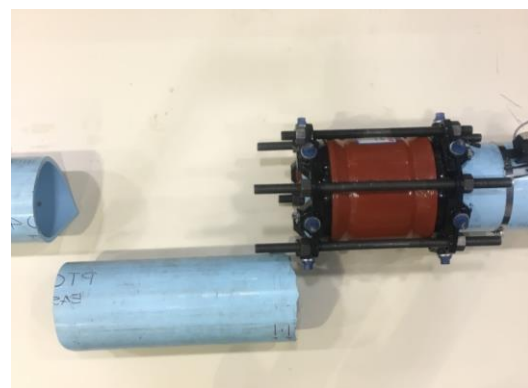
The following section provides results from axial tension tests performed on different pipe connections. A total of six axial tension tests are reported in the following sections. For all tests, displacement is applied at a rate of 1 in. (25 mm) per minute.

#### 3.1 Tension Test (PT04)- fPVC w/ Megalug Coupling

Fusible PVC piping with a Megalug-coupling restraint was used for this test. Images of the centered coupling connection before and after the test are shown in Figure 3.1. As shown by the blue line in Figure 3.2, water pressure was held relatively constant at ~63 psi (435 kPa) for the duration of the test. Figure 3.2 also shows the actuator force and displacement relative to time during the test. The slight fluctuation in pressure is a function of the increasing internal volume during applied tensile loading. Figure 3.3 shows the relationship between the actuator force and actuator displacement. Actuator forces and displacements are direct measurements of the hydraulic load cell and piston, respectively. Displacement was applied at a rate of 1 in. (25 mm) per minute, and the force feedback of the load cell was recorded. The maximum force recorded in the load cell of the actuator was 29.6 kips (132 kN) and the maximum displacement was 2.4 in. (61 mm). Figure 3.4 shows the actuator force vs the joint displacement. Joint displacement was measured using two string potentiometers located 3 in (75 mm) away from the coupling on both ends of the coupling, shown in Figure 3.1 (a). The joint displacement reached a total of about 0.9 in (23 mm) just before failure. The true joint displacement does not include the stretch of the pipe over the 3 in. (75 mm) on either side of



(a)



(b)

Figure 3.1. Image of PT04 (a) before the start of testing and (b) after failure



the coupling, but the elongation due to that strain was negligible, accounting for only 0.03 in. (0.8 mm) of additional displacement on either side of the joint. The west side reached just under 0.4 in. (10 mm), while the east side reached about 0.5 in. (13 mm). Failure occurred on the east side of the coupling, fracturing in two different locations along the pipe, shown in Figure 3.1 (b).

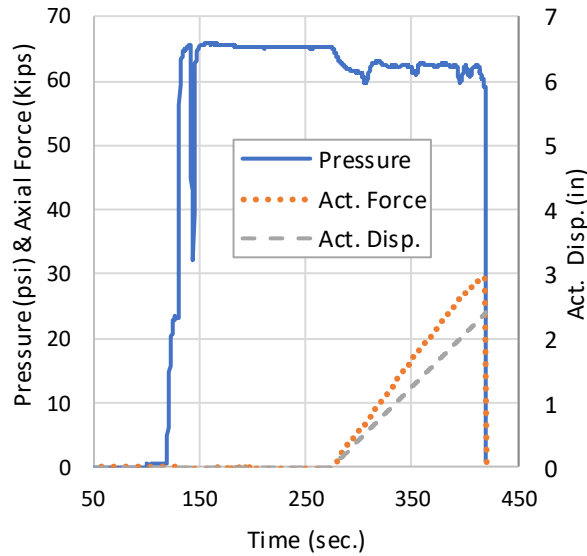


Figure 3.2. PT04 results for internal pressure, actuator displacement and axial force vs time

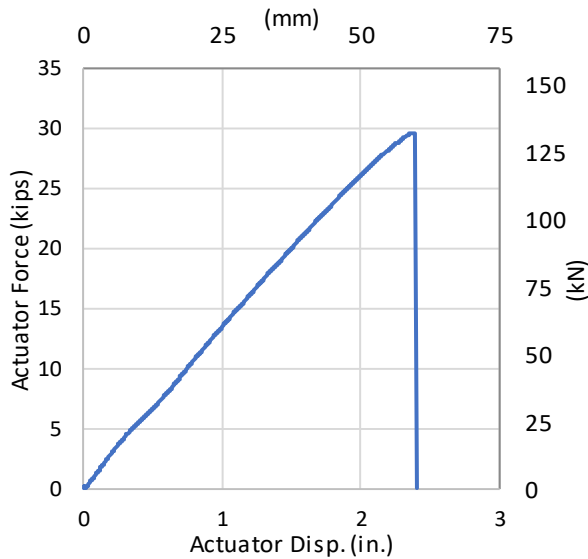


Figure 3.3. PT04 force vs actuator displacement

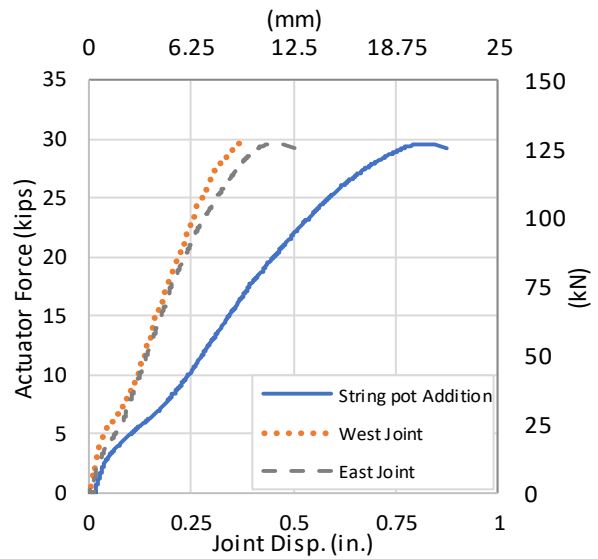


Figure 3.4. PT04 force vs joint displacement



Figure 3.5 shows the average axial and circumferential strains for the duration of the test. At the start of the test, the system was fully pressurized, and an increase in circumferential strain was observed. Once loading began, the circumferential strains began to decrease, while the axial strains increased. As the actuator applied tensile loading to the system, the pipe began to elongate, causing the increase in axial strains. Due to Poisson's effect, the circumferential strain decreased as the tensile load was applied. The maximum axial strain was measured at about 0.9% strain prior to failure. The average axial strain was used in a stress strain relationship seen in Figure 3.6. From this data, a representative modulus of elasticity of 401 ksi (2763 MPa) was estimated using data collected from 0-0.5% strain, shown by the orange trendline. The representative modulus of elasticity estimated from data collected between 0 and 1.0% strain is 383 ksi (2639 MPa), shown by the blue trendline.

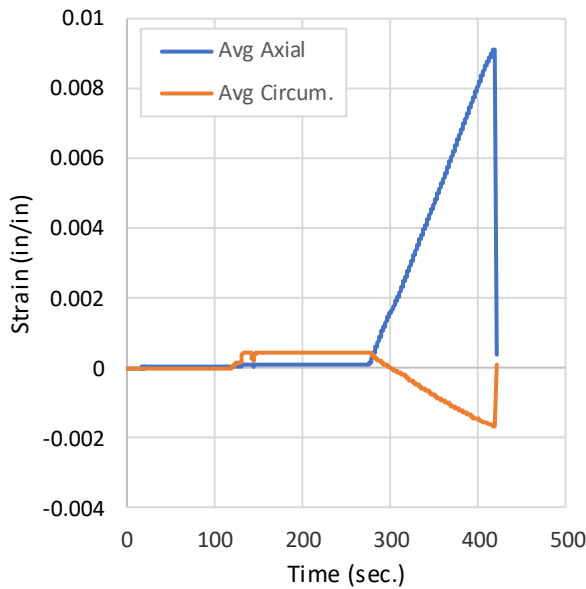


Figure 3.5. PT04 average axial and circumferential strains.

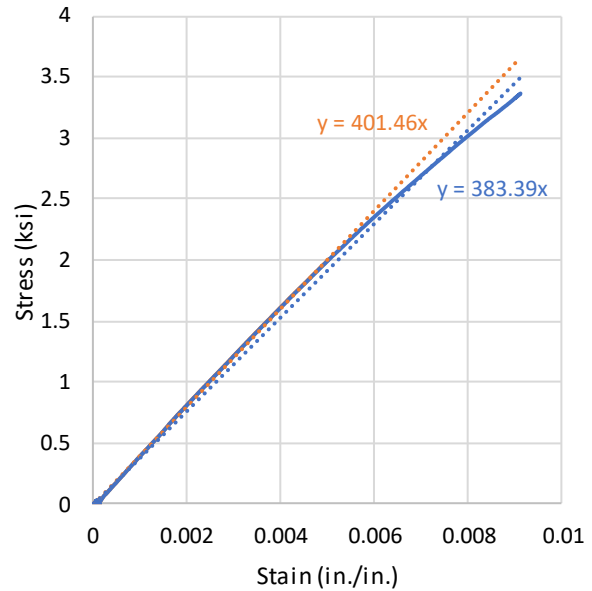


Figure 3.6. PT04 stress vs strain

### 3.2 Tension Test (PT07)- fPVC w/ Fused Connection

Fusible PVC pipe with a fused connection at the midpoint was used for this test. Figure 3.7 shows the relationship among actuator force, internal pressure, and actuator displacement relative to time. Actuator displacements and force are direct measurements of the hydraulic piston and inline loadcell, respectively. Displacement was applied at a rate of 1.0 in./min. (25 mm/min.), and the force feedback of the load cell



was recorded. Figure 3.8 shows that the maximum force recorded in the load cell was 52.5 kips (234 kN) at an actuator displacement of 5.02 in. (127.5 mm). A constant internal water pressure of  $63 \pm 3$  psi ( $434 \pm 20$  kPa) throughout the duration of the test. Figure 3.9 shows the actuator force relative to joint displacement. Joint displacement was measured using two LVDTs located on the north and south spring lines of the specimen, as shown in Figure 3.10. The LVDTs were fixed to the pipe at 3 in (75 mm) on either side of the fuse to measure displacements along a 6 in (152 mm) initial gauge length. The joint displacement reached an average of about 0.25 in. (6.5 mm) just before failure. Each of the LVDTs measured the joint displacement for the fused connection and were averaged to get the total joint displacement. Failure occurred on the east end of the specimen, fracturing at the contact point between the pipe and the restraint, shown in Figure 3.11.

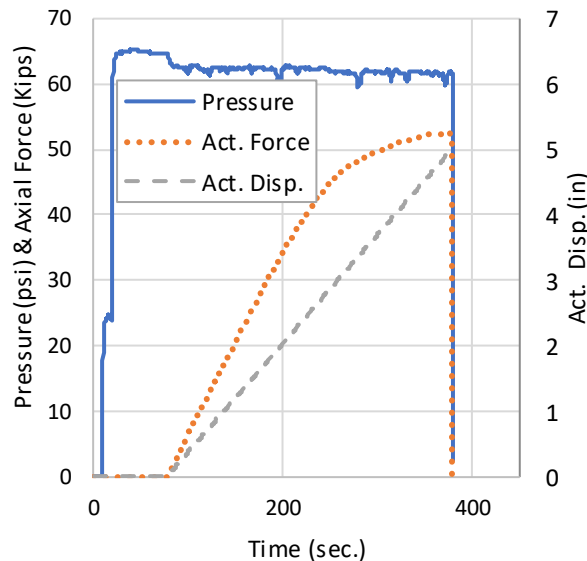


Figure 3.7. Specimen PT07 results for pressure, axial force, and actuator displacement vs time

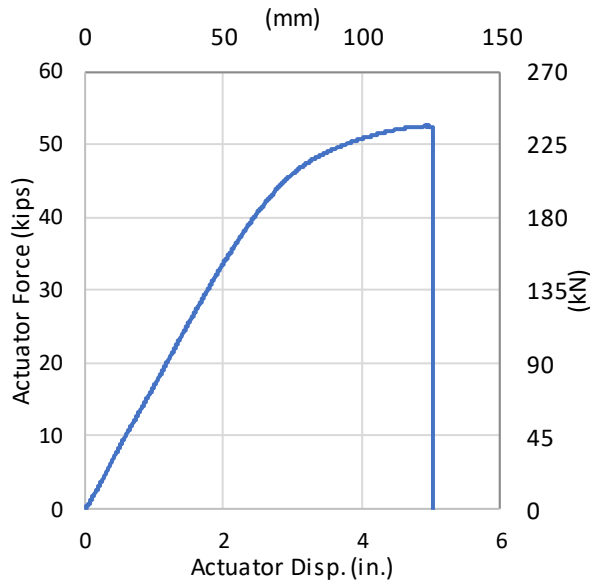


Figure 3.8. PT07 force vs actuator displacement

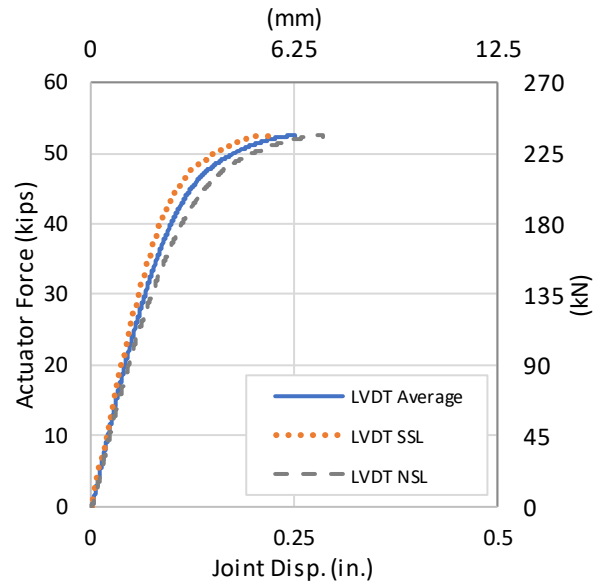


Figure 3.9. PT07 force vs joint displacements



Figure 3.10. LVDT locations for PT07



Figure 3.11. Failure at east end for PT07

Figure 3.12 shows all strains measured at a plane 36 in (910 mm) way from the fused connection. Figure 3.13 shows the average axial and circumferential strains for the duration of the test. At the start of the test, the system was fully pressurized, and an increase in circumferential strain was observed. Once loading began, the circumferential strains began to decrease, while the axial strains increased. As the actuator applied tensile loading to the system, the pipe began to elongate, causing an increase in axial strains. Due to Poisson's effect, the circumferential strain decreased as the tensile load was applied. Figure 3.14 shows the stress curve relative to axial strain. Three different representative moduli of elasticities are estimated at



406 ksi (2800 MPa), 391 ksi (2700 36MPa), and 369 ksi (2545 MPa) using data collected between 0 and 0.5% strain, 0 and 1.0% strain, and 0 and 1.5% strain, respectively.

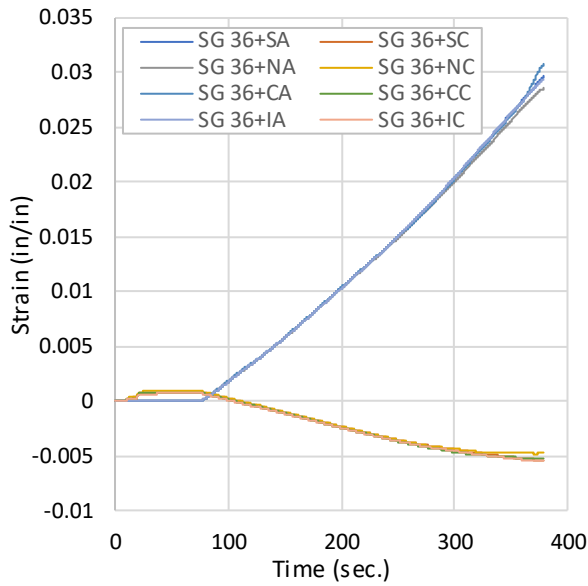


Figure 3.12. PT07 axial and circumferential strains vs time

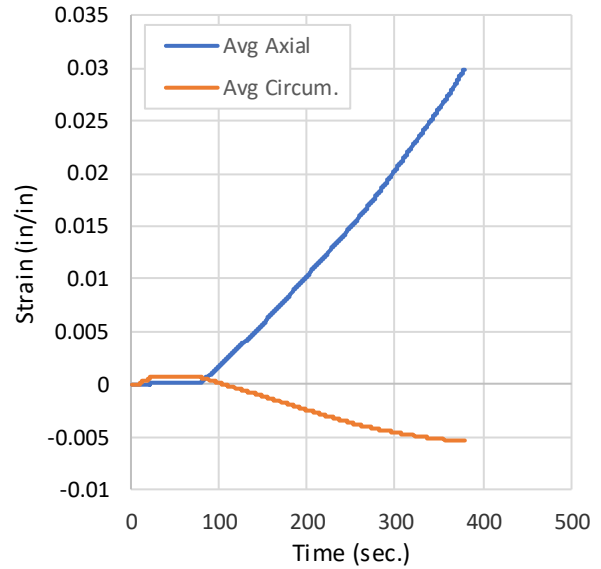


Figure 3.13. PT07 average axial and circumferential strains vs time

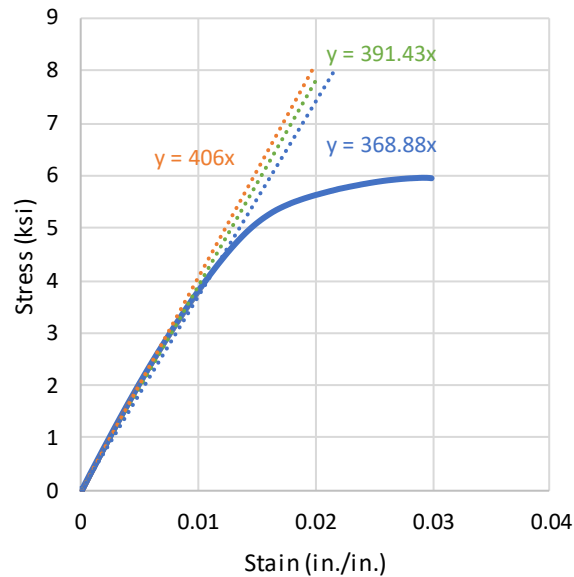


Figure 3.14. PT07 stress vs strain

### 3.3 Tension Test (PT08)- fPVC w/ Megalug Coupling

Fusible PVC pipe with a Megalug coupling restraint was used for this test. Figure 3.15 shows the relationship among actuator force, internal pressure, and actuator displacement relative to time. Actuator force and displacement are direct measurements of the hydraulic load cell and piston, respectively. Displacement was applied at a rate of 1.0 in./min. (25 mm/min.), and the force feedback of the load cell was recorded. Figure 3.16 shows that the maximum force recorded in the load cell was 19.6 kips (89 kN) at an actuator displacement of 1.74 in. (44 mm). There was no leakage of the endcaps during the duration of the test, which resulted in a constant internal water pressure of about 61 psi (420 kPa). Figure 3.17 shows the actuator force vs the joint displacement. Joint displacement was measured using two LVDTs located on both ends of the coupling, shown in Figure 3.18. The joint displacement reached an average of about 0.9 in. (23 mm) just before failure. Each of the LVDTs measured relative joint displacement for each side of the Megalug coupling, which were added together to get the total joint displacement. Failure occurred on the west side of the coupling, fracturing at the contact point between the pipe and the coupling, shown in Figure 3.19.

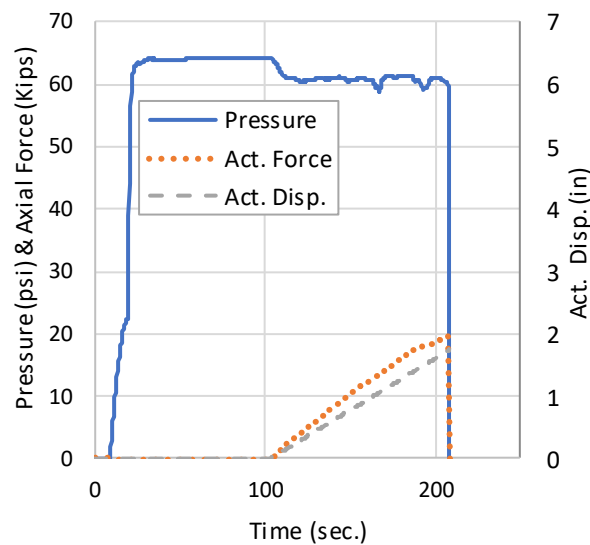


Figure 3.15. Specimen PT08 results for pressure, axial force, and actuator displacement vs time

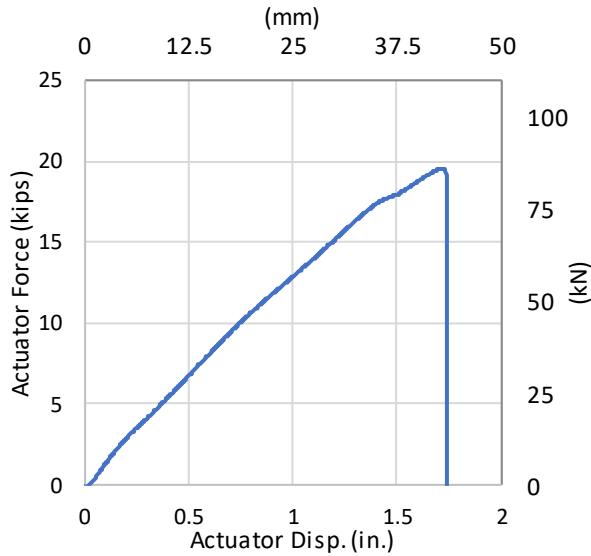


Figure 3.16. PT08 force vs actuator displacement

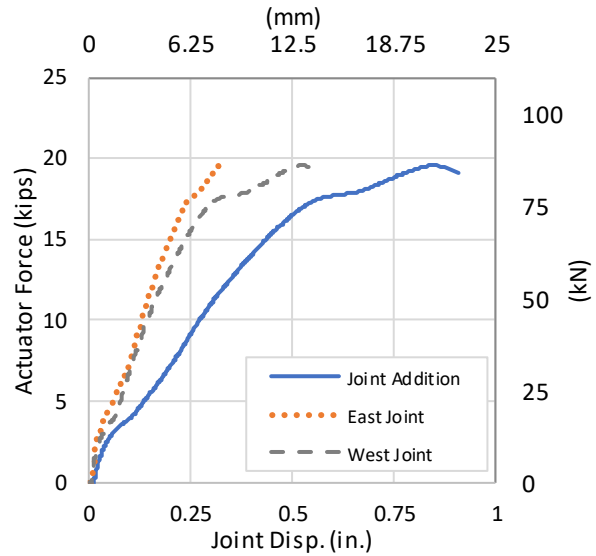


Figure 3.17. PT08 force vs joint displacements



Figure 3.18. LVDT locations for PT08



Figure 3.19. Failure at west joint for PT08

Figure 3.20 shows the average axial and circumferential strains for the duration of the test. At the start of the test, the system was fully pressurized, and an increase in circumferential strain was observed. Once loading began, the circumferential strains began to decrease, while the axial strains increased. As the actuator applied tensile loading to the system, the pipe began to elongate, causing the increase in axial strains. Due to Poisson's effect, the circumferential strain decreased as the tensile load was applied. The maximum axial strain was measured at about 0.4% prior to failure. A representative modulus of elasticity is derived from the linear relationship of stress and strain, established from Figure 3.21 to be 578 ksi (3985 MPa).

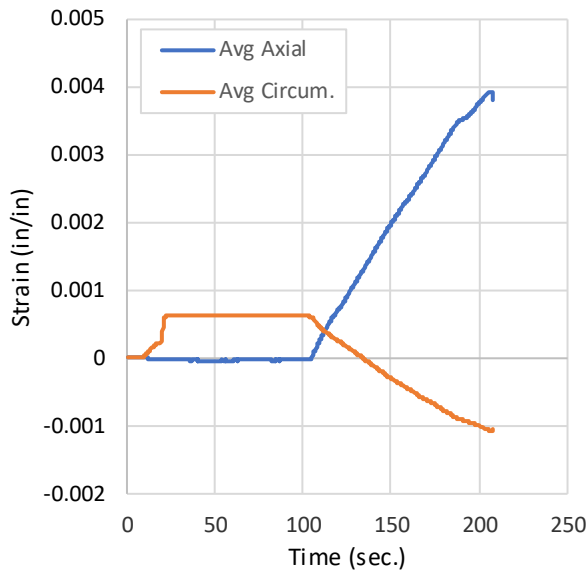


Figure 3.20. PT08 average axial and circumferential strains vs time

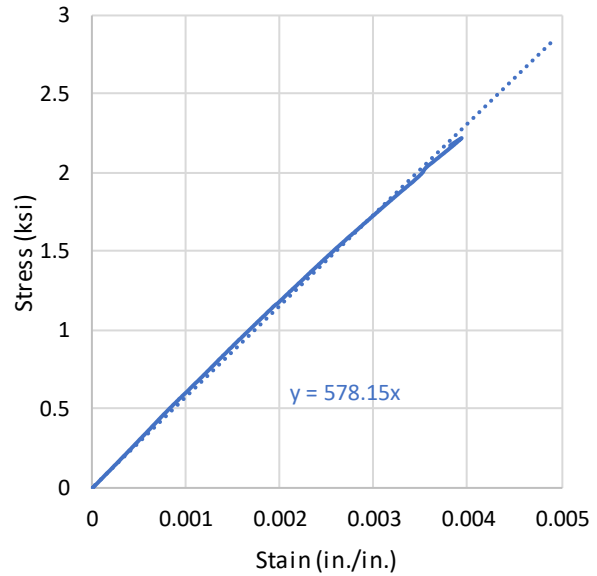


Figure 3.21. PT08 stress vs strain

### 3.4 Tension Test (PT14)- fPVC w/ Fused Connection

Fusible PVC pipe with a fused connection at the midpoint was used for this test. Figure 3.22 shows the relationship among actuator force, internal pressure, and actuator displacement relative to time. Actuator displacement and force are direct measurements of the hydraulic piston and loadcell, respectively. Displacement was applied at a rate of 1.0 in./min. (25 mm/min.), and the force feedback of the load cell was recorded. Figure 3.23 shows that the maximum force recorded in the load cell was 53 kips (234 kN) at an actuator displacement of 4.46 in. (113 mm). A constant internal water pressure of  $7 \pm 3$  psi ( $48 \pm 20$  kPa) was applied throughout the test. Figure 3.24 shows the actuator force relative to joint displacement. Joint displacement was measured using two LVDTs located on the north and south spring lines of the specimen, as shown in Figure 3.25. The LVDTs were fixed to the pipe at 3 in. (75 mm) on either side of the fused connection to measure displacements along a 6 in. (152 mm) initial gauge length. The joint displacement reached an average of about 0.17 in. (4 mm) just before failure. Each of the LVDTs measured the joint displacement at the fused connection and were averaged to get the total joint displacement. Failure occurred at the fuse, fracturing on both sides of the joint, shown in Figure 3.26.

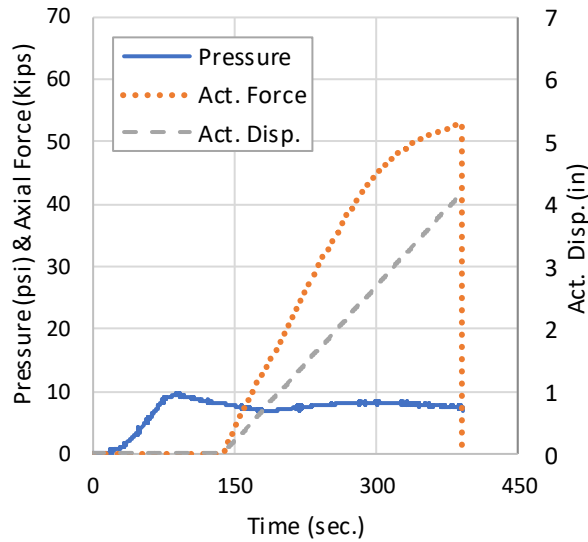


Figure 3.22. Specimen PT14 results for pressure, axial force, and actuator displacement vs time

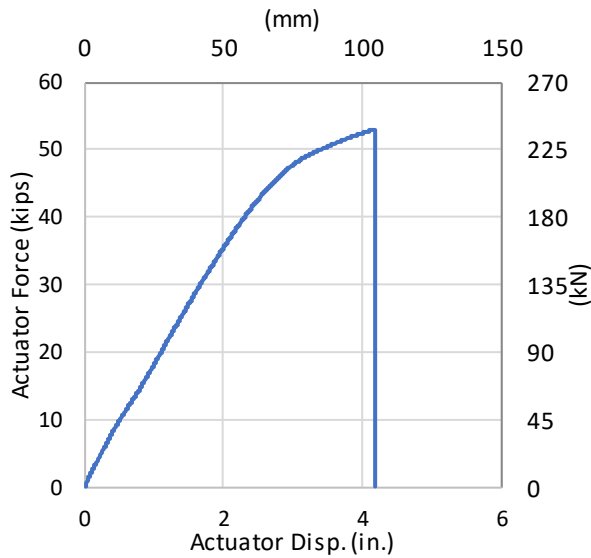


Figure 3.23. PT14 force vs actuator displacement

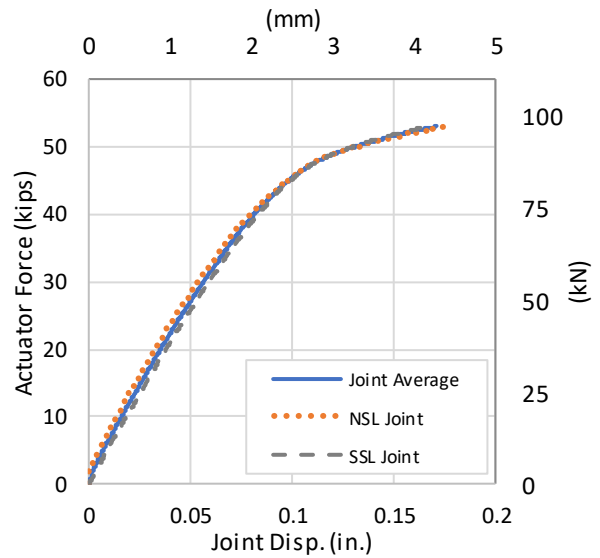


Figure 3.24. PT14 Force vs joint displacements



Figure 3.25. LVDT locations for PT14



Figure 3.26. Failure at joint for PT14

Figure 3.27 shows the average axial and circumferential strains throughout the duration of the test. At the start of the test, the system was fully pressurized and an increase in circumferential strain was observed. Once loading began, the circumferential strains began to decrease, while the axial strains increased. As the actuator applied tensile loading to the system, the pipe began to elongate, causing an increase in axial strains. Due to Poisson's effect, the circumferential strain decreased as the tensile load was applied. Figure 3.28 shows the stress curve relative to axial strain. Three different representative moduli of elasticities are

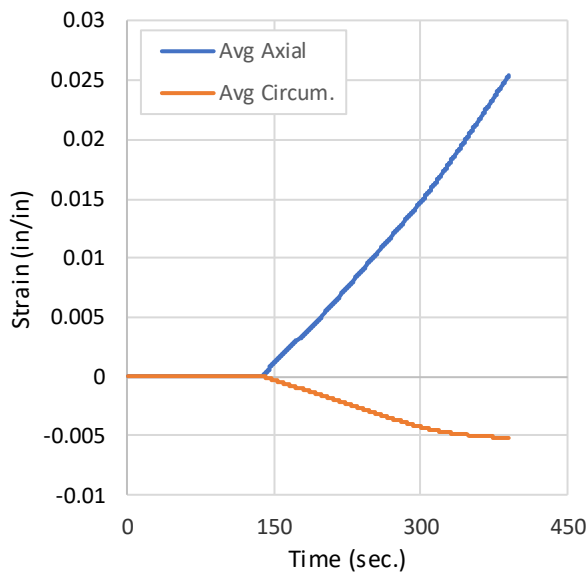


Figure 3.27. PT14 average axial and circumferential strains vs time

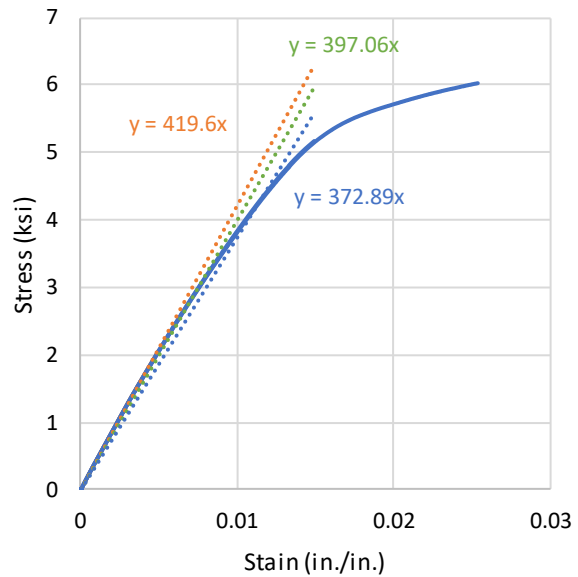


Figure 3.28. PT14 stress vs strain

estimated at 420 ksi (2894 MPa), 397 ksi (2735 MPa), and 373 ksi (2570 MPa) using data collected between 0 and 0.5% strain, 0 and 1.0% strain, and 0 and 1.5% strain, respectively.

### 3.5 Tension Test (PT15)- fPVC w/ Megalug Coupling

Fusible PVC pipe with a Megalug coupling at the midpoint was used for this test. Figure 3.29 shows the relationship of actuator force, internal pressure, and actuator displacement vs time. Actuator displacement and force are direct measurements of the hydraulic piston and loadcell, respectively. Displacement was applied at a rate of 1.0 in./min. (25 mm/min.), and the force feedback of the load cell was recorded. Figure 3.30 shows that the maximum force recorded in the load cell was 24.5 kips (110 kN) at an actuator displacement of 1.9 in. (48 mm). A constant internal water pressure of  $7 \pm 1$  psi ( $48 \pm 7$  kPa) was applied throughout the test. Figure 3.31 shows the actuator force relative joint displacement. Joint displacement was measured using two LVDTs located on the north and south spring lines of the specimen, as shown in Figure 3.32. The LVDTs were fixed to the pipe at 3 in. (75 mm) on either side of the coupling to measure joint displacement. The LVDT on the west side of the joint recorded 0.52 in (13 mm) while the LVDT on the east side recorded 0.28 in (7 mm) The joint displacement reached a total of 0.85 in. (22 mm) just before failure. Failure occurred at the east side of the joint where the pipe contacts the restraint, as shown in Figure 3.33.

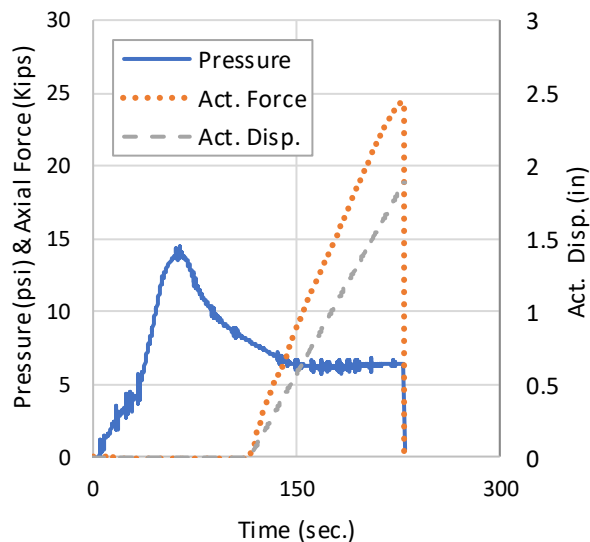


Figure 3.29. Specimen PT15 results for pressure, axial force, and actuator displacement vs time

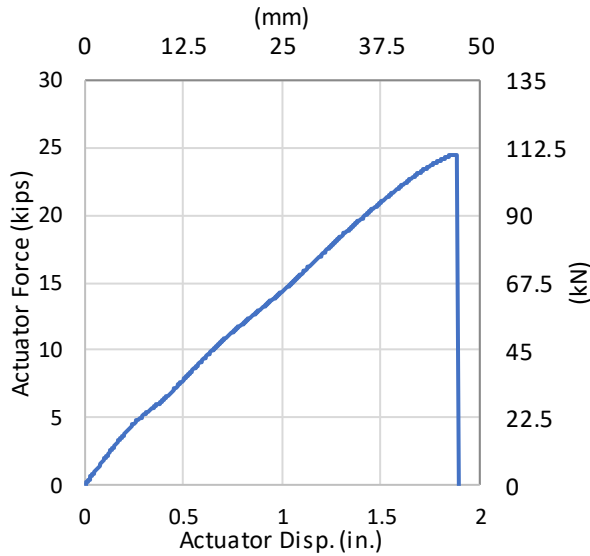


Figure 3.30. PT15 force vs actuator displacement

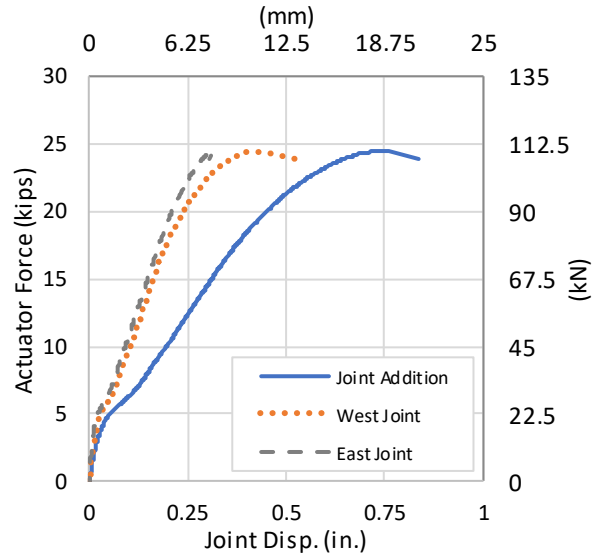


Figure 3.31. PT15 force vs joint displacements



Figure 3.32. LVDT locations for PT15



Figure 3.33. Failure at coupling for PT15

Figure 3.34 shows the average axial and circumferential strains throughout the duration of the test. At the start of the test, the system was fully pressurized, and an increase in circumferential strain was observed. Once loading began, the circumferential strains began to decrease, while the axial strains increased. As the actuator applied tensile loading to the system, the pipe began to elongate, causing an increase in axial strains. Due to Poisson's effect, the circumferential strain decreased as the tensile load was applied. The average axial strain was used in a stress strain relationship seen in Figure 3.35. The representative modulus of elasticity estimated from data collected between 0 and 0.5% strain is 411 ksi (2837 MPa), shown by the



orange trendline. The representative modulus of elasticity estimated from all data collected (0 to 0.7% strain) is 400 ksi (2758 MPa), shown by the blue trendline.

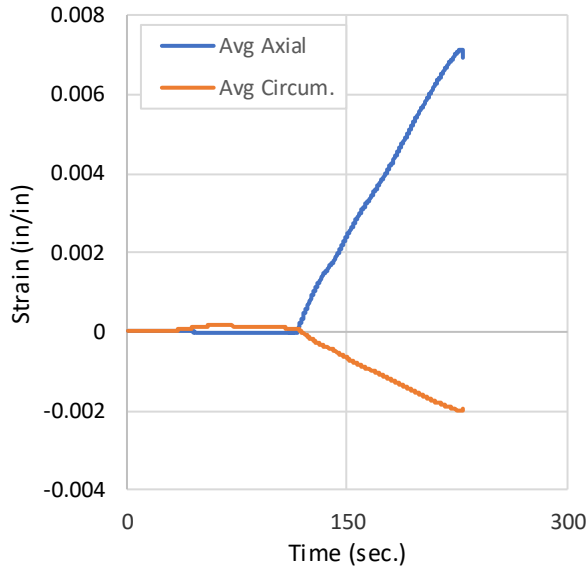


Figure 3.34. PT15 average axial and circumferential strains vs time

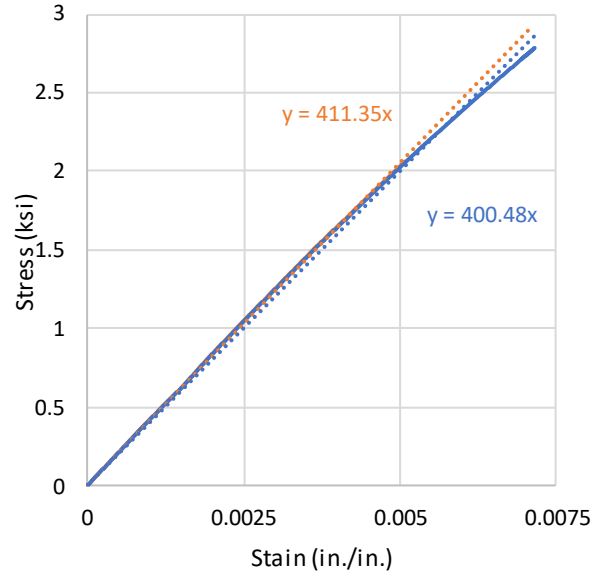


Figure 3.35. PT15 stress vs strain



### 3.6 Tension Test (PT16)- fPVC w/ Megalug Coupling and Stiffeners

Fusible PVC pipe with a Megalug coupling at the midpoint was used for this test. This test specimen also included pipe stiffener inserts installed in both pipe ends inside the Megalug coupling. The stiffeners were supplied by Underground Solutions and were manufactured by Cascade Waterworks. The pipe stiffeners were made for a pipe inner diameter of 6.13 inches and were slightly too large for the pipe being used. The installation of the stiffeners was modified by placing the stiffener in the pipe fully and then hammering the stiffener wedge in as far as it could reasonably go. The remaining portion of the wedge outside of the pipe was then cut off. Figure 3.36 shows a stiffener insert installed in one of the pipe segments before assembling the coupling joint. The internal water pressure was held at approximately 64 psi (440 kPa) during loading. Displacement was applied at a rate of 1.0 in./min. (25 mm/min.). Actuator displacement and force are direct measurements of the hydraulic piston and loadcell, respectively. Joint displacement was measured using two LVDTs on the crown of the specimen, as shown in Figure 3.37. One LVDT measured the joint displacement at the east segment of pipe and the other measured joint displacement at the west segment of pipe. The LVDTs were fixed to the pipe at approximately 4 in. (100 mm) on either side of the coupling to measure joint displacement.

Figure 3.38 shows the actuator force, internal pressure, and actuator displacement vs time. Figure 3.39 shows force relative to actuator displacement. The maximum force was 24.6 kips (109 kN) at an actuator displacement of 1.72 in. (43.7 mm). Figure 3.40 shows actuator force relative to joint displacement. At maximum force (just before failure), the west side joint displacement was 0.211 in (5.36 mm) and the east side was 0.306 in (7.77 mm). The total joint displacement was therefore 0.52 in. (13.1 mm). Failure occurred at the east side of the coupling. The pipe broke in multiple places at or near the location of the restraint wedges as seen in Figure 3.41.

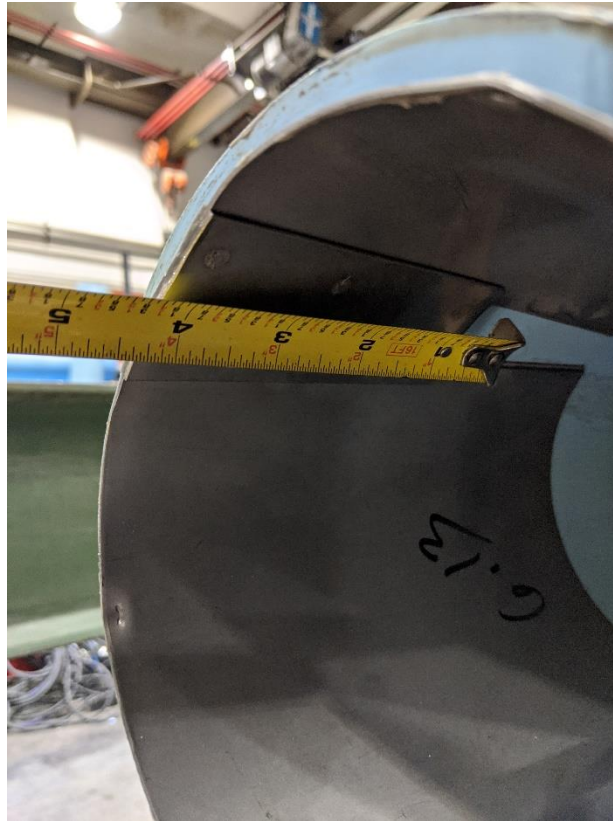


Figure 3.36. Typical installation of stiffener insert.

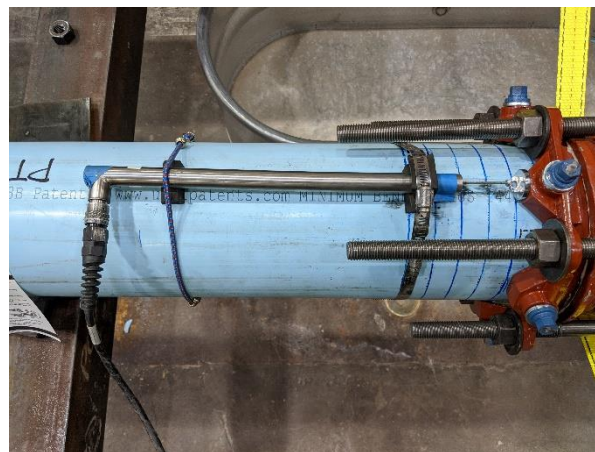


Figure 3.37. Typical LVDT attachment for PT16

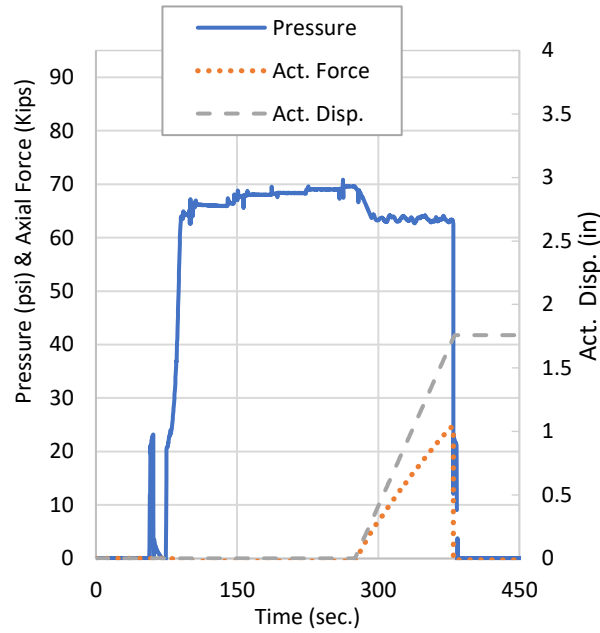


Figure 3.38. Specimen PT16 results for pressure, axial force, and actuator displacement vs time

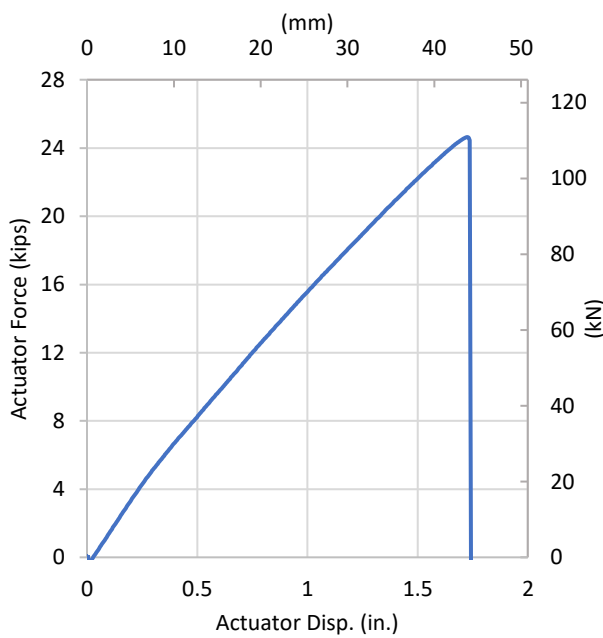


Figure 3.39. PT16 force vs actuator displacement

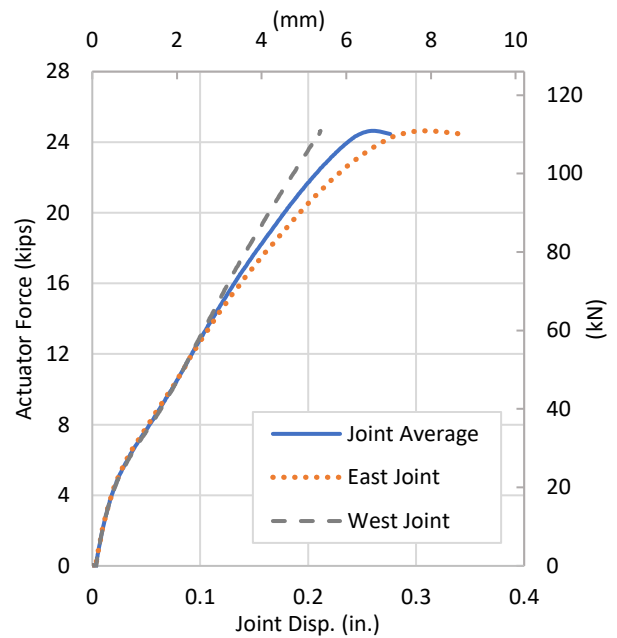


Figure 3.40. PT16 force vs joint displacements



(a) Fracture of the pipe



(c) Exposed pipe stiffener

Figure 3.41. PT16 failure at joint.

Figure 3.42 shows the average axial and circumferential strains throughout the duration of the test. At the start of the test, the system was fully pressurized resulting in an increase in circumferential strain. Once loading began, the circumferential strains began to decrease, while the axial strains increased. A stress-strain curve based on the average axial strain and the stress calculated from actuator force and typical pipe dimensions is shown in Figure 3.43. The modulus of elasticity calculated between 0 and 0.5% strain is 448.4 ksi (3092 MPa).

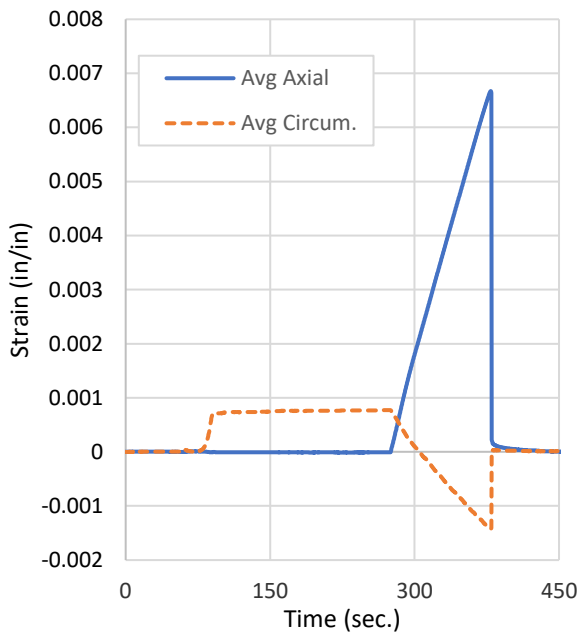


Figure 3.42. PT16 average axial and circumferential strains vs time

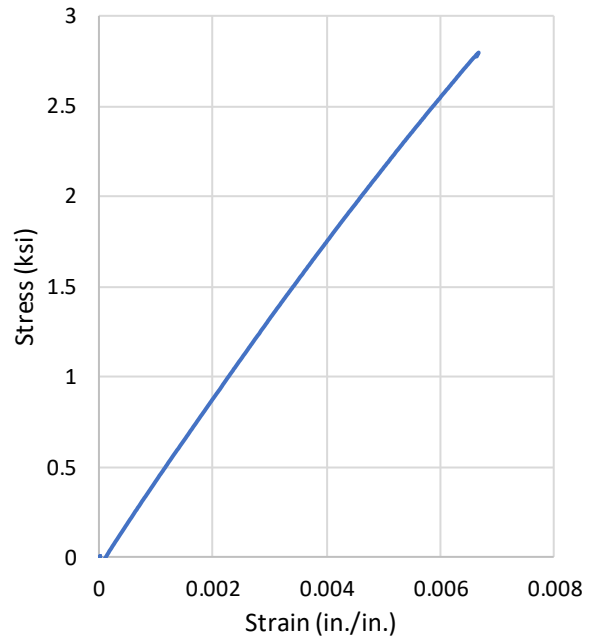


Figure 3.43. PT16 stress vs strain



### 3.7 Tension Test (PT34) – fPVC w/ Lokx Coupling

Fusible PVC pipes with a Lokx coupling at the midpoint was used for this test. Figure 3.45 shows the relationship of actuator force, internal pressure, and actuator displacement relative to time. Actuator displacement and force are direct measurements of the hydraulic piston and loadcell, respectively. Displacement was applied at a rate of 1.0 in./min. (25 mm/min.), and the force feedback of the load cell was recorded. Figure 3.46 shows that the maximum force recorded in the load cell was 46.4 kips (206.4 kN) at an actuator displacement of 3.66 in. (93 mm). A constant internal water pressure of  $67 \pm 3$  psi ( $462 \pm 20$  kPa) was applied throughout the test. Figure 3.47 shows the actuator force relative to joint displacement. Joint displacement was measured using four string potentiometers located on the north and south spring lines of the specimen, as well as the crown and invert, as shown in Figure 3.44. The north and south string pots were fixed to the pipe at 6 in (152 mm) on either side of the coupling to measure displacements along a 6 in (152 mm) initial gauge length. The string pot on the north spring line measured the relative displacement between the west segment and the joint, while the string pot on the south spring line measured the relative displacement between the east segment and the joint. The north-west string pot measured a joint displacement of 0.49 in (12 mm) and the south-east string pot measured a joint displacement of 0.44 in (11 mm). The crown and invert string pots measured the relative joint displacement across the entire joint, with an average of 1.11 in (28 mm) just before failure. Failure occurred just east side of the Lokx coupling, fracturing at the contact point between the pipe and the coupling, shown in Figure 3.48.



Figure 3.44. Sting pot attachment for PT34

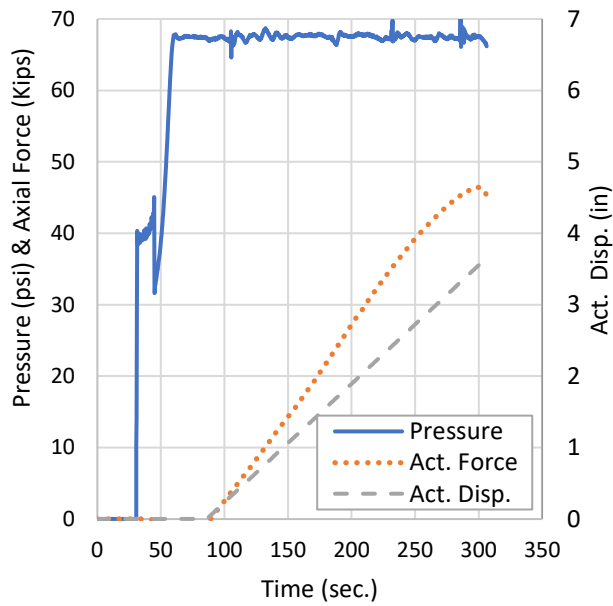


Figure 3.45. PT34 – Pressure, Act. Disp., and Act. Force vs. Time

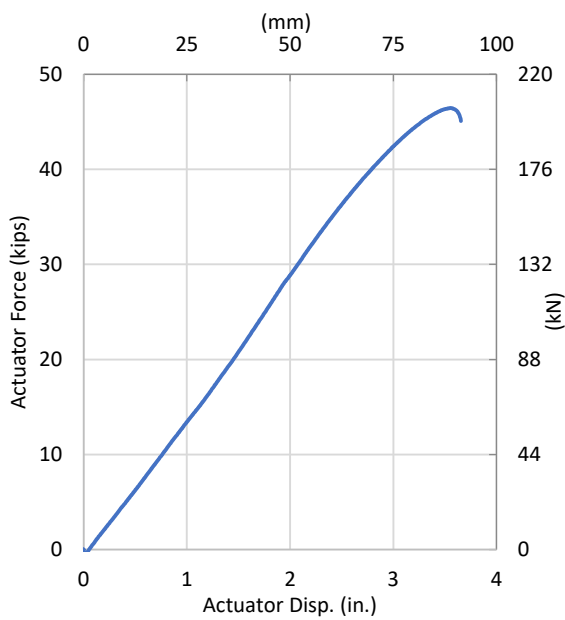


Figure 3.46. PT34 force vs actuator displacement

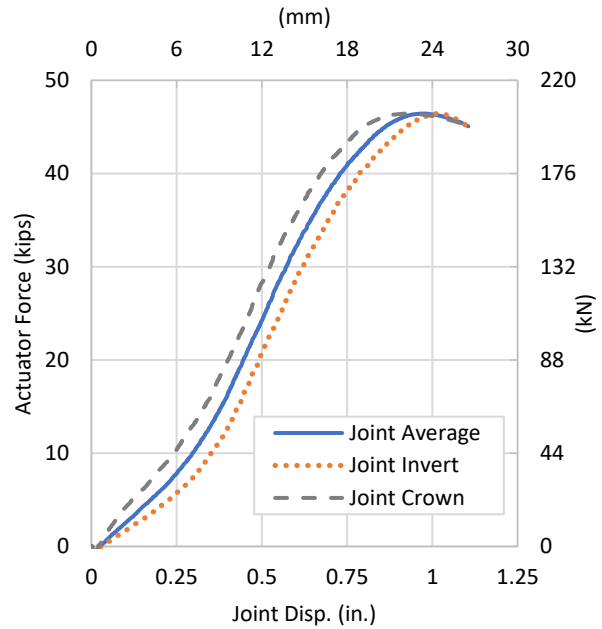
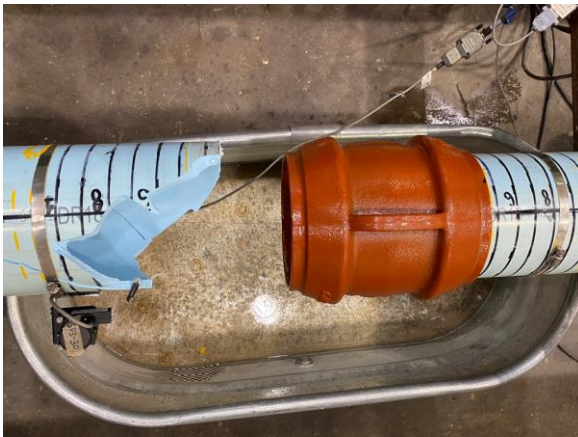
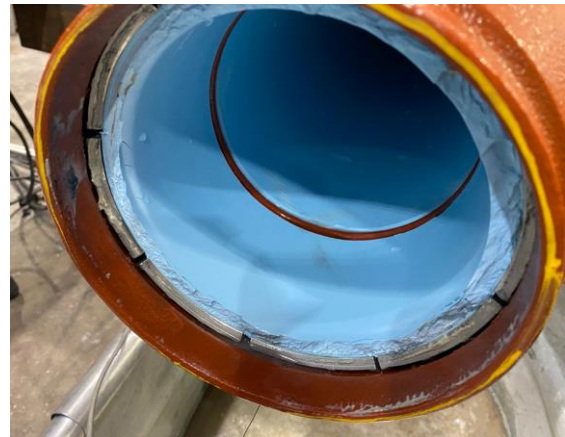


Figure 3.47. PT34 force vs joint displacements



(a) Fracture of pipe east of coupling



(b) Interior view of pipe fracture

Figure 3.48. PT34 failure at joint.

Figure 3.49 shows the average axial and circumferential strains for the duration of the test. At the start of the test, the system was fully pressurized resulting in an increase in circumferential strain. Once loading began, the circumferential strains began to decrease, while the axial strains increased. A stress-strain curve based on the average axial strain and the stress calculated from actuator force and typical pipe dimensions is shown in Figure 3.50. The modulus of elasticity calculated between 0 and 0.5% strain is 419.6 ksi (2893 MPa).

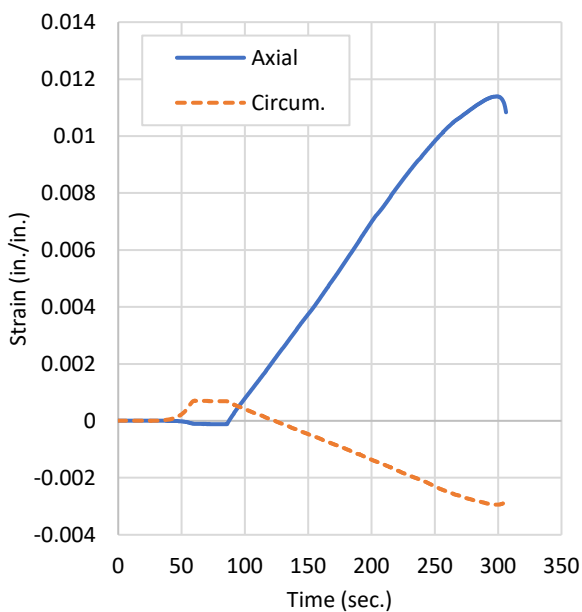


Figure 3.49. PT34 average axial and circumferential strains vs time

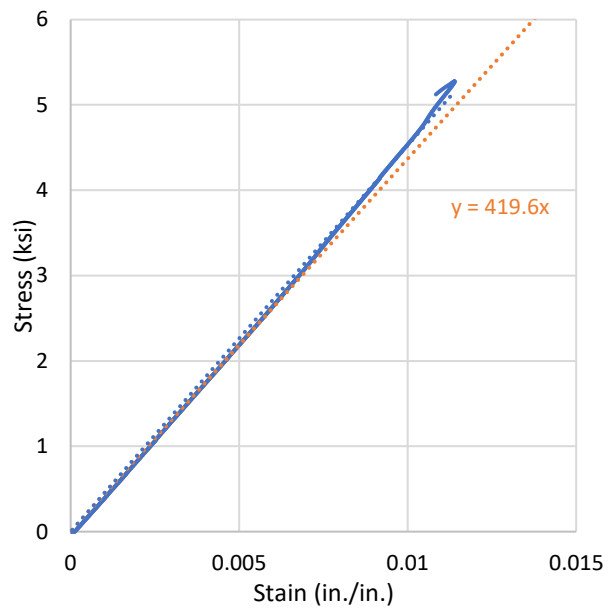


Figure 3.50. PT34 stress vs strain



### 3.8 Tension Test Overview

The following figures provide comparisons of tension tests performed in this testing program. Table 3.1 shows a summary of the axial tests performed. Table 3.2 shows a summary of the different apparent moduli of elasticities recorded for each tension test.

Table 3.1. Summary of Tension Test Results

Test ID	Pipe-Connection	Max Axial Force		Max Axial Strain		Max Act. Disp.		Joint/connection Disp.	
		kips	(kN)	in/in	%	in	(mm)	in	(mm)
PT07	Fused PVC - Fused	52.5	(234)	0.0296	2.96	5.02	(128)	0.25	(6.5)
PT14	Fusible PVC - Fused	53.1	(236)	0.0254	2.54	4.46	(113)	0.17	(4)
PT04	Fusible PVC - Megalug	29.6	(133)	0.0091	0.91	2.40	(61)	0.90	(22)
PT08	Fusible PVC - Megalug	19.7	(89)	0.0037	0.37	1.74	(44)	0.91	(23)
PT15	Fusible PVC - Megalug	24.5	(109)	0.0065	0.65	1.89	(48)	0.84	(21)
PT16	Fusible PVC - Megalug with stiffeners	24.6	(109)	0.0067	0.67	1.72	(44)	0.52	(13.1)
PT34	Fusible PVC – Lokx Coupling	46.4	(206)	0.0114	1.14	3.66	(93)	1.11	(26)

Table 3.2. Summary of Apparent Moduli of Elasticities for Tension Tests

Test ID	Pipe-Connection	E, 0.5% Strain		E, 1.0% Strain		E, 1.5% Strain	
		ksi	(MPa)	ksi	(MPa)	ksi	(MPa)
PT07	Fusible PVC - Fused	406.0	(2800)	391.4	(2700)	368.9	(2543)
PT14	Fusible PVC - Fused	419.6	(2893)	397.1	(2738)	372.8	(2570)
<b>Fused Average</b>		<b>437.5</b>	<b>(3017)</b>	<b>411.5</b>	<b>(2838)</b>	<b>370.8</b>	<b>(2407)</b>
PT04	Fusible PVC - Megalug	401.5	(2768)	383.4	(2643)	-	-
PT08	Fusible PVC - Megalug	578.2	(3987)	-	-	-	-
PT15	Fusible PVC - Megalug	411.4	(2837)	400.5	(2761)	-	-
PT16	Fusible PVC – Megalug with stiffeners	448.4	(3092)	-	-	-	-
<b>Megalug Average</b>		<b>459.9</b>	<b>(3171)</b>	<b>392.0</b>	<b>(2702)</b>	-	-
PT34	Fusible PVC – Lokx	419.6	(2893)	-	-	-	-
<b>Lokx Average</b>		<b>419.6</b>	<b>(2893)</b>	-	-	-	-



Figure 3.51 shows the actuator force relative to the actuator displacement for each fused tension test. PT07 was completed under the same internal water pressure conditions and yielded a maximum actuator force of 52.5 kips (234 kN). PT14 tested the same specimen with a water pressure of approximately 7.5 psi (52 kPa). This test also yielded a maximum actuator force of 53.1 kips (236 kN), concluding that internal water pressure has a negligible effect on the overall strength of the specimen. However, higher water pressure resulted in a larger overall displacement.

Figure 3.52 shows the joint displacement (displacement across the fuse along 6 in. (150 mm) gage length, shown in Figure 3.10) for each of the fused tests. PT07 at ~65 psi (448 kPa) yielded a displacement of 0.26 in. (7 mm) while PT14 (at approximately 7 psi (48 kPa) pressure) yielded a displacement of 0.19 in (5 mm). This accounts for some of the difference observed in the overall actuator displacement, but lower water pressure may have also played a part. When lower water pressure is applied to the specimen, the end restraints holding the pipe are less engaged than they would be at higher pressure states (due to the increase in circumferential expansion at high pressure). As a result, more slippage in the end restraints occurred, contributing to the discrepancy in actuator force shown in Figure 3.51.

Figure 3.53 and Figure 3.54 compare the axial and circumferential strains from PT07 and PT14, respectively. The circumferential strain difference between PT07 and PT14 is interesting because they

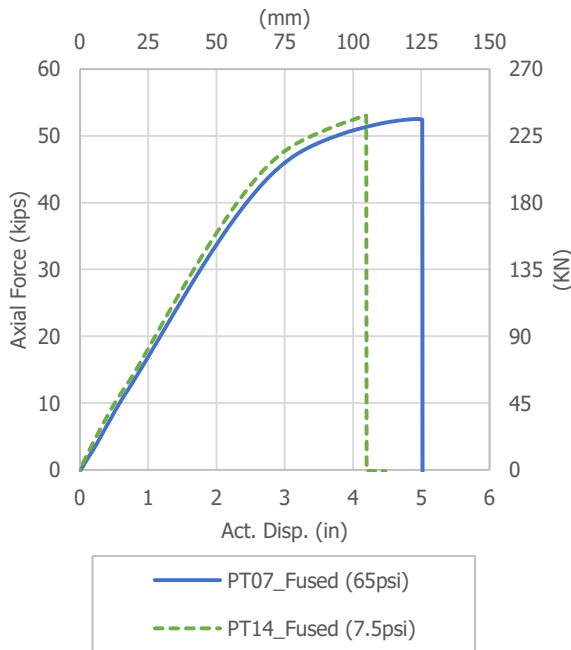


Figure 3.51. Fused pipe axial force vs actuator displacement

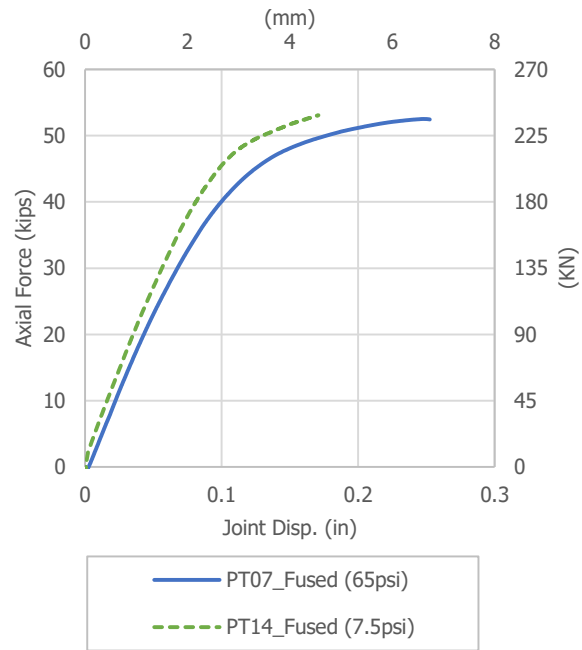


Figure 3.52. Fused pipe axial force vs joint displacement

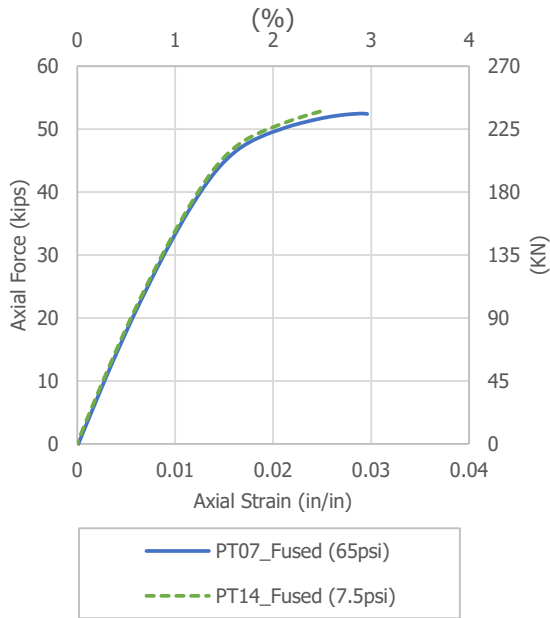


Figure 3.53. Fused pipe axial force vs axial strain

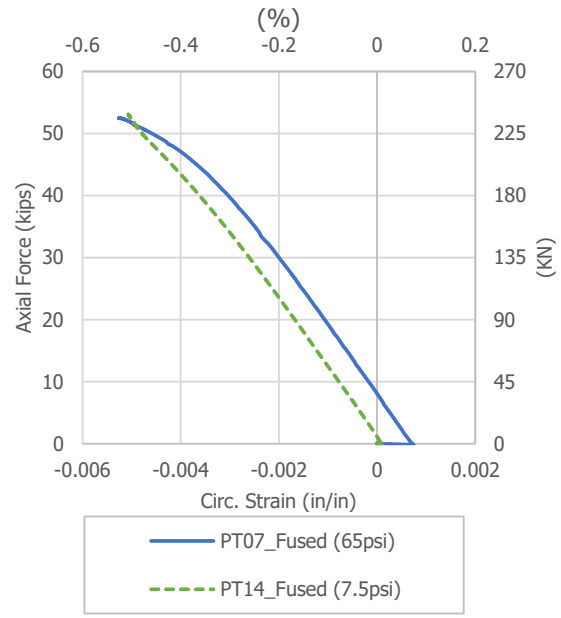


Figure 3.54. Fused pipe axial force vs circumferential strain

result in different initial strain conditions (due to pressurization differences) but ultimately fail at the same circumferential strain.

Figure 3.55 shows the actuator force relative to the actuator displacement for each Megalug coupling tension test. PT04 and PT08 were both tested under the same internal water pressure of ~65 psi (448 kPa). However, PT04 yielded a maximum force of 30 kips (133 kN), which was 10 kips (45 kN) more than the maximum force recorded from PT08 of 20 kips (89 kN). The total actuator displacements recorded for PT04 and PT08 were 2.4 in (61 mm), and 1.74 in (44 mm), respectively. PT15 tested the same specimen with a water pressure of approximately 5 psi (35 kPa). This test yielded a maximum actuator force of 24.5 kips (109 kN) and a maximum actuator displacement of 1.89 in (48 mm).

Figure 3.56 shows the joint displacement for each of the Mega-coupling tests. Each test resulted in approximately the same joint displacement, independent of the differing failure loads. The variation in total actuator displacement can be attributed to inconsistent material properties between the specimens. Water pressure did not have a visible effect on the joint displacement of the specimen.

PT08 yielded the lowest ultimate strength but recorded a marginally large representative modulus of elasticity. Figure 3.57 illustrates that the more load a specimen took to reach a given strain, the earlier the specimen failed. Similar to the fusible tests, the specimen with the largest representative modulus of elasticity resulted in the lowest overall strength. Figure 3.58 shows the circumferential strain for each of



the Megalug coupling tests. As seen in the fusible data, the circumferential strain had an initial difference due to variations in applied water pressure. However, this difference remained constant throughout the duration of the tests, unlike in the fused data.

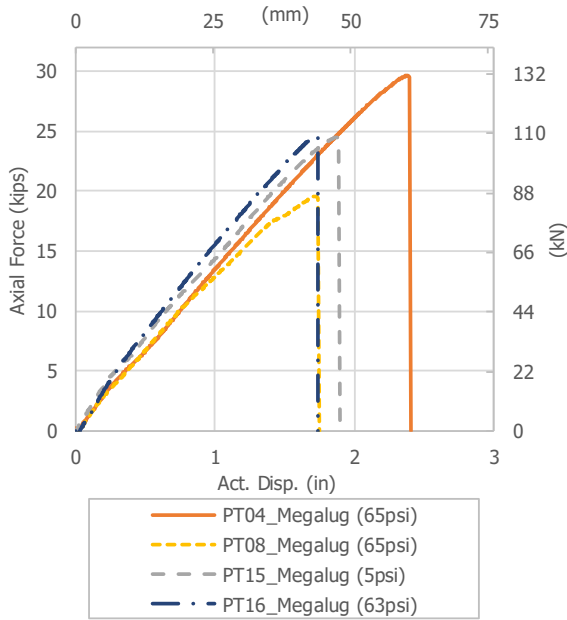


Figure 3.55. Megalug coupling axial force vs actuator displacement

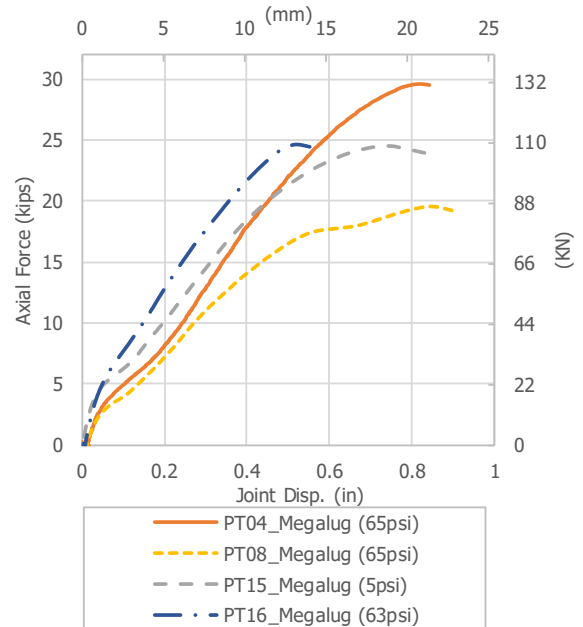


Figure 3.56. Megalug coupling axial force vs joint displacement

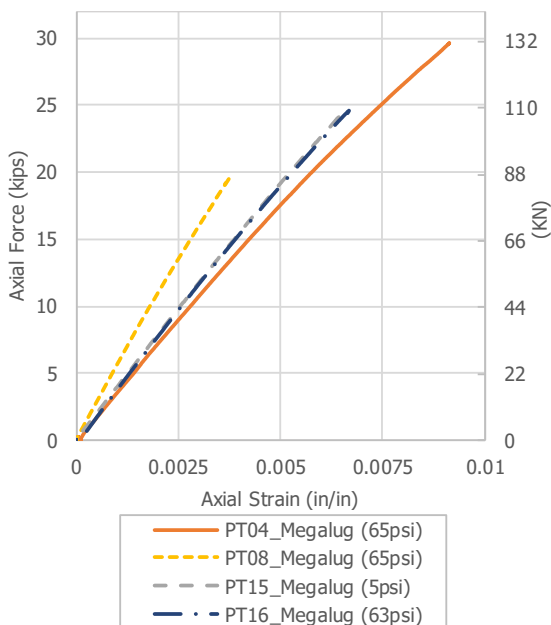


Figure 3.57. Megalug coupling axial force vs axial strain

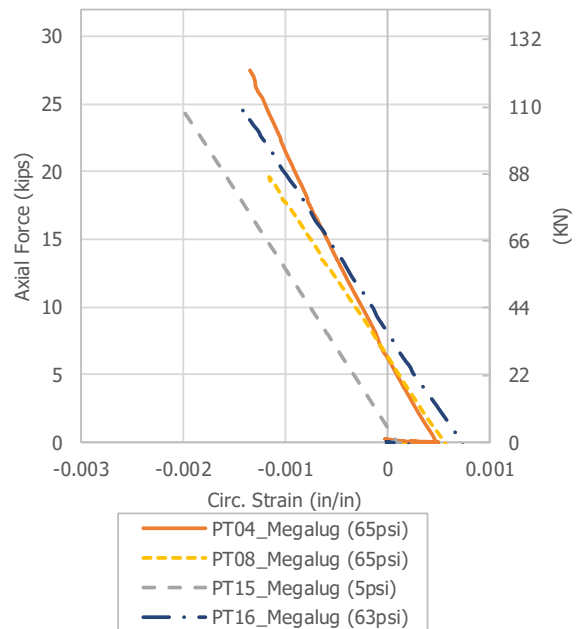


Figure 3.58. Megalug coupling axial force vs circumferential strain



Figure 3.59 shows the relationship between all tension tests performed on fusible PVC. Overall, the fused connection reaches the highest axial load and displacement. The Lokx connection exhibits notable performance, as it falls between results on the fused connection tests and the tests with Megalug connection.

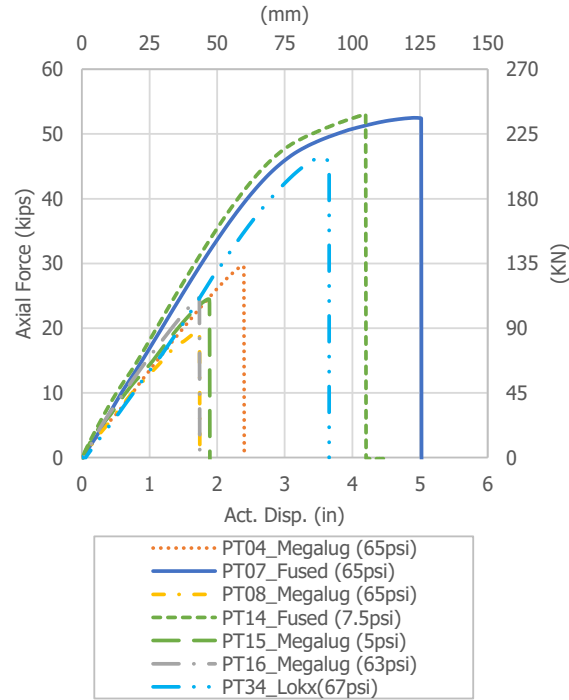


Figure 3.59. Axial Force vs. Act. Disp. for all fusible PVC tension tests



#### 4. Axial Compression Test Results

This section reports on two compression tests performed on fusible PVC pipe with a field installation fuse and Megalug coupling at the center of the specimen. The compression tests were setup similarly to the tension tests, shown in Figure 4.1. The setup varied from the previously reported tension tests in the following ways: (1) Lateral supports were provided to limit out-of-plane (global) buckling of the specimen; (2) End restraints were positioned opposite of the tension tests (as shown in Figure 4.2) to engage the necessary loading direction of Megalug end restraints; (3) The specimen was approximately 12 in. (300 mm) longer to reduce the buckling length of the threaded rods while the stroke of the piston, of length 11.2 in. (284 mm), was fully retracted and (4) Positive values are shown for compressive forces and displacements throughout this section of the report.

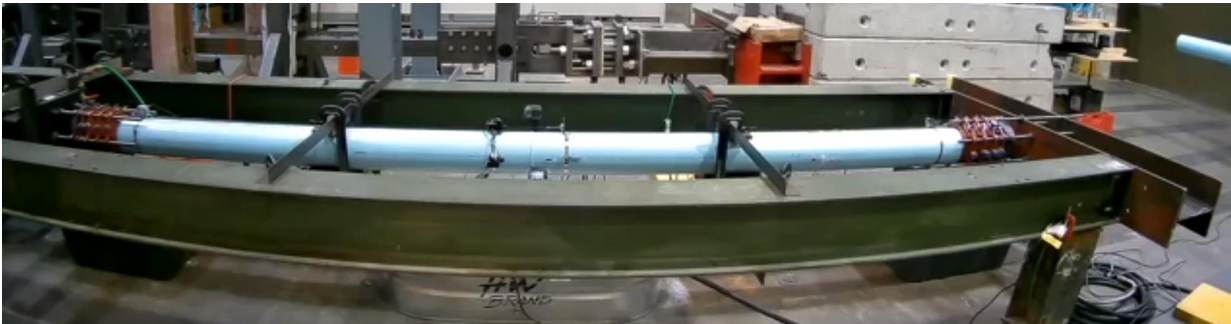


Figure 4.1. Compression test setup



Figure 4.2. Megalug end restraint orientation for compression



#### 4.1 Compression Test (PC10)- fPVC w/ Megalug Coupling

Fusible PVC pipe with a Megalug coupling restraint was used for this test. Figure 4.3 shows the relationship of actuator force, internal pressure, and actuator displacement versus time. Actuator force and displacement are direct measurements of the hydraulic load cell and piston, respectively. Displacement was applied at a rate of 1.0 in./min. (25 mm/min.), and the force feedback of the load cell was recorded. Figure 4.4 shows that the maximum force recorded in the load cell was 47.4 kips (211 kN) at an actuator displacement of 4.7 in. (119 mm). Pressure was adjusted throughout the test to account for pressure build up caused from decreasing volume. Prior to failure, pressure ranged from about 60 psi to 75 psi, with an average pressure of about 65 psi (448 kPa). Figure 4.5 shows the actuator force vs the joint displacement. Joint displacement was measured using two LVDTs located on both ends of the coupling, shown in Figure 4.6. The joint displacement reached an average of about 1.84 in (27 mm) just before failure. Each of the LVDTs measured relative joint displacement for each side of the Megalug coupling, which were then added together to get the total joint displacement. Failure for this test occurred due to a localized buckle on the west side of the specimen, shown in Figure 4.7.

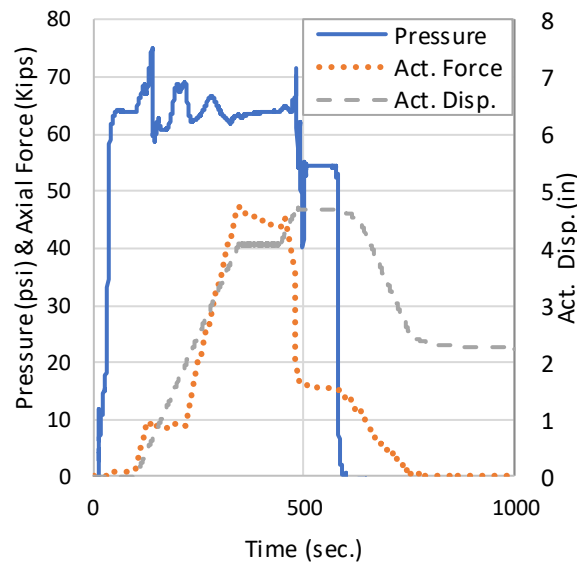


Figure 4.3. Specimen PC10 results for pressure, axial force, and actuator displacement vs time

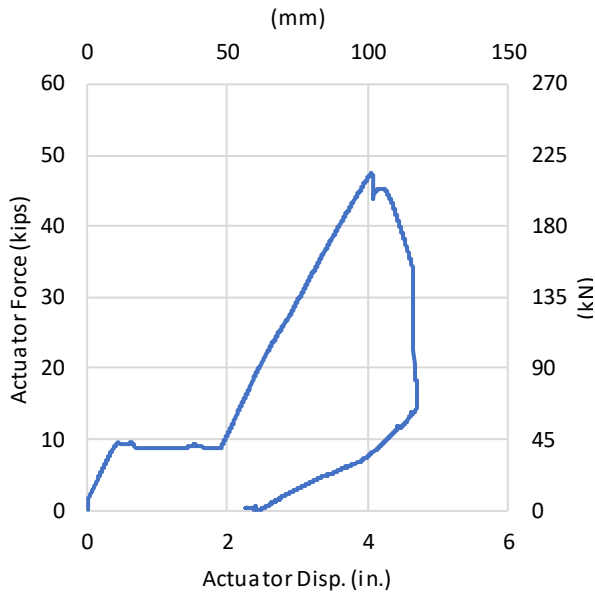


Figure 4.4. PC10 force vs actuator displacement

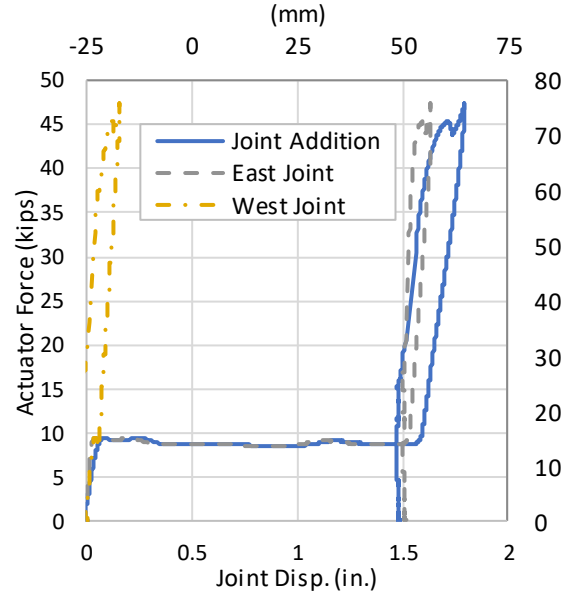


Figure 4.5. PC10 force vs joint displacements



Figure 4.6. LVDT locations for PC10

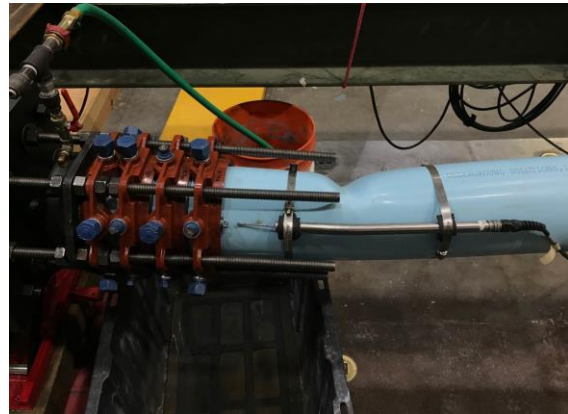


Figure 4.7. Failure at west end for PC10

Figure 4.8 shows the axial and circumferential strains for the duration of the test. These strains are not as consistent as seen in PT07 due to bending of the pipe during compression. Figure 4.9 shows the average axial and circumferential strains. For this data, compressive displacements were considered to be negative strain, while circumferential expansion was considered positive. Due to Poisson's effect, as the pipe was compressed axially (negative axial strain), the circumferential strain increased proportionally. The average maximum axial strain was measured at about 1.3% prior to failure. The average axial strains were used to develop the stress strain relationship shown in Figure 4.10. The representative modulus of elasticity estimated from data collected between 0 and 0.5% strain is 465.6 ksi (3210 MPa), shown by the orange



trendline. The representative modulus of elasticity estimated from data collected between 0 and 1.0% strain is 444.1 ksi (3041 MPa), shown by the blue trendline.

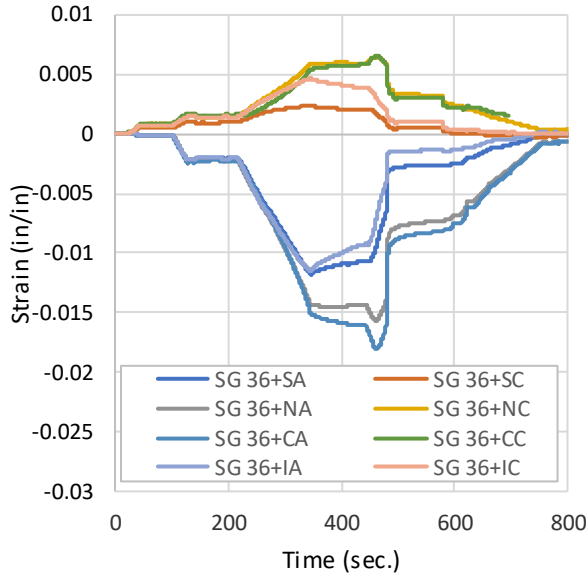


Figure 4.8. PC10 axial and circumferential strains vs time

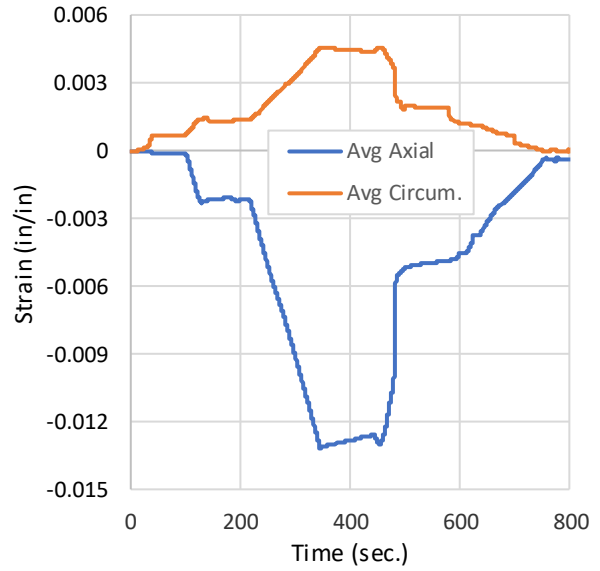


Figure 4.9. PC10 average axial and circumferential strains vs time

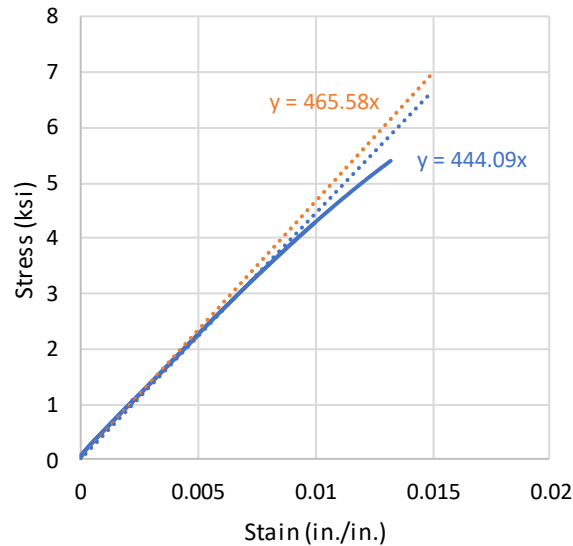


Figure 4.10. PC10 stress vs strain



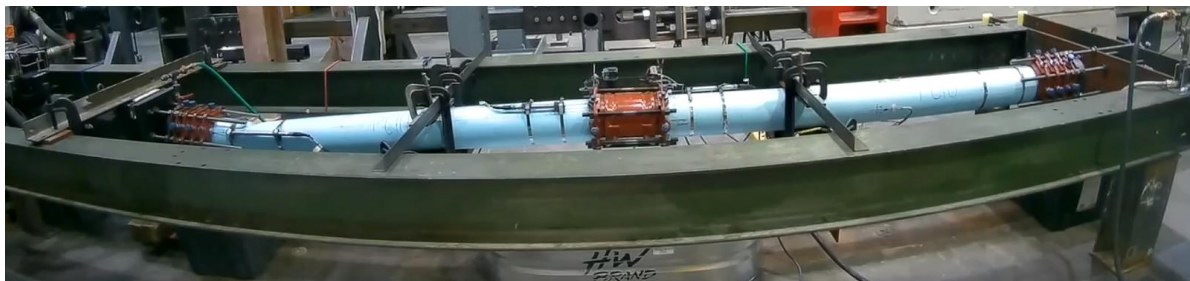
(a) Start of loading



(b) Progression loading



(c) Maximum loading



(d) Unloaded

Figure 4.11. Compression test progression



## 4.2 Compression Test (PC13)- fPVC w/ Fused Connection

Fusible PVC pipe with a fused connection was used for this test. Figure 4.12 shows the relationship among actuator force, internal pressure, and actuator displacement. Actuator forces and displacements are direct measurements of the hydraulic load cell and piston, respectively. Displacement was applied at a rate of 1.0 in./min. (25 mm/min.), and the force feedback of the load cell was recorded. Figure 4.13 shows that the maximum force recorded in the load cell was 41.4 kips (184 kN) at an actuator displacement of 2.9 in. (74 mm). Pressure was adjusted throughout the duration of the test to account for pressure build up caused from decreasing volume. Prior to failure, pressure ranged from about 60 psi (413.6 kPa) to 67 psi (461.9 kPa), with an average pressure of about 65 psi (448 kPa). Figure 4.14 shows the actuator force vs the joint displacement. Joint displacement was measured using three string potentiometers located on the crown and the north and south spring line. During the test, the string pot located on the crown of the specimen slipped and therefore was not included with the other data, shown in Figure 4.15. Each of the spring line string pots recorded only about 0.1 in (2.5 mm). Instabilities in the testing system caused termination of this test prior to failure. Slight local buckling occurred on the west end of the specimen, but no ultimate failure was reached.

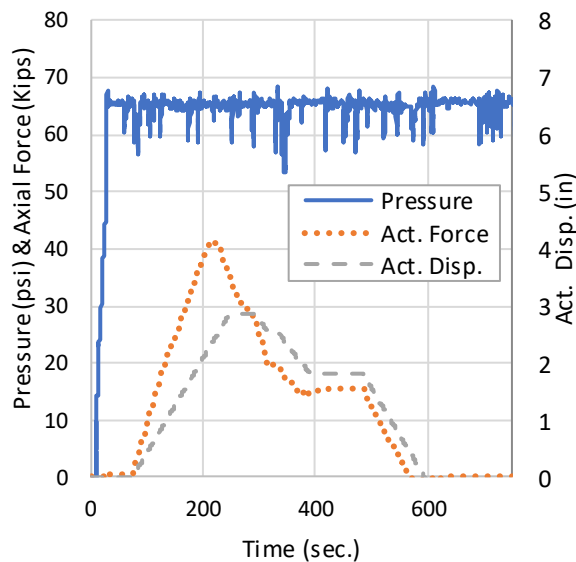


Figure 4.12. Specimen PC13 results for pressure, axial force, and actuator displacement vs time

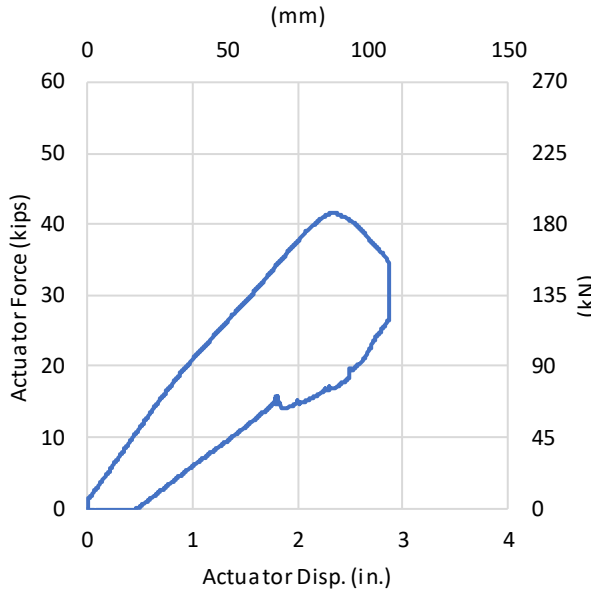


Figure 4.13. PC13 Force vs actuator displacement

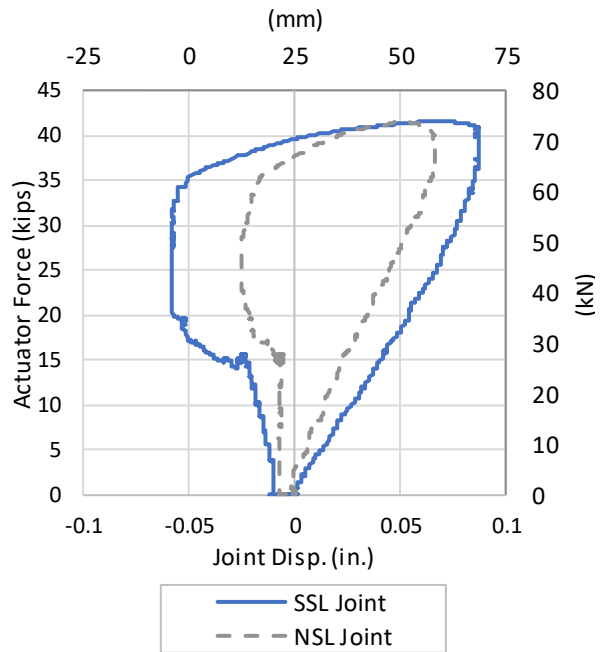


Figure 4.14. PC13 force vs joint displacements



Figure 4.15. String potentiometer locations for PC13

Figure 4.16 shows the axial and circumferential strains for the duration of the test. Figure 4.17 shows the average axial and circumferential strains for the duration of the test. For this data, axial compressive displacements along the barrel were considered negative while circumferential expansion was considered positive. Due to Poisson's effect, as the pipe was compressed axially (negative axial strain), the



circumferential strain increased proportionally. The maximum axial strain (average) was measured at about 1.1% prior to stoppage of the test. The average axial strains were used to develop the stress strain relationship shown in Figure 4.18. The representative modulus of elasticity estimated from data collected between 0 and 0.5% strain is 450.7 ksi (3107 MPa), shown by the orange trendline. The representative modulus of elasticity estimated from data collected between 0 and 1.0% strain is 432.1 ksi (2980 MPa), shown by the blue trendline.

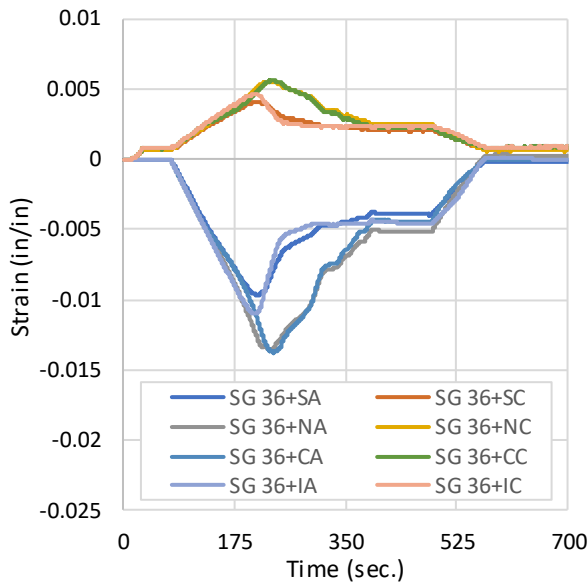


Figure 4.16. PC13 axial and circumferential strains vs time

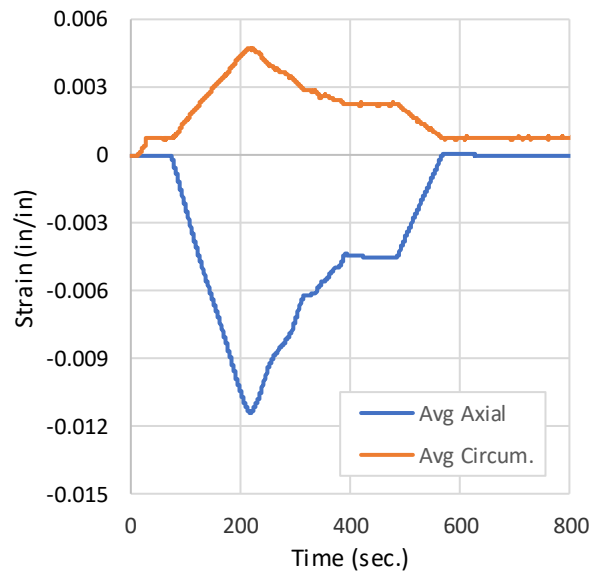


Figure 4.17. PC13 average axial and circumferential strains vs time

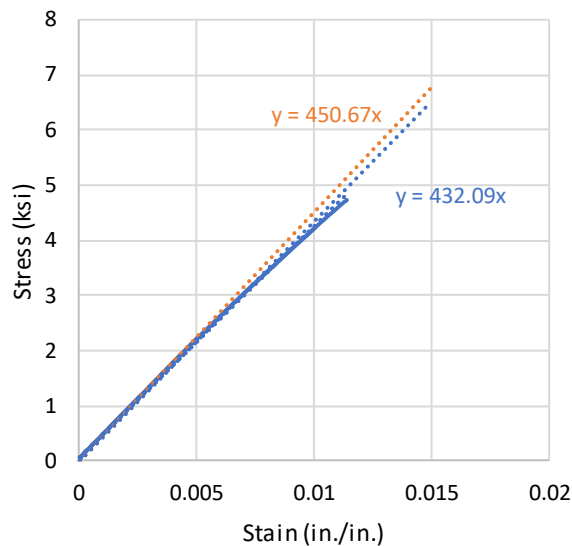


Figure 4.18. PC13 Stress vs strain



(a) Start of loading



(b) Progression loading



(c) Maximum loading



(d) Unloaded

Figure 4.19. Compression test (PC13-Fuse) progression



### 4.3 Compression Test Summary

The following figures provide comparisons of compression tests performed. Table 4.1 shows a summary of the axial compressive tests performed. Table 4.2 shows a summary of the different apparent moduli of elasticities recorded for each compression test.

Table 4.1. Summary of Compression Test Results

Test ID (CIEST)	Pipe-Connection	Max Axial Force		Max Axial Strain		Max Act. Disp.		Joint Disp.	
		kips	(kN)	in/in	%	in	(mm)	in	(mm)
PC10	Fusible PVC - Megalug	47.4.2	(206)	0.0131	1.31	4.7	(119)	1.84	(27)
PC13	Fusible PVC - Fused	41.4	(184)	0.0111	1.11	2.9	(74)	0.07	(2)

Table 4.2. Summary of Apparent Moduli of Elasticity for Compression Tests

Test ID	Pipe-Connection	E, 0.5% Strain		E, 1.0% Strain		E, 1.5% Strain	
		ksi	(MPa)	ksi	(MPa)	ksi	(MPa)
PC10	Fusible PVC - Megalug	465.6	(3210)	444.1	(3041)	-	-
PC13	Fusible PVC - Fused	450.7	(3107)	432.1	(2980)	-	-
<b>Compression Average</b>		<b>458.15</b>	<b>(3159)</b>	<b>438.1</b>	<b>(3010)</b>	-	-

Figure 4.20 shows the actuator force relative to the actuator displacement for each compression tension test. Both the Mega-coupling and the fused connection performed exceptionally well, reaching a maximum actuator force of 46.2 kips (206 kN) and 41.4 kips (184 kN), respectively. PC13 was stopped early due to a stability issue during testing, which prevented any conclusive determination of which of the tests performed better. Both tests were completed using approximately 65 psi (448 kPa) of water pressure, and no external leakage was observed in either test. For PC10, at a load of about 10 kips (45 kN), the east side of the joint lost grip between the pipe and the Megalug, resulting in rapid deformation with no load change. After about 1.5 in (31 mm) of displacement, the east end of the pipe engaged the west end of the pipe at the joint and loading continued. As a result of this slip, the total actuator displacement for PC10 yielded 4.7 in (119 mm), compared to 2.9 in (74 mm) observed in PC13.

Figure 4.21 shows the joint displacement for each of the compression tests. As previously stated, the joint displacement of the Mega-coupling was much larger than that of the fused connection due to the slipping of the pipe and the Megalug restraints. Ultimately, for the Megalug coupling, joint displacement reached a



maximum value of 1.84 in (27 mm), compared to the ultimate joint displacement of 0.07 in (2 mm) for the fused connection.

Both compression tests yielded similar measures for the modulus of elasticity. Figure 4.22 and Figure 4.23 compare the axial and circumferential strains, respectively. Both the axial and circumferential strains for the two compression tests were very similar.

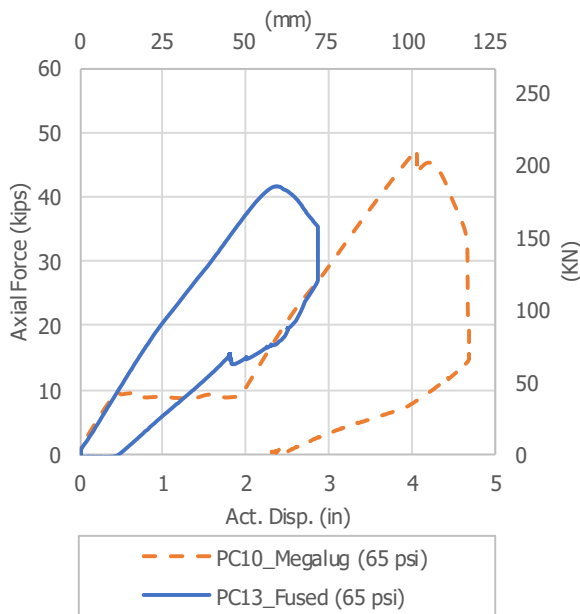


Figure 4.20. Axial force vs Act. Disp. for fPVC pipe with Megalug coupling & fused connection

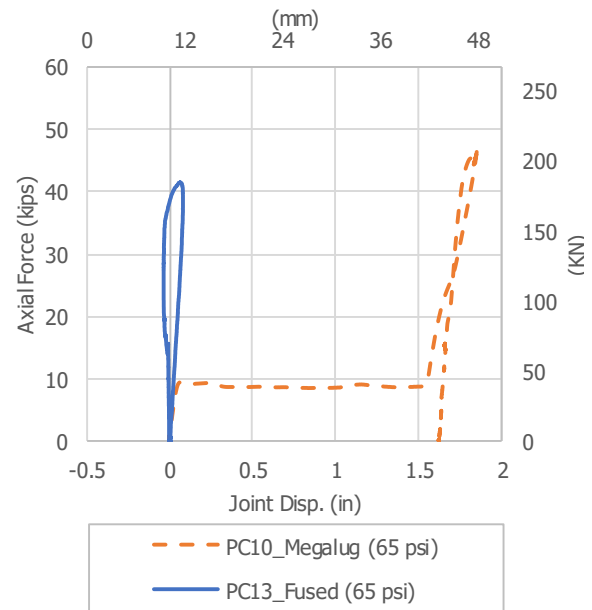


Figure 4.21. Axial force vs Joint Disp. comparison for fPVC pipe with coupling & fused connection

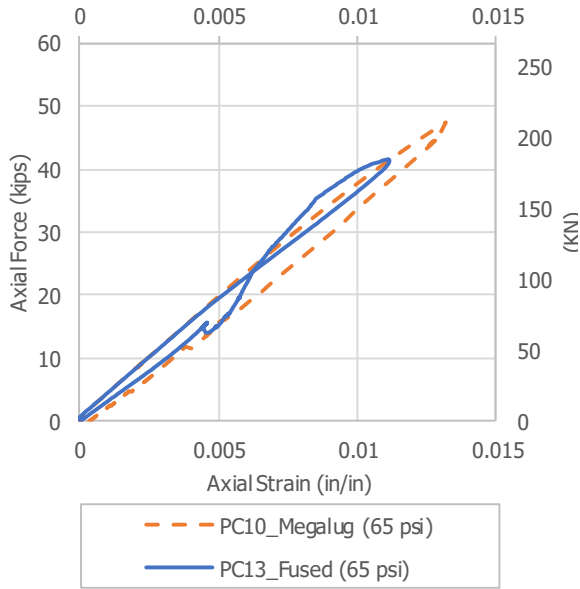


Figure 4.22. Axial compression force vs Axial strain for fusible pipe with Megalug & fused connection

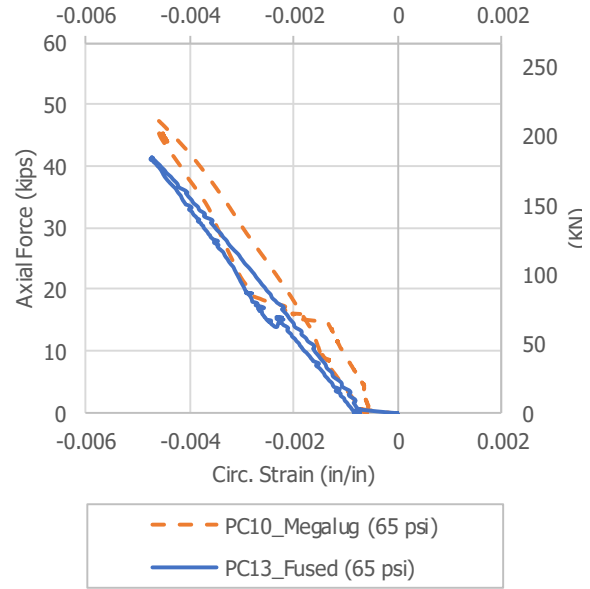


Figure 4.23. Axial compression force vs Circumferential strain for fusible pipe with Megalug & fused connection



## 5. Axial Tests Discussion and Conclusion

This section assesses the axial performance of thermoplastic pipe under external loading conditions associated with earthquakes and other sources of significant ground deformation. Axial tests on three types of pipe connections with the same type of pipe were performed. Tests included seven monotonic axial tension, two monotonic axial compression, and one axial cyclic test (discussed in appendix A). The axial cyclic test imposed increasingly larger cycles of tensile and compression loading prior to a monotonic axial pull to failure. Table 5.1 shows a summary of the axial tests performed while Table 5.2 shows a summary of the different apparent moduli of elasticities recorded for each test.

Both axial tension tests performed on Fusible PVC® with a fused connection achieved similar levels of axial force of 52.5–53.1 kips (234–236 kN). For these two tests, one was pressurized with 65 psi (448 kPa) of water pressure, while the other was only pressurized to approximately 5 psi (35 kPa) of water pressure. This concludes that water pressure has an insignificant effect of the ultimate strength of the pipe and the fused connection.

Three axial tension tests were also performed on the Megalug coupling. Unlike the fused connection, each test performed did not yield a consistent ultimate strength. Two of the three tests were conducted using a water pressure of 65 psi (448 kPa). PT04 resulted in an ultimate strength of 30 kips (133 kN) while PT08 only yielded 20 kips (89 kN). Differences in actuator and joint displacement are also found to be inconsistent between each test. Similar to the fused connections, these differences can be attributed to a number of different variables, including changes in material properties between the pipe or weather of the pipe. When water pressure was reduced to 5 psi (35 kPa), for test PT15, the ultimate strength of the pipe was 24.5 kips (109 kN). Because there is not a clear understanding of how the pipe should perform at higher pressures, it is difficult to draw conclusions on how lower water pressures might affect the system. To answer these questions, more tension tests on both fused and Mega-coupling connections are required to provide sufficient data to draw better conclusions.

Lastly, one axial tension test (PT34) was performed with a Lokx coupling, which performed better than the Mega-coupling, reaching a maximum force of 46.4 kips (206 kN) and 3.66 in (93 mm) of axial deformation. Since only one test was performed with this coupling, not many conclusions can be drawn from the data.

For the compression tests, both the fused connection and the Mega-coupling performed exceptionally well. Both compression tests achieved similar levels of axial force of 41.4–47.4 kips (184–212 kN). The limiting factor for both tests was the inability to Modifications to the testing frame will need to be made to push these specimens to their ultimate compressive loads.



Table 5.1. Summary of All Axial Test Results

Test #	Pipe-Connection	Max Axial Force		Max Axial Strain		Max Act. Disp.		Joint Disp.	
		kips	(kN)	in/in	%	in	(mm)	in	(mm)
PT07	Fused PVC - Fused	52.5	(234)	0.0296	2.96	5.02	(128)	0.505	(13)
PT14	Fusible PVC - Fused	53.1	(236)	0.0254	2.54	4.46	(113)	0.171	(4)
PT04	Fusible PVC - Megalug	30.0	(133)	0.0091	0.91	2.40	(61)	0.870	(22)
PT08	Fusible PVC - Megalug	20.0	(89)	0.0037	0.37	1.74	(44)	0.908	(23)
PT15	Fusible PVC - Megalug	24.5	(109)	0.0065	0.65	1.89	(48)	0.839	(21)
PT16	Fusible PVC with stiffeners - Megalug	24.6	(109)	0.0067	0.67	1.72	(44)	0.517	(13)
PT34	Fusible PVC – Lokx Coupling	46.4	(206)	0.01139	1.139	3.66	(93)	1.105	(26)
PC10	Fusible PVC - Megalug	46.2	(206)	0.0111	1.11	4.7	(119)	1.84	(27)
PC13	Fusible PVC - Fused	41.4	(184)	0.0131	1.31	2.9	(74)	0.07	(2)

Table 5.2. Summary of All Apparent Moduli of Elasticities

Test #	Pipe-Connection	E, 0.5% Strain		E, 1.0% Strain		E, 1.5% Strain	
		ksi	(MPa)	ksi	(MPa)	ksi	(MPa)
PT07	Fusible PVC - Fused	406.0	(2800)	391.4	(2700)	368.9	(2543)
PT14	Fusible PVC - Fused	419.6	(2893)	397.1	(2738)	372.8	(2570)
<b>Tension Fused Average</b>		<b>437.5</b>	<b>(3017)</b>	<b>411.5</b>	<b>(2838)</b>	<b>370.8</b>	<b>(2407)</b>
PT04	Fusible PVC - Megalug	401.5	(2768)	383.4	(2643)	-	-
PT08	Fusible PVC - Megalug	<b>578.2</b>	<b>(3987)</b>	-	-	-	-
PT15	Fusible PVC - Megalug	411.4	(2837)	400.5	(2761)	-	-
PT16	Fusible PVC with stiffeners - Megalug	448.4	(3092)	-	-	-	-
<b>Tension Megalug Average</b>		<b>463.7</b>	<b>(3197)</b>	<b>392.0</b>	<b>(2702)</b>	-	-
PT34	Fusible PVC – Lokx	419.6	(2893)	-	-	-	-
<b>Lokx Average</b>		<b>419.6</b>	<b>(2893)</b>	-	-	-	-
PC10	Fusible PVC - Megalug	465.6	(3210)	444.1	(3041)	-	-
PC13	Fusible PVC - Fused	450.7	(3107)	432.1	(2980)	-	-
<b>Compression Average</b>		<b>458.15</b>	<b>(3159)</b>	<b>438.1</b>	<b>(3010)</b>	-	-

The results demonstrate the available axial capacity of the Mega-coupling and fused connection. These values can be used in assessing a system’s expected performance when earthquake-induced ground



deformation occurs. While this testing program provides valuable results for assessing earthquake performance, additional assessment is recommended. Not all pressure classes and loading regimes were investigated for each joint type. Most tests were performed at a reasonably representative operating pressure. Note that variations may be possible based on internal pressure, specifically for Mega-coupling responses. Repeating tests to identify variability in the experimental results would be highly valuable for incorporation into seismic design assessments.



## 6. Four-point Bending Tests

This section reports on the test setup and results of three four-point bending tests. The intent of these tests is to apply lateral deformation to a pipeline system, simulating the conditions of significant transverse ground deformation. Specifically, the four-point bending test setup used for this study provides a constant moment across the center third of the specimen, simulating worst-case bending associated with buried conditions. The setup also aims to limit artificial and localized shear. By applying constant moment across the region of interest, bending strain can be accurately measured regardless of failure location within the region. These tests are designed to focus on the upper bound performance of a pipe system when subjected to lateral displacement and applied moments.

### 6.1 Bending Test Experimental Setup

An MTS 661.32 Universal Testing Machine with 1000-kip (4450-kN) compression capacity was adapted to conduct four-point bending tests on 15 ft (4.6 m) sections of nominal 6-in. (150-mm) diameter PVC pipes and joints. The large deflection capacity test setup is shown in Figure 6.1. The load is applied through downward displacement of the test frame crosshead. A spreader beam is employed to distribute force to two circumferentially oriented loading harnesses located at the middle third points. In general, it is advisable to apply vertical loads at least 3 pipe diameters (3D) from the central connection of interest for flexible pipes. For the 6 in. (150mm) diameter PVC tested, approximately 5 diameters or 30 in. (760 mm) on each side of the joint was specified. Resistance is provided by two loading saddles supporting the specimen near its ends. These saddles are positioned on columns attached to a stiff beam that transfers the force into the piston at the bottom of the test frame.

All load-points are unrestrained in the horizontal direction to limit the development of undesirable axial forces at large vertical displacements. As shown in Figure 6.2, high-capacity roller bearings, attached to the loading saddles, allow the specimen to displace laterally with minimal resistance/friction. The inner loading bearings are free to translate along the bottom of the spreader beam while the outer support bearings area allocated approximately 9 in. (230 mm) of lateral displacement on top of each support column. Restraining plates are fixed to either support column so that once either side reaches its maximum displacement, the boundary condition acts as a pinned connection and the test may continue uninterrupted. Testing of the 6-in. (150-mm) diameter PVC pipes suggests the frame can displace vertically approximately 35 in. (890 mm) before axial load is applied at the support points.

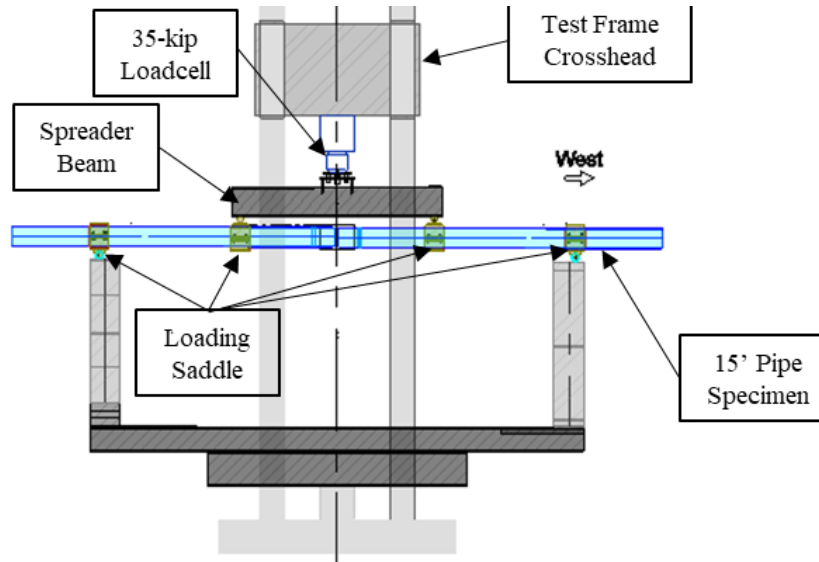


Figure 6.1. Test frame with 6-in. diameter PVC

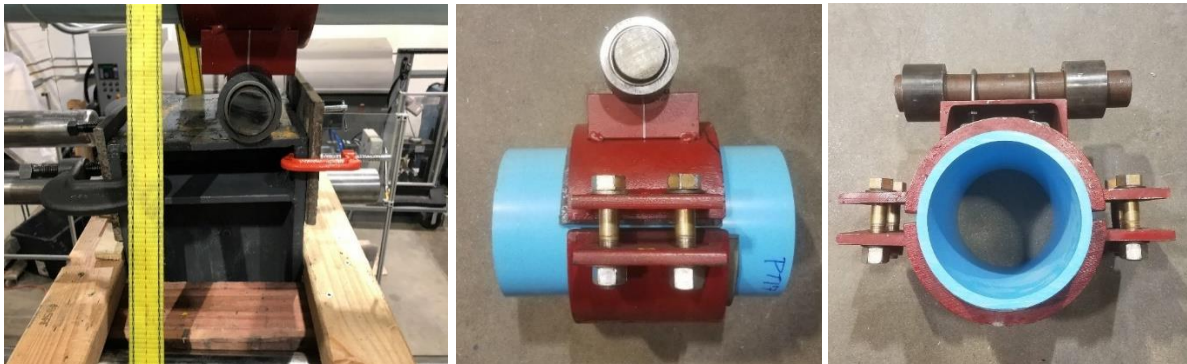


Figure 6.2. Pipe loading saddles with high-capacity bearings



### 6.1.1 Bending Test Instrumentation

A detailed list of instrumentation used in each test is identified in each test overview section. The primary measuring devices are variable string pots (VSP) for displacement and either biaxial or uniaxial strain gauges (SG) for strain. Each instrument uses a system of labeling beginning with either “VSP” or “SG” and are followed by a positive or negative number representing the distance (inches) from the centerline of the specimen. Positive numbers indicate the instrument is west of specimen centerline (CL), while negative numbers indicate the instrument is east of centerline. Strain gauges are placed at either the top (crown), bottom (invert), or on either the north or south sides (north or south springline). Table 6.1 contains the instrumentation naming conventions.

Table 6.1. Instrumentation Naming Convention

Instrument Name: <b>SG+20CA</b>	
Code	Description
SG	SG = Strain Gauge VSP = Vertical String Pot
+	+ = west of CL - = east of CL
20	Inches from CL
C	C = Crown I = Invert N = North Spring Line S = South Spring Line
A	A = Axial C = Circumferential

## 6.2 Experimental Measures of Pipeline System Response

To date, research focused on the characterization of jointed pipeline response to transverse loading has not reached a consensus on the parameters needed to quantify response. Previous work by Wham et al. (2017) reported global pipeline response as the relationship between applied force and lateral displacement at the loading points. They also used strains measured at the outer fiber vs. applied displacement to assess local response. While these parameters are useful to quantify the performance of the pipe system that was tested, advancements have been included in this report to quantify responses into measures that are independent of test frame attributes (i.e., location of load application, distance between load/support points) while also corresponding to the measure of ground deformation demands on pipeline systems that have been proposed by Davis et al. (2019) and correspond directly to developing seismic design guidelines.



The current state of practice does not consider the load (i.e. moment) capacity of a pipeline system in determining response to transverse loading. Therefore, the results from the global deflection of the system imposed by the movement of soil is of interest in quantifying system performance. As global demands of pipeline systems have been quantified as radius of curvature, the same measure can be employed to consider system capacity. As current joint mechanisms for continuous pipeline systems are designed to be stronger than the pipe segments they connect, the local response of interest is the bending strain achieved by the individual pipe segments. Therefore, to quantify the impact of globally imposed displacement demands on continuous pipelines, both the global deflection response in terms of curvature, and the local response, in terms of bending strain, are compared. The following sections outline the parameters used to quantify both the global and local response of a continuous pipeline system.

### **6.2.1 Crosshead Displacement**

Measurements of vertical displacement captured by VSP located at the bottom of the two inner loading saddles are averaged to represent the total imposed crosshead displacement. During imposed vertical displacement, the loading and support points move laterally inward (toward the specimen centerline), resulting in a slight misalignment of the VSPs. Given the small angle theorem, errors in vertical displacement are less than 1% of the physical displacement of the specimen and are thus assumed negligible (the ratio of vertical to horizontal displacement is on the order of 30 to 1).

### **6.2.2 Applied Moment**

The moment applied to the pipeline consists of a primary contribution and several secondary contributions. The primary applied load is imposed by the weight of the load frame crosshead moving downward relative to the test specimen and is applied at the location of the two inner loading saddles. Load due to crosshead displacement is calculated as two point loads equal to the difference between the load cell reading during the test and the initial reading of the load cell, which includes the weight of the loading beam.

Secondary contributions to the imposed moment within the middle third region of the specimen include: (1) the self-weight of pipe and any joint mechanism, (2) weight of two inner load saddles, and (3) the weight of water within the pipe. Specimen weights are calculated from reported manufacturer values while other non-specified components are weighed in the lab. Values are applied as either distributed loads or point loads as applicable. Moment contributions from specimen self-weight, weight of the water, and weight of the loading saddles are applied during post-test analysis linearly over the first two inches of crosshead displacement. Additional details and equations used to determine moment capacity are included in Appendix E.



### **6.2.3 Radius of Curvature**

The global response of the system is measured by vertical string pots (VSP) positioned along the invert of the specimen. As VSP locations are fixed along the specimen horizontally and measured vertically throughout the test, geospatial information is known about each VSP plane of the specimen throughout the test. Appendix F details the equations used to calculate the center of a circle from three known positions along its circumference, from which the radius of curvature (R) is calculated. By taking an average of the radius of curvature calculated for combinations of the two inner loading saddles and each VSP plane located between these loading saddles, the representative global radius of curvature can be determined for the middle third of the pipeline system tested. Due to connection mechanisms allowing for localized joint deflection/rotation, this calculation is representative of the transverse response between loading points that considers both the pipe barrel deflection and joint rotation. The following sections present experimental results as a function of pipe curvature ( $\phi$ ), which is simply the inverse of the radius of curvature ( $\phi = 1/R$ ), and used to simplify the presentation of results (curvature increases with additional displacement, while R decreases with greater deformation).

### **6.2.4 Internal Pressure**

Internal water pressure of the pipe is maintained at a constant value to provide testing conditions representative of those of an operating pipeline system. During an earthquake, it is expected that a pipeline system is likely to contain standard operating pressure [typically 50 to 120 psi (345 to 830 kPa)], or limited pressure due depressurization of the system at another location. Therefore, approximately 62 psi (430 kPa) was used for two of the tests enclosed, representing typical operating pressure. Reduced internal pressure is prescribed for the third test to identify potential influence of internal pressure on transverse system response.

## **6.3 Bending Test Procedure**

The following section provides details of the overall test sequence separated into three parts: pretest, test sequence, and discussion of pause or stop criteria.

### **6.3.1 Pretest**

Once the specimen is secured in the loading frame and the calibrated instrumentation is installed, the measuring systems are verified. The pipe is filled with water with the air bleed in the open position. The air bleed is closed once water has streamed from it and the system is pressurized to the laboratory pressure of approximately 65 psi (450 kPa) to check for leaks. Water is introduced into the specimen more than five hours before testing to ensure thermal acclimation to ambient laboratory conditions. Temperature readings



of the external wall of the pipe are taken at several locations. Multiple pressurization sequences are completed to seat and verify readings of strain gauges. In each of the cycles the air bleed valve is opened to release any accumulating air. For each sequence, data was analyzed to ensure proper function of all measuring systems. The area surrounding the testing frame is cleared of all tools and other objects. Once ready for the test, a pretest meeting is conducted to review installation conditions, walk through instrumentation locations and expectations, and discuss safety equipment and concerns.

### ***6.3.2 Test Sequence***

Each specimen was equipped with strain gauges and loading saddles before installation into the test frame. Careful consideration was taken to ensure strain gauges lie along the extreme outer fibers of the specimen. Once placed within the frame, a small hand-jack was placed one-foot east of center to counteract sagging of the specimen due to self-weight. Once instrumented, placed within the test frame, and connected to the data collection system, pressurization sequences were performed by increasing the pressure within the pipe from 0 psi to approximately 65 psi (430 kPa) where it was maintained for approximately 30 seconds and then depressurized back to 0 psi. This sequence was performed for ten cycles to properly seat end caps, joint mechanisms, and gages, while also providing an initial data set to ensure that testing equipment is working properly. Once it was established that all equipment was functioning, the crosshead was lowered to approximately 1 in. (25 mm) above the specimen, data acquisition was turned on, pipe pressure was increased from 0 psi to the test pressure, and the center jack used to level the pipe was removed. Typical sag of the pipe from self-weight was ~2 in. (50 mm) and was captured in the crosshead displacement data. The crosshead was then lowered with minimal pauses until failure, or the full displacement capacity of the frame was reached. Due to the manual lowering of the crosshead, displacement rates vary marginally among tests and can be viewed in individual test sections.

### ***6.3.3 Stop or Pause Criteria***

Several predetermined interruptions to the test sequence are identified prior to testing. The test is paused if the specimen lost all water pressure during the test. If any leakage is observed at the coupling or center of the specimen, the test is paused briefly, leakage rate assessed, and the test resumed until ultimate failure. The test is paused if any fundamental instrumentation malfunctions during the test, or if power is lost in any part of the testing laboratory. The test is terminated when the specimen is unable to hold internal water pressure, which occurs due to structural failure of the pipe body or connection.



## 7. Bending Test Results

A total of three tests were completed in which pipe diameter, specimen geometry, and loading saddle location remained constant. Table 7.1 provides an overview of the tests. The following sections provide an overview of attributes specific to each of the three tests as well as experimental results.

Some minor modifications to the test frame and loading protocol occurred during the progression of the tests, as noted in the following sections. Radius of curvature values are displayed as curvature, the inverse of radius of curvature, to better graphically represent the data. A comparison of data plotted as a function of radius of curvature vs curvature can be found in Appendix F. Data is shown for instrumentation functioning properly and discarded when extreme changes in values are present, signifying a failure of the equipment. Reasons for loss of VSP data collection include the loss of signal through connections to the data collection system, and the VSP reaching its full displacement capacity. SG data was lost at some locations due to delamination of the gage from the specimen at values around +/-4%.

Table 7.1. Overview of Bending Tests

Test ID (pipe)	Pipe Barrel	Pipe Class [DR]	Joint Type	Pipe Wall Thickness <sup>1</sup> , in. (mm)	Internal Pressure, psi (kPa)
PB03	fPVC	235 [DR18]	Megalug (EBAA)	0.43 (10.9)	62 (427)
PB04	fPVC	235 [DR18]	Fused (UGS)	0.43 (10.9)	62 (427)
PB05	fPVC	235 [DR18]	Fused (UGS)	0.43 (10.9)	16-20 (110-138)

<sup>1</sup>minimum manufacturer wall thickness: 0.38 in. (9.65mm)

### 7.1 PB03 – fPVC w/ Megalug Coupling

Fusible PVC piping with a mechanical joint (Megalug) straight coupling at the midpoint was tested. The Megalug connection uses torque-controlled bolts to apply forces normal to the surface of the pipe to provide friction. Normal forces and a post-test image are shown in Figure 7.1. Examination of the failure surfaces, shown in Figure 7.1b, suggests that the fracture initiated at the invert of the pipe where maximum tensile strain was located, and the external restraint's coupling teeth localized the stress concentration. A summary of instrumentation description and locations are provided in Table 7.2. A series of images depicting test progression is shown in Figure 7.2.



(a) Pre-test depicting applied normal forces

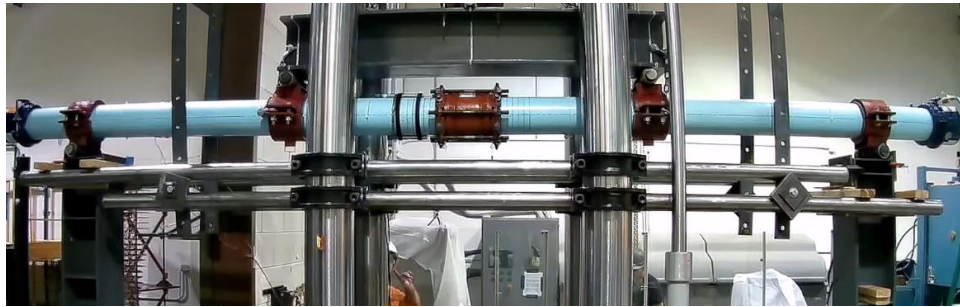


(b) Post-test showing pipe fracture

Figure 7.1. PB03 with Megalug connection

Table 7.2. Instrumentation of PB03

Location	Instrument Description	Local Instrument Name
57 in. east of CL	Crown, Axial Strain	SG-60CA
	Crown, Circumferential Strain	SG-60CC
	Invert, Axial Strain	SG-60IA
	Invert, Circumferential Strain	SG-60IC
19.5 in. east of CL	Crown, Axial Strain	SG-20CA
	Crown, Circumferential Strain	SG-20CC
	Invert, Axial Strain	SG-20IA
	Invert, Circumferential Strain	SG-20IC
70 in. east of CL	Vertical String Pot	VSP-70
33 in. east of CL	Vertical String Pot	VSP-30
18.25 in. east of CL	Vertical String Pot	VSP-20
6 in. east of CL	Vertical String Pot	VSP-6
6in. west of CL	Vertical String Pot	VSP+6
18.25 in. west of CL	Vertical String Pot	VSP+20
33 in. west of CL	Vertical String Pot	VSP+30
70 in. west of CL	Vertical String Pot	VSP+70



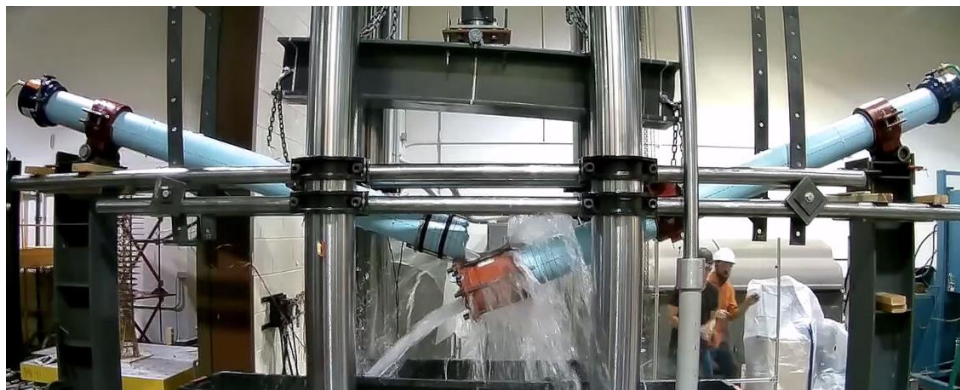
(a) Start of test



(b) Prior to failure



(c) Initiation of failure



(d) Failure

Figure 7.2. Images of PB03 during the test progression



Figure 7.3 shows pressure, crosshead displacement, and the applied load until failure at approximately 600 seconds. Pressure was maintained at approximately 62 psi (427 kPa) and the crosshead displacement reached a maximum value of 7.21 in. (183 mm) while the applied force reached a maximum of 1.43 kips (6.36 kN). Displacement was applied continuously by the weight of the crosshead at an average rate of 1.53 in./min (39 mm/min). VSP-30 did not measure during the test, and it was determined through video analysis that VSP+30 was approximately symmetric to VSP-30 during loading.

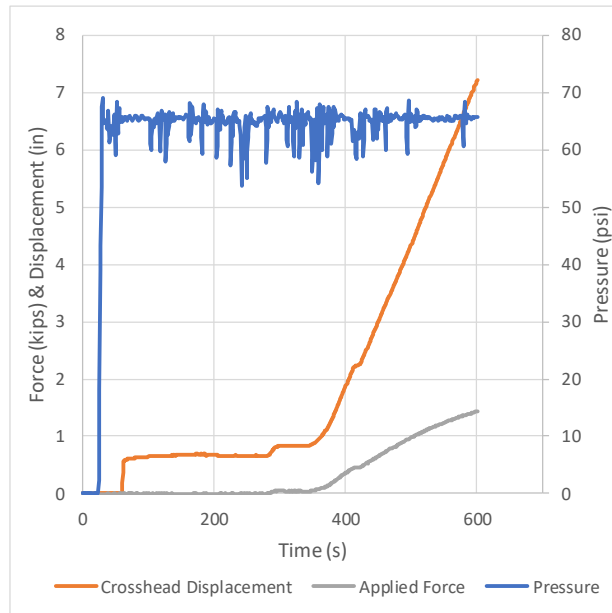
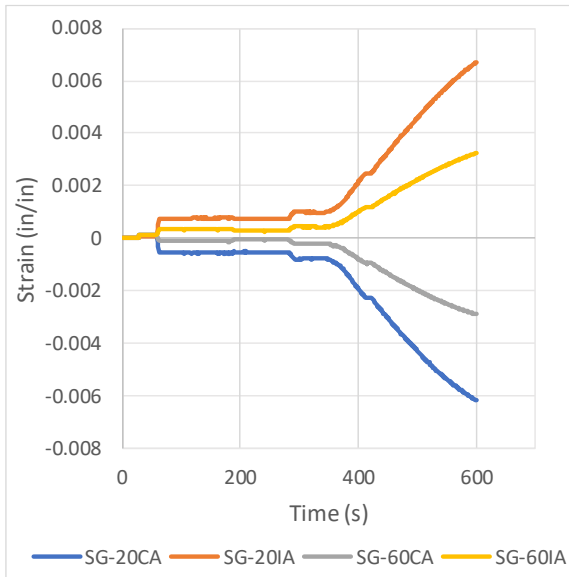


Figure 7.3. PB03 Time history of crosshead displacement, applied force, and pressure

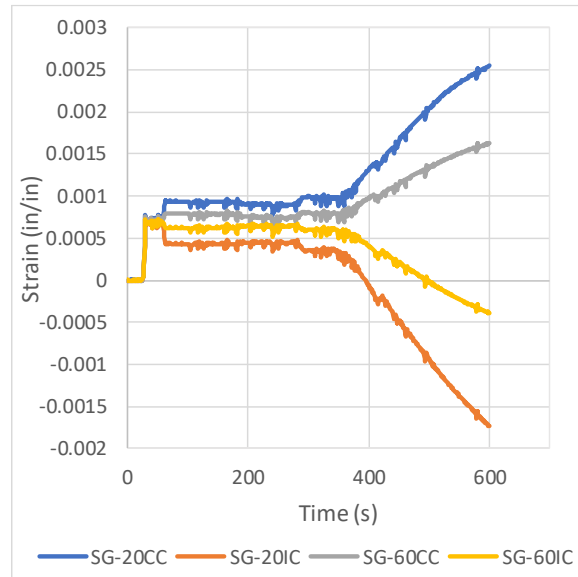
A total of eight strain gages measured axial and circumferential strains at the locations identified in Table 7.2. A full loading sequence can be observed in Figure 7.4 with maximum values shown in Table 7.3. Axial strains located at SG-20 are within the inner loading saddles and considered the maximum recorded strain.

Table 7.3. Maximum Strain Values at Rupture for PB03

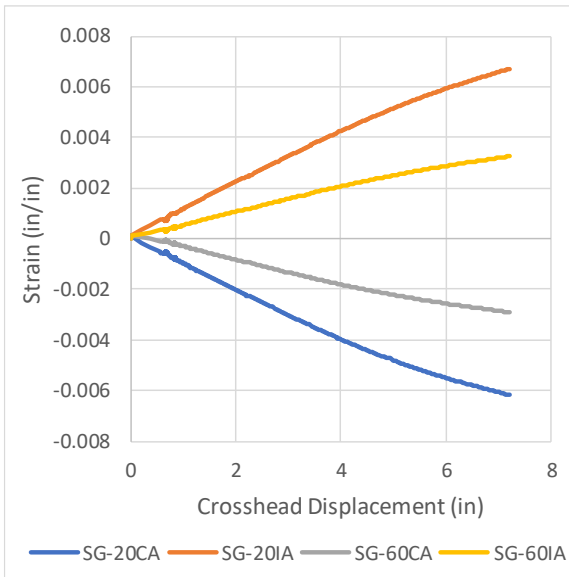
Location	SG-60CA	SG-20CA	SG-60IA	SG-20IA
Strain (in./in.)	-0.00290	-0.00619	0.00325	0.00672



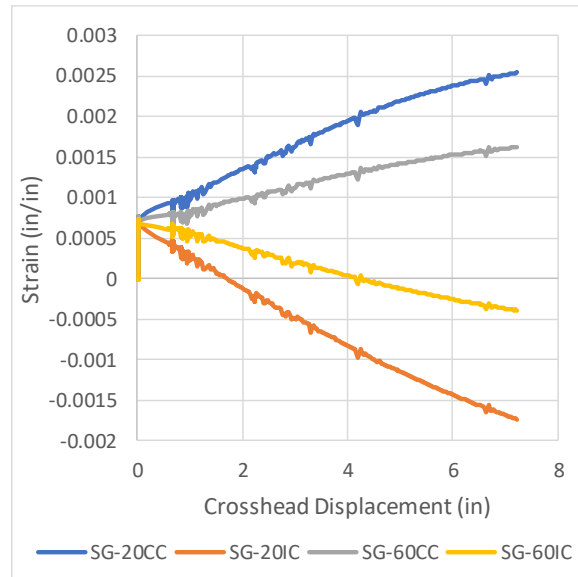
(a) axial strains vs. time



(b) circumferential strains vs. time



(c) axial strains vs. imposed displacement



(d) circumferential strains vs. displacement

Figure 7.4. PB03 axial strains and circumferential strains vs. time and imposed crosshead displacement

The relationship between crosshead displacement and moment, as well as the curvature and pressure are shown in Figure 7.5. A maximum moment of 40.0 kip-in (4.52 kN-m) and a minimum radius of curvature of 191 in. (4850 mm), or a curvature of 0.0052 1/in. (0.0002 1/mm), was achieved. Table 7.4 contains a summary of key experimental results.

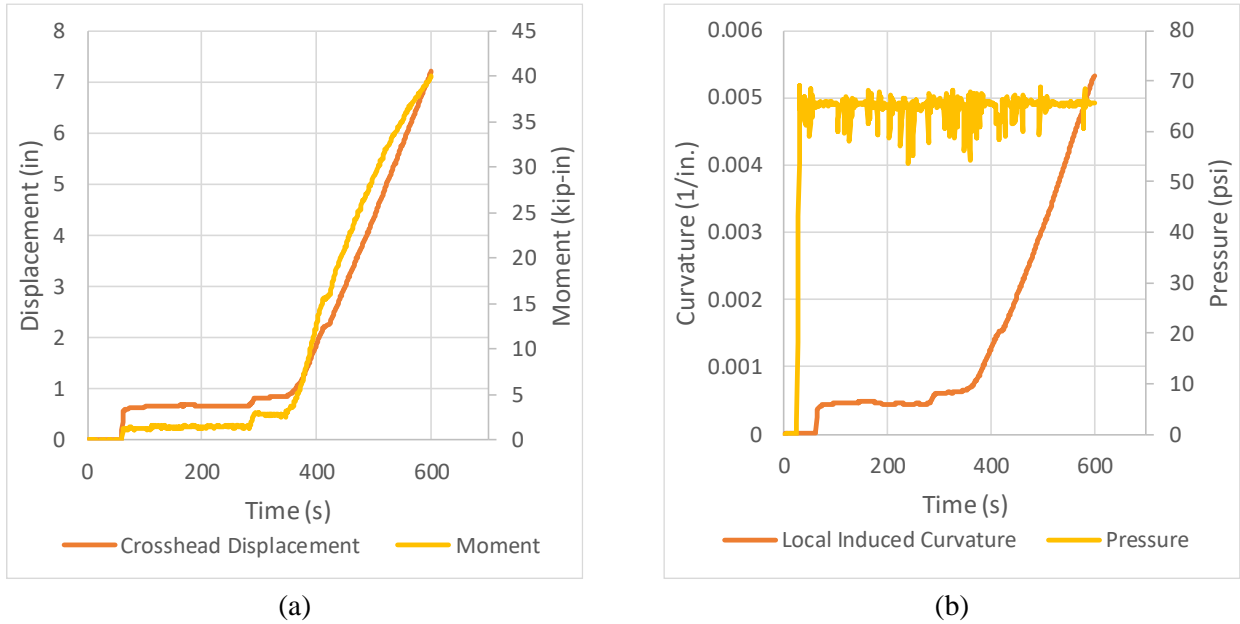


Figure 7.5. PB03 results for (a) applied displacement & resisting moment and (b) curvature & internal pressure

Table 7.4. Maximum Parameter Values of PB03

Maximum Applied Displacement (in.) [mm]	Maximum Resisting Force (kip) [kN]	Maximum Resisting Moment (kip-in) [kN-m]	Minimum Radius of Curvature (in.) [mm]
7.21 [183]	1.43 [6.36]	40.0 [4.52]	191 [4,850]

Figure 7.6(a) shows the linear relationship between crosshead displacement and curvature. Figure 7.6(b) shows applied moment vs. curvature which demonstrates a nonlinear relationship between the imposed loading and resulting deformation. A similar nonlinear response is shown in the axial strain vs. curvature results of Figure 7.7.

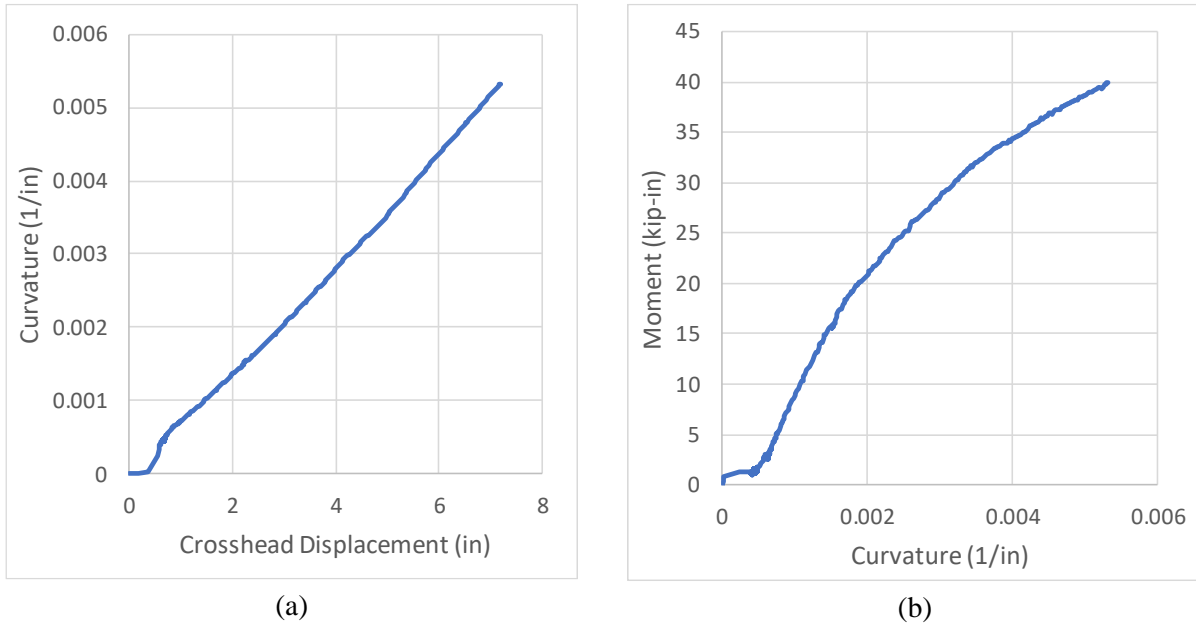


Figure 7.6. PB03: (a) crosshead displacement vs. curvature and (b) moment vs. curvature

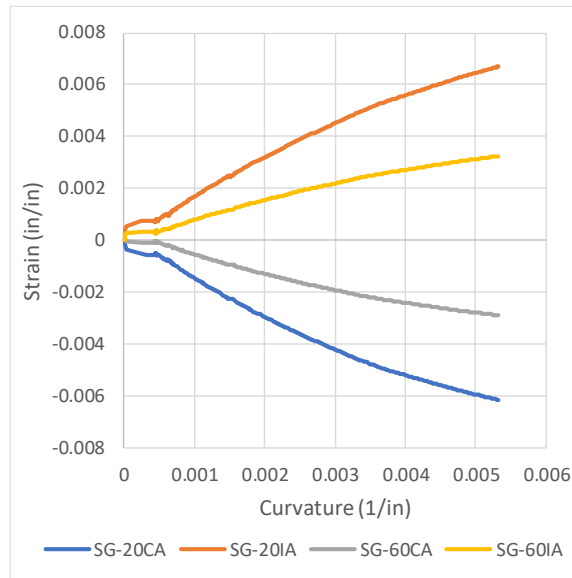


Figure 7.7. PB03 curvature history of axial strain



## 7.2 PB04 – fPVC w/ Fused Connection

Fusible PVC piping with a fused connection at midpoint was tested, as shown in Figure 7.8. The fused connection uses a temperature fusing process to develop a bond between the lengths of pipeline. This fused pipe specimen is representative of a continuous pipe with limited localized deflection provided by the connection. A summary of instrumentation description and locations are provided in Table 7.5. Images of the test progression is shown in Figure 7.9. No leakage or buckling of the pipe wall was observed prior to rupture.

Table 7.5. Instrumentation of PB04

Location	Instrument Description	Local Instrument Name
57 in. east of CL	Crown, Axial Strain	SG-60CA
	Invert, Axial Strain	SG-60IA
	Crown, Circumferential Strain	SG-60CC
	Invert, Circumferential Strain	SG-60IC
19.5 in. east of CL	Crown, Axial Strain	SG-20CA
	Invert, Axial Strain	SG-20IA
	Crown, Circumferential Strain	SG-20CC
	Invert, Circumferential Strain	SG-20IC
12 in. east of CL	Crown, Axial Strain	SG-12CA
	Invert, Axial Strain	SG-12IA
	Crown, Circumferential Strain	SG-12CC
	Invert, Circumferential Strain	SG-12IC
20 in. west of CL	Crown, Axial Strain	SG+20CA
	Invert, Axial Strain	SG+20IA
	Crown, Circumferential Strain	SG+20CC
	Invert, Circumferential Strain	SG+20IC
70 in. east of CL	Vertical String Pot	VSP-70
33 in. east of CL	Vertical String Pot	VSP-30
18.25 in. east of CL	Vertical String Pot	VSP-20
6 in. east of CL	Vertical String Pot	VSP-6
6in. west of CL	Vertical String Pot	VSP+6
18.25 in. west of CL	Vertical String Pot	VSP+20
33 in. west of CL	Vertical String Pot	VSP+30
70 in. west of CL	Vertical String Pot	VSP+70

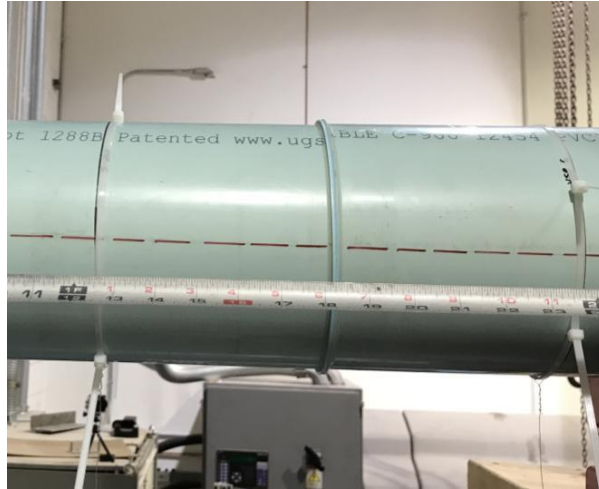
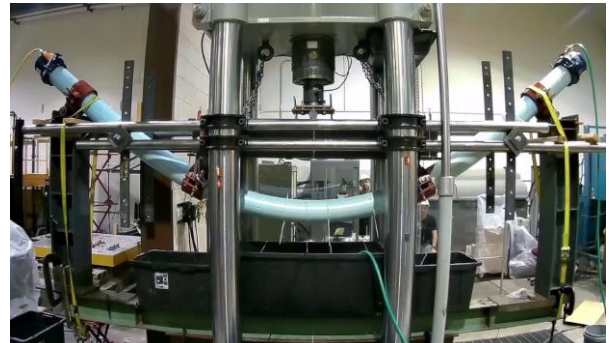


Figure 7.8. PB04 6-in. (150 mm) diameter fusible PVC with fused connection



(a) Beginning of test



(b) Prior to failure



(c) Failure



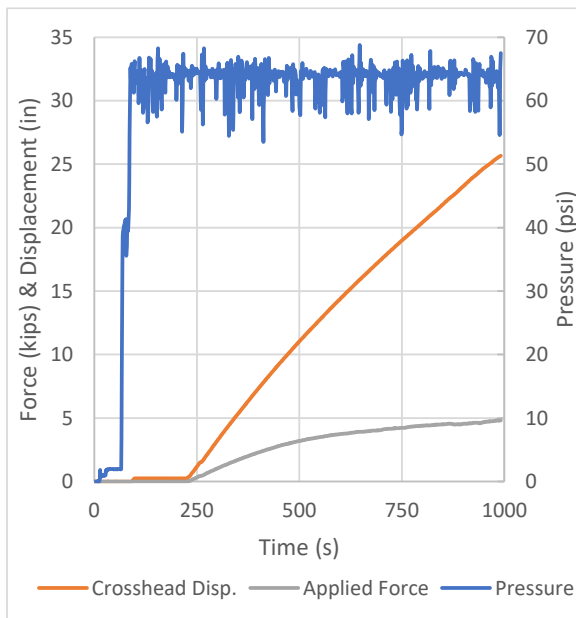
(d) Post-failure

Figure 7.9. Images of PB04 during the test progression

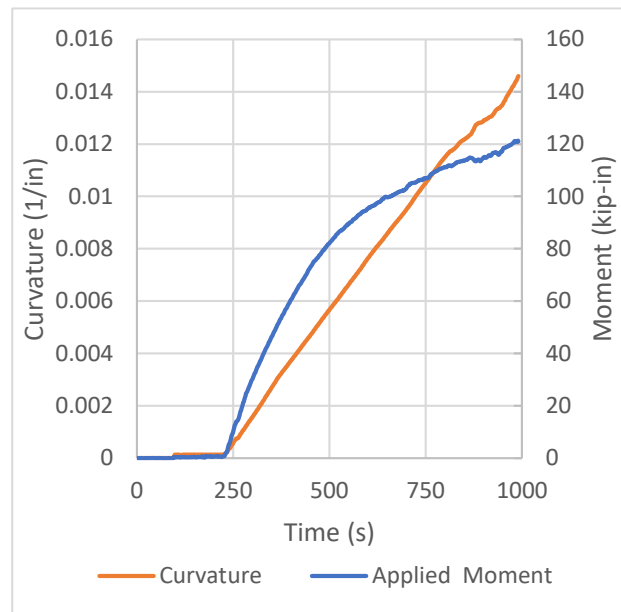


Pressure, crosshead displacement, and applied force were recorded and are shown in Figure 7.10 until failure at approximately 1,000 seconds. The average internal pressure was 62 psi (427 kPa) and was maintained during the test by a combination of a pressure regulator set to 58 psi (400 kPa) and backpressure regulator set to 63 psi (434 kPa); fluctuations between these values can be observed. The crosshead displacement reached a maximum value of 25.7 in. (650 mm) while the applied force reached a maximum of 5.03 kips (22.4 kN). Displacement was applied continuously by the weight of the crosshead at an average rate of 0.88 in./min (22.3 mm/min). Crosshead position was calculated as the average of VSP-30 and VSP+30 displacements.

The relationships between curvature and applied moment vs. time are shown in Figure 7.10(b). A maximum moment of 121 kip-in (13.7 kN-m) and a minimum radius of curvature of 70 in. (1.78 m), or a curvature of 0.0143 1/in. (0.56 1/m), were calculated from test measurements just prior to rupture. Table 7.6 contains a summary of maximum values achieved.



(a)



(b)

Figure 7.10. PB04 test results for (a) crosshead displacement, applied force, & pressure vs. time and (b) calculated curvature & applied moment



Table 7.6. Maximum Parameter Values of PB04

Maximum Applied Displacement (in.) [mm]	Maximum Resisting Force (kip) [kN]	Maximum Resisting Moment (kip-in) [kN-m]	Minimum Radius of Curvature (in.) [m]
25.7 [650]	5.03 [22.4]	121 [13.7]	70 [1.78]

Figure 7.11(a) shows the approximate linear correlation between crosshead displacement and pipe curvature, which is expected given the geometry of the test setup. Some deviation for linearity is observed at significant levels of deformation. Figure 7.11(b) proves the key experimental result. The moment vs. curvature relationship is approximately linear up to a curvature of approximately 0.005 1/in., ( $R = 200$  in. or 16.7 ft), after which the specimen behaves non-linearly, requiring less applied load per increment of deformation.

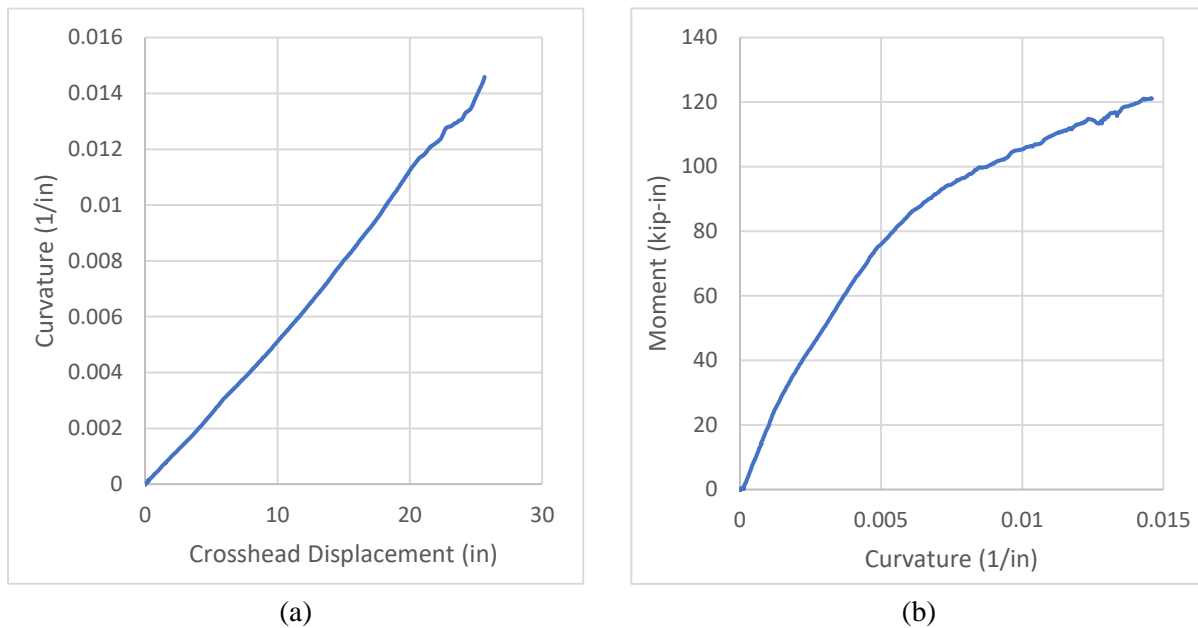


Figure 7.11. PB04: (a) crosshead displacement vs. curvature and (b) moment vs. curvature

A total of sixteen strain measurements were recorded at four locations: 60, 20, and 12 in. (1500, 500, and 300 mm) east of centerline and 20 in. (500 mm) west of centerline with axial and circumferential strains recorded at both crown and invert for all locations (Table 7.5). The development of strains vs. time and crosshead displacement are provided Figure 7.12 with maximum values given by Table 7.7. Figure 7.13 provides the same axial strain measurements vs. applied specimen curvature.

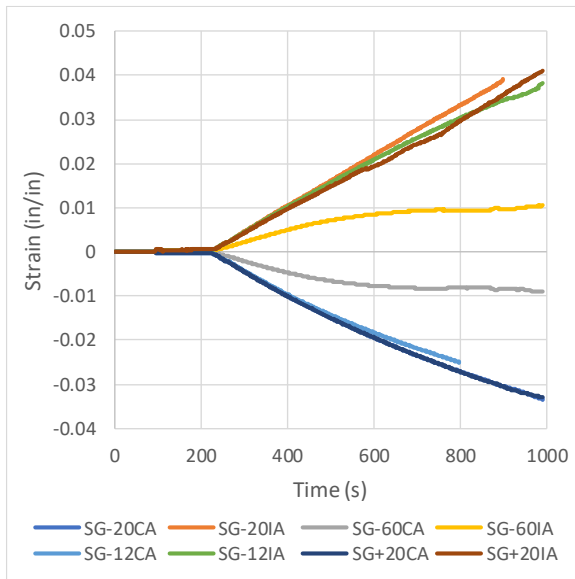


Figure 7.12(c) shows that both tensile and compression strains (located along the pipe invert and crown, respectively) maintain a linear relationship with respect to crosshead displacement both before and after reaching the material proportional limit strain of approximately 0.01 (0.1%, refer to Section 1.3). The circumferential strains demonstrate similar trends (with reverse signs) at low levels of cross-head displacement, but demonstrate deviation from linearity at higher displacement levels, suggesting ovalization of the pipe cross-section, shown in Figure 7.12 (d). The strain results demonstrate that the largest localized deformations occur at the specimen invert, suggesting the likely location of a tensile rupture failure mechanism.

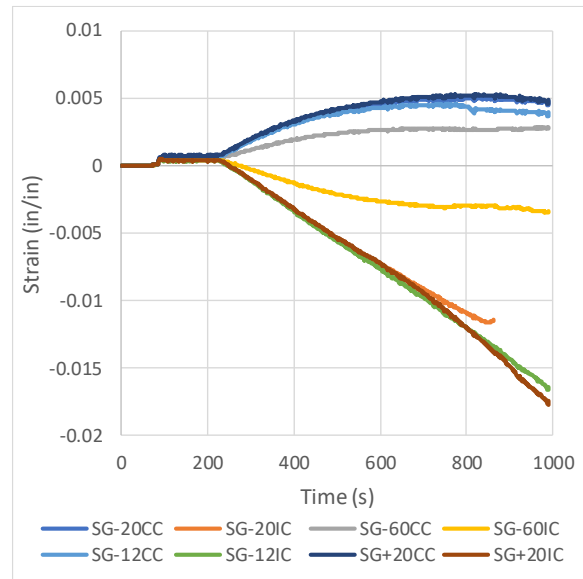
Another observation is the relationship of SG-60 strain values to strain values measured within the inner loading saddles. As the inner strain values continue linearly, both axial and circumferential SG-60 strain values level off. This could be due to the large displacement imposed by the test frame, shifting the angle that laterally applied loads are subjected to through the loading saddles. As load increases due to the displacement of the crosshead, so does the angle to which load is applied, countering the increased load by a decreased effective lateral load.

Table 7.7. Maximum Strain Values Recorded in PB04

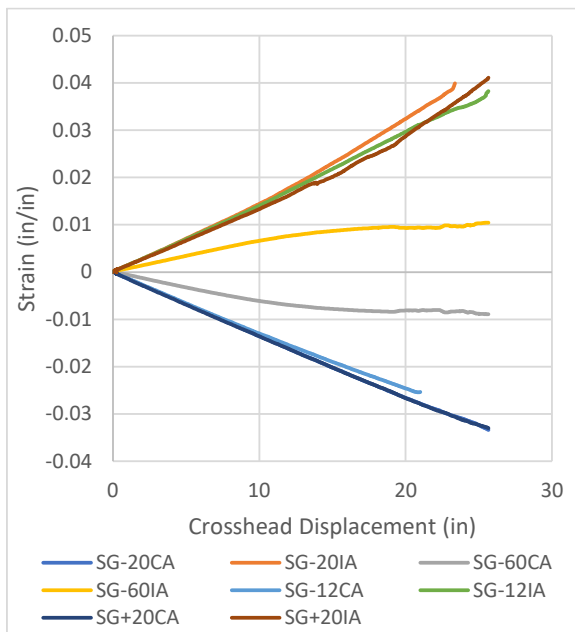
Location	SG-60	SG-20	SG-12	SG+20
<b>Crown Axial Strain: in./in. (%)</b>	-0.0029 (-0.29%)	-0.00619 (-0.619%)	-0.0254 (-2.5%)	-0.0330 (-3.3%)
<b>Invert Axial Strain: in./in. (%)</b>	0.00325 (0.325%)	0.00672 (0.672%)	0.0383 (3.83%)	0.0411 (4.11%)



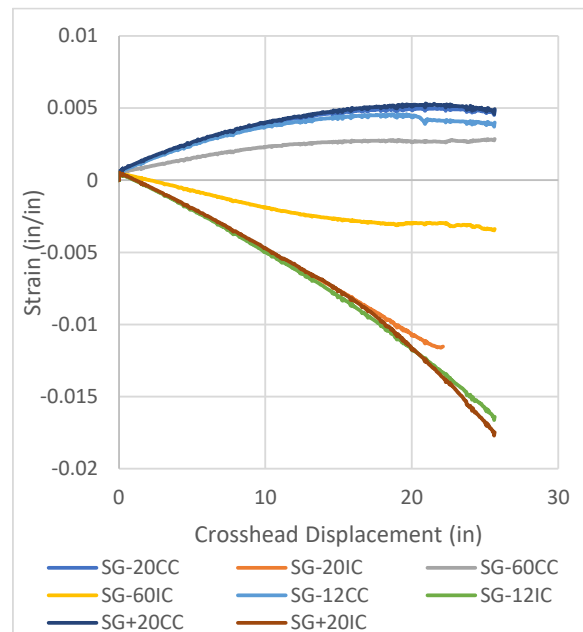
(a)



(b)



(c)



(d)

Figure 7.12. PB04 strain evolution for (a)(c) axial and (b)(d) circumferential strains vs. time and applied crosshead displacement

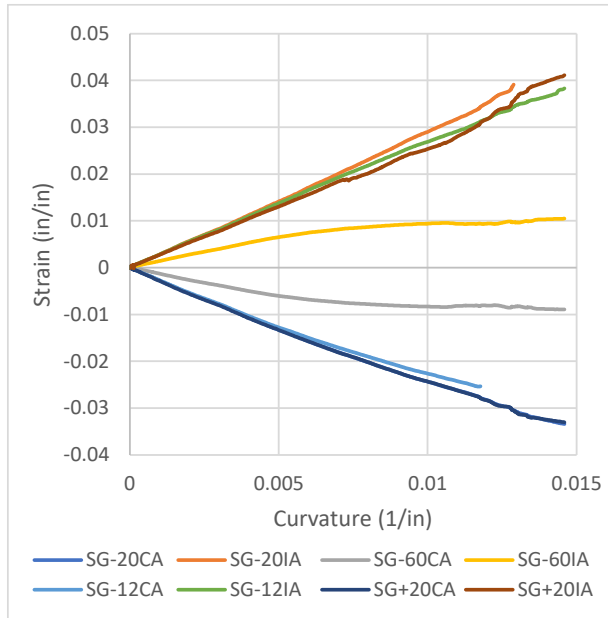


Figure 7.13. PB04 curvature history of axial strain



### 7.3 PB05– Fused Pipe with Fused Connection

Fusible PVC piping with a fused connection at midpoint was tested and can be viewed in Figure 7.14(a). This test followed the same specimen and connection as PB04 with strains measured in additional locations and a reduced internal water pressure. During the initial test sequence, it was observed that VSP data was not being collected at all VSP locations as several instruments reached their full stroke. The test was paused, and the specimen was unloaded. Analysis was completed on the initial data collected and it was determined that the specimen had undergone some plastic deformation and would not return to its original position. Before retesting, data was collected to compare the plastic deformation in terms of crosshead displacement that was sustained by the specimen. This value was then considered the baseline of VSP data collected once testing was resumed. Strain data in the second test used the baselines of the initial test in analysis. Data from the first and second sequences are combined in the PB05 test data outlined below. Due to the significant displacements at unloading and reloading, several strain gauges unbonded from the specimen,

Table 7.8. Instrumentation of PB05

Location	Instrument Description	Local Instrument Name
57 in. east of CL	Crown, Axial Strain	SG-60CA
	Invert, Axial Strain	SG-60IA
19.5 in. east of CL	Crown, Axial Strain	SG-20CA
	Crown, Circumferential Strain	SG-20CC
	Invert, Axial Strain	SG-20IA
	Invert, Circumferential Strain	SG-20IC
	Spring Line North, Axial	SG-20NA
	Spring Line South, Axial	SG-20SA
12 in. east of CL	Crown, Axial Strain	SG-12CA
	Invert, Axial Strain	SG-12IA
12 in. west of CL	Crown, Axial Strain	SG+12CA
	Invert, Axial Strain	SG+12IA
20 in. west of CL	Crown, Axial Strain	SG+20CA
	Invert, Axial Strain	SG+20IA
70 in. east of CL	Vertical String Pot	VSP-70
33 in. east of CL	Vertical String Pot	VSP-30
18.25 in. east of CL	Vertical String Pot	VSP-20
6 in. east of CL	Vertical String Pot	VSP-6
6in. west of CL	Vertical String Pot	VSP+6
18.25 in. west of CL	Vertical String Pot	VSP+20
33 in. west of CL	Vertical String Pot	VSP+30
70 in. west of CL	Vertical String Pot	VSP+70



and their data has been appropriately truncated. All the data collected and the corresponding locations can be found in Table 7.8.



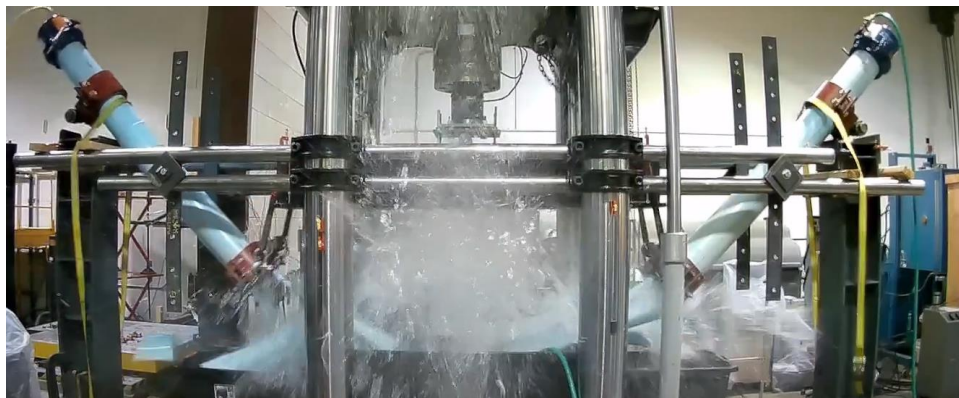
(a) Start of test



(b) Mid-loading point



(c) Maximum loading



(d) Failure

Figure 7.14. Images of PB05 during the test progression



Displacement was applied by the weight of the crosshead at an average rate of 0.78 in./min (20 mm/min) and crosshead movement was stopped before failure and unloaded. Crosshead movement was then continued four days later continuously until failure. The full loading sequence can be seen in Figure 7.15 with the stop in loading occurring at ~2,100 seconds. VSP data was not recorded from 1,100 seconds to 2,145 seconds and is the cause for pausing the test between initial and secondary sequences. VSP data was resumed at the level of crosshead displacement equivalent to the sag of the system due to plastic deformation. Because the radii of curvature calculations are based on VSP data within the inner loading saddles, radius of curvature was not calculated during the latter part of the first sequence.

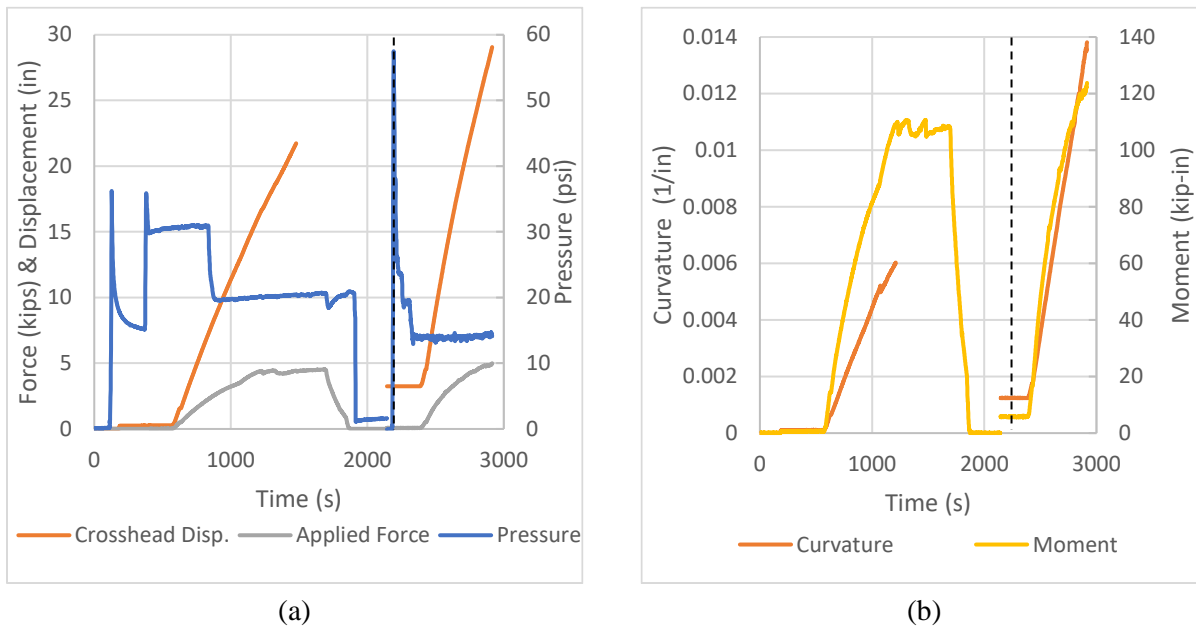


Figure 7.15. PB05 (a) applied displacement & moment and (b) curvature & internal pressure vs. time

Internal pressure of the first sequence was set to approximately 20 psi (138 kPa) but experienced some fluctuation due to poor backpressure regulation. Internal pressure during the second sequence loading was set to 16 psi (110 kPa) and was maintained until failure without leakage. Maximum values, which occurred at failure during the second sequence, are provided in Table 7.9.

Table 7.9. Maximum Parameter Values of PB05

Max. Applied Displacement (in.) [mm]	Max. Applied Force (kip) [kN]	Max. Moment (kip-in) [kN-m]	Max. Curvature (1/in.) [1/m]	Min. Radius of Curvature (in.) [m]
29.1 [739]	4.98 [22]	123 [13.9]	0.138 [0.54]	72.4 [1.84]

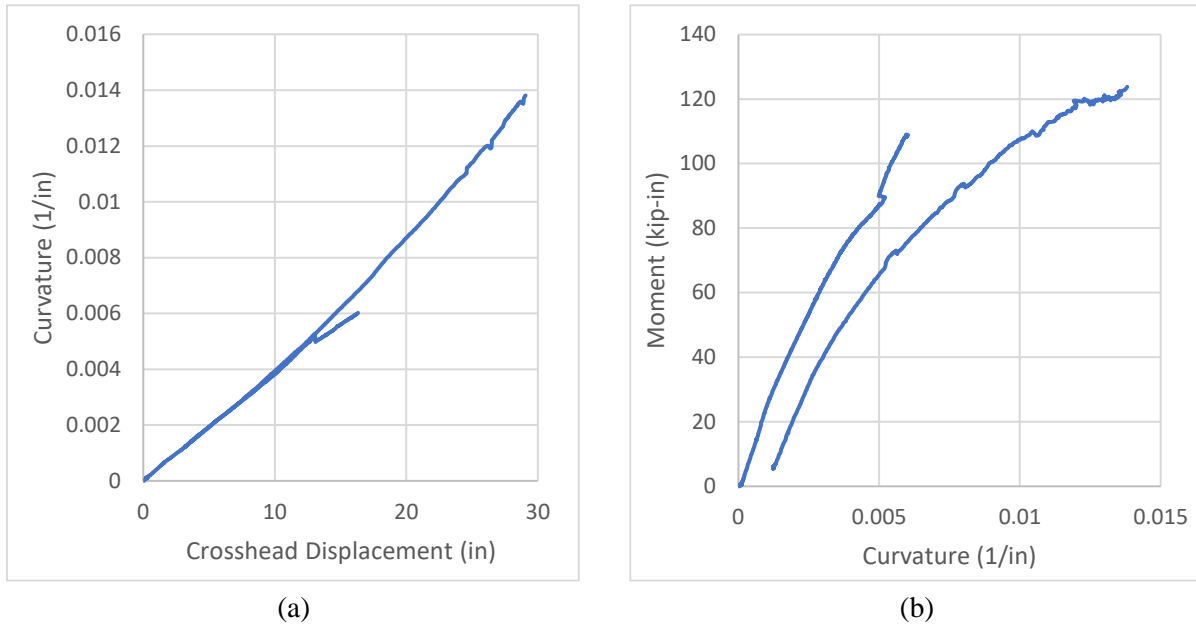


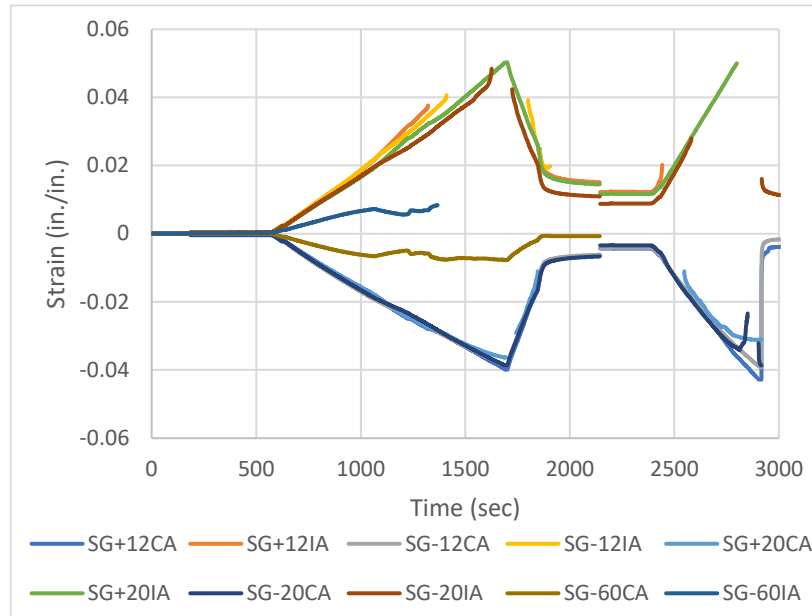
Figure 7.16. PB05: (a) crosshead displacement vs. curvature and (b) moment vs. curvature

A total of fourteen strain measurements, detailed in Table 7.8, were recorded at four locations: 60, 20, and 12 in. (1500, 500, and 300 mm) east of centerline and 12 and 20 in. (300 and 500 mm) west of centerline. Axial strain was measured at all locations and circumferential strain was measured at SG-20 east of centerline. Additional strain gauges were placed along the spring line 20 in. (500 mm) east of centerline to observe the strain distribution across the specimen throughout loading. The full loading sequence is shown in Figure 7.17 while maximum values are provided in Table 7.10.

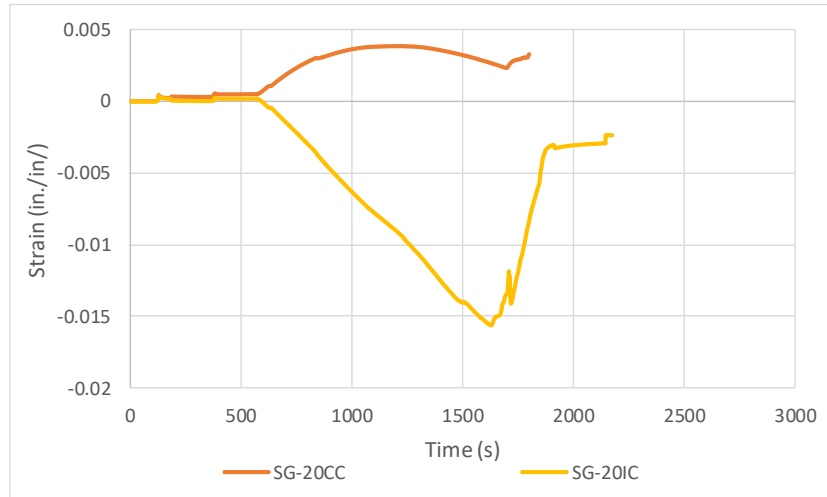
Strain data in secondary testing appears irregular due to errors in the data reading for various lengths of time. SG-60IA and SG+12IA were both lost early in the testing sequence due to damage of the connection wires.

Table 7.10. Extreme Axial Strain Values Recorded in PB05

Location	SG-60	SG-20	SG-12	SG+12
Crown Axial Strain (in./in.)	-0.0078 (-0.8%)	-0.0387 (-3.9%)	-0.0393 (-3.93%)	-0.0428 (-4.3%)
Invert Axial Strain (in./in.)	NA	0.0483 (4.8%)	0.0406 (4.1%)	NA



(a)



(b)

Figure 7.17. Time history of PB05 (a) axial and (b) circumferential strains



## 7.4 Summary of Bending Tests Results

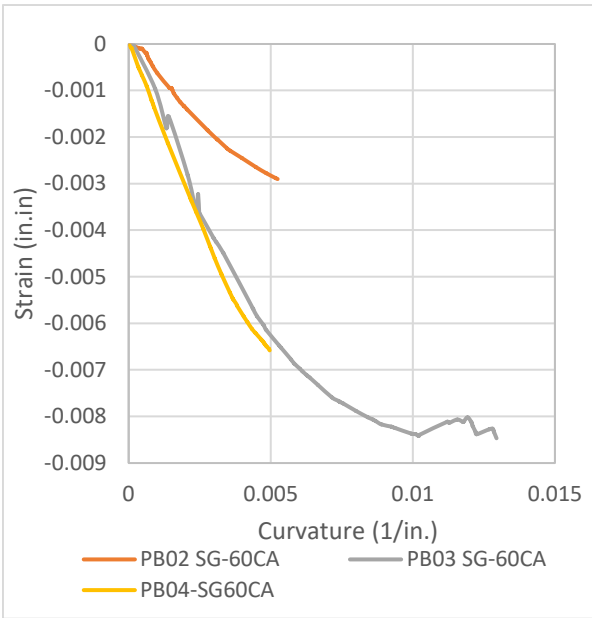
Axial strain values are compared among tests at varying levels of curvature and applied moment. All specimens were fusible PVC pipe [PC235, DR18] with a wall thickness of 0.43 in. (11 mm). Table 7.11 contains a summary of results.

Table 7.11. Overview of Fused Bending Test Results

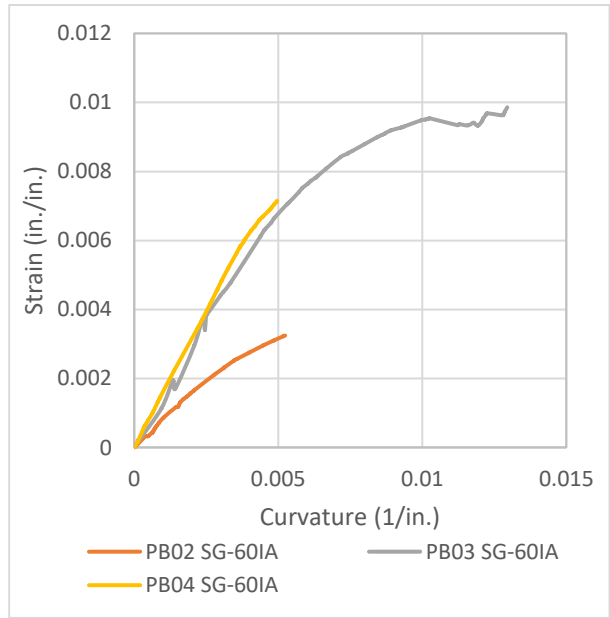
Test ID	Joint Type (Company)	Max. Applied Displacement (in.) [mm]	Max. Resisting Moment (kip-in) [kN-m]	Min. Radius of Curvature (in.) [m]	Max. Tensile Strain (%)	Max. Comp. Strain (%)
PB03	Megalug (EBAA)	7.21 [183]	40.0 [4.52]	191 [4.85]	0.67	-0.619
PB04	Fused (UGS)	25.7 [653]	121 [13.7]	70.0 [1.78]	4.11	-3.30
PB05	Fused (UGS)	30.5 [775]	123 [13.9]	72.4 [1.84]	4.83	-4.28

Strain readings are grouped together by the joint mechanism used in each test. Strains are plotted at two locations, SG-60 that is located outside of the region of maximum moment and SG-20 that is located within the region of maximum moment, shown in Figure 7.18. SG-20 was selected due to all fusible and Megalug connection tests having strain values measured at the location. A comparison of these strains can be seen in Figure 7.19. As individual test data show strain values measured within the region of maximum moment to be equal, comparison is only needed at a single location. When comparing joint mechanisms, the lower the strain demand per applied curvature, the greater the joint rotation allowed by the joint mechanism.

The fused connection shows the highest strain demand per applied curvature, indicating that the fused connection acts as a continuous member, absent of any localized joint deflection. The Megalug connection (PB03) is slightly lower, implying a small quantity of joint rotation, but failing before reaching the pipe tensile elongation at yield (3.1%, referenced in Section 1.3). This is likely due to the applied normal forces of the restraint wedges increasing the local strain demand through the stress vector acting normal to the surface of the pipe. Therefore, it shifts the principal stresses and strains closer to failure in three-dimensional analysis. Further testing is suggested to confirm performance and repeatability.

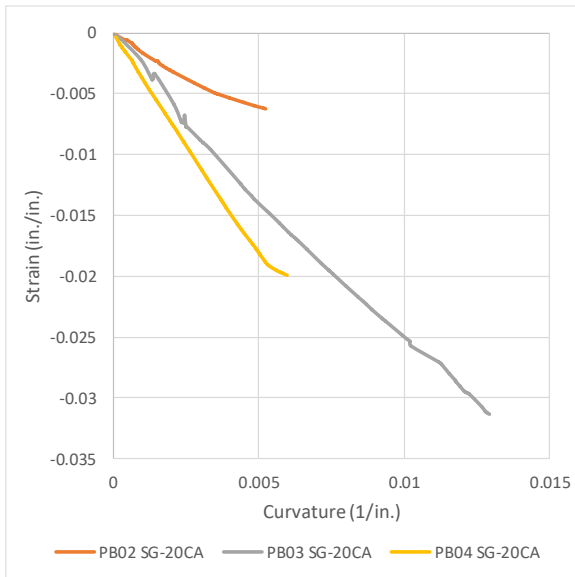


(a) Crown axial strains

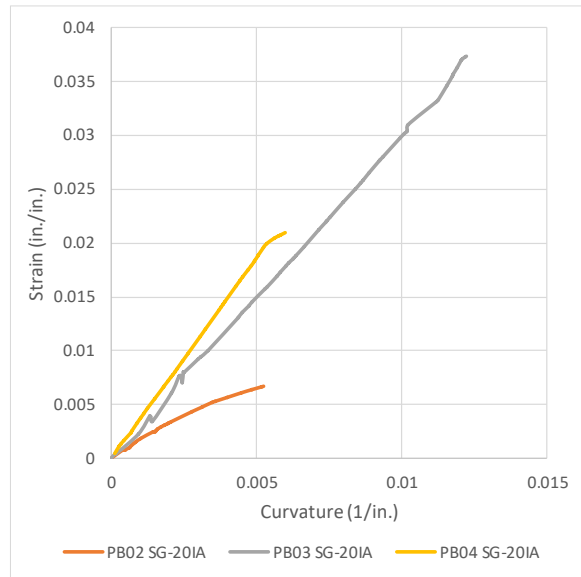


(b) invert axial strains

Figure 7.18. Axial strains at SG-60 (a) crown and (b) invert as a function of applied curvature



(a) Crown axial strains



(b) invert axial strains

Figure 7.19. Axial strains at SG-20 (a) crown and (b) invert as a function of applied curvature



The moment-curvature relationship is plotted for each test in Figure 7.20. Similar to the strain demands, joint mechanisms that provide less joint rotation, such as the fused connection, have a higher moment capacity per curvature demand when compared to joint mechanisms such as the Megalug fitting, which has a small plateau at the onset of loading, characteristic of joint rotation.

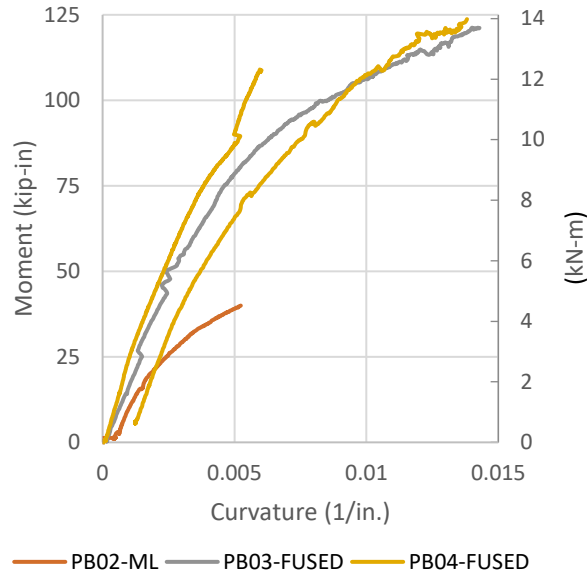
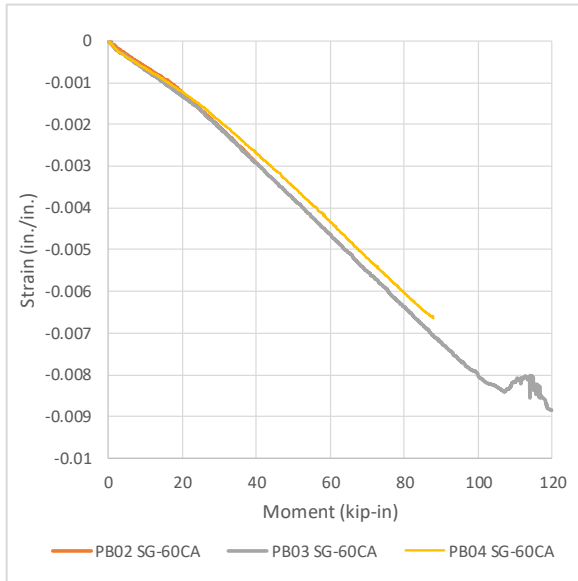
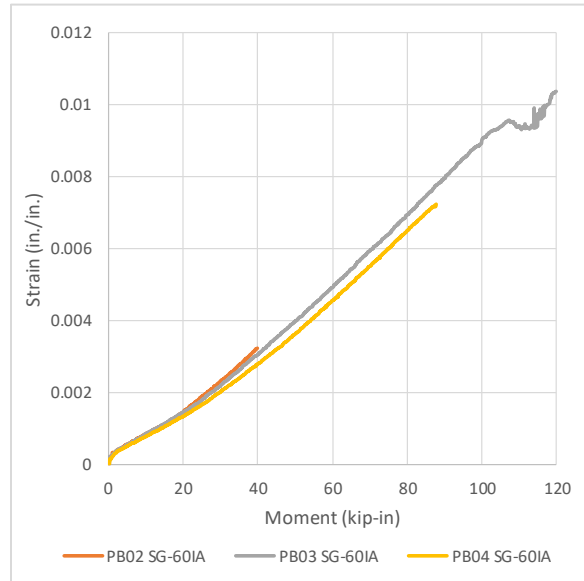


Figure 7.20. Comparison of bending test moment vs. curvature

Strain readings are grouped together by the joint mechanism used in each test. Strains are then plotted at three locations. SG-60 is located outside of the region of constant moment (Figure 7.21), and SG-20 and SG-12 that are both located within the region of constant maximum moment (Figure 7.22).

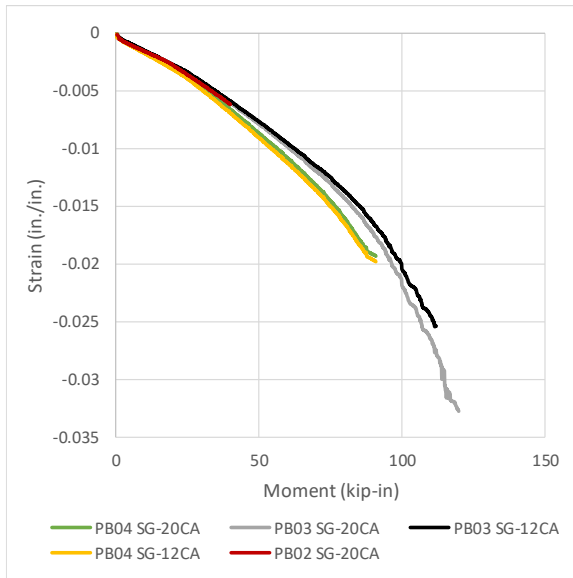


(a)

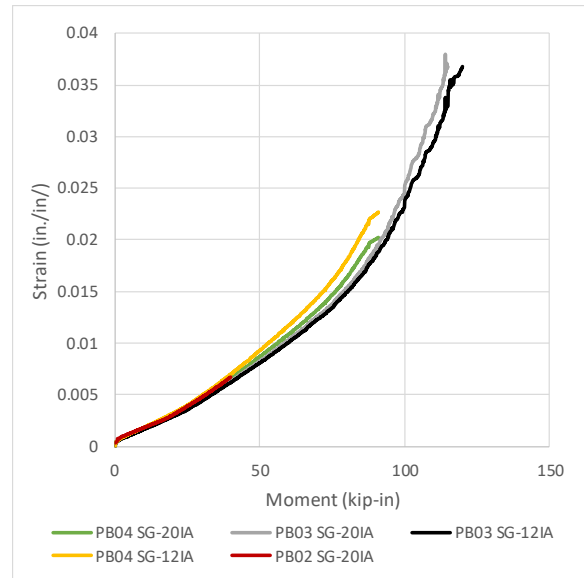


(b)

Figure 7.21. Comparison of applied moment vs (a) crown and (b) invert axial strains located at SG-60



(a)



(b)

Figure 7.22 Applied moment vs. (a) crown and (b) invert strains within constant moment region



### 7.5 Bending Test Classification

This testing allows for direct classification of system response due to imposed bending from ground deformation classified by Davis et al., (2019). This classification is also described in Table 7.12 and is being considered in the development of a seismic design standard for water and wastewater pipelines. Results are from preliminary tests and are intended to show the capabilities of the test frame. Further testing would be needed to validate these results. Classification for each system relative to lateral capacity is provided in Figure 7.12. Results of minimum radius of curvature are taken as the maximum value recorded for each pipeline system. All systems qualify by a large margin as the threshold to achieve the maximum seismic rating is a minimum radius of curvature achieved of 150 ft (46 m).

Table 7.12. Seismic Ground Strain Demand Levels for Buried Pipes (Davis et al. 2019)

Parameter (+ and -)	Class	Seismic Strain Demand	
Axial Strain ( $\alpha$ )	$\alpha_A$	0.01% up to 0.1%	
	$\alpha_B$	0.1% up to 0.5%	
	$\alpha_C$	0.5% up to 1%	
	$\alpha_D$	1% or greater	
Radius of Curvature (R)/ Deflection Angle ( $\phi$ )	$\rho_A$	$R_A > 344\text{m}$ (1130 ft)	$\phi_A/L_g < 0.167$ deg./m (0.051 deg./ft)
	$\rho_B$	$115\text{ m}$ (376 ft) $< R_B \leq 344\text{m}$ (1130 ft)	$0.167 \leq \phi_B/L_g < 0.5$ deg./m (0.152 deg./ft)
	$\rho_C$	$46\text{ m}$ (150 ft) $< R_C \leq 115\text{ m}$ (376 ft)	$0.5 \leq \phi_C/L_g < 1.25$ deg./m (0.381 deg./ft)
	$\rho_D$	$R_D \leq 46\text{ m}$ (150 ft)	$\phi_D/L_g \geq 1.25$ deg./m (0.381 deg./ft)

Table 7.13. Seismic Classification of Pipeline Systems Tested (all 6-in. diameter)

Continuous Pipeline System	Test Number	Minimum Radius of Curvature in. (ft) [m]	Seismic Classification	% Exceeding Class D?
<b>fPVC with Megalug joint</b>	PB03	15.9 [4.8]	D	9.4
<b>fPVC with fused joint</b>	PB04	5.8 [1.8]	D	25.7
<b>fPVC with fused joint</b>	PB05	6.0 [1.84]	D	24.8

\* Class D requires radius of curvature of 150 ft (46 m)

\*\* Min. allowable manufacturer bend radius: 144 ft. Bend Radius calculations assume that a fitting or flange is present/to be installed in the bend. The Bend Radius for PVC is calculated using 250 times the outside diameter of the pipe, which is based on an axial tensile stress due to bending of 800 PSI and which includes a safety factor of 2.5. This is compared to the long-term stress capacity [Unibell Handbook of PVC, 4th Edition].



The moment-curvature plots of each pipeline system shown in Figure 7.20 demonstrate that joint rotation has an important effect on the moment capacity of each system. The test results demonstrate that pipelines accommodate transverse loading through a flexural component provided by the pipe segments and a rotational component provided by the joint.

For future testing, a baseline should be established, measuring the moment capacity of a pipe segment with no joint. By accurately measuring the bending strain at failure (leakage or fracture) within the region effected by the joint, a comparison between the bending strain of a segment with and without joint effects can be made. From this comparison, a weak point of the system can be identified. By understanding the impact of the joint mechanism on the system, further refinement of K-values used within the fragility curve equations that account for system material can be made (American Lifelines Alliance (ALA), 2001).



## 8. Conclusions

The tests performed reflect on the performance of nominal 6-in. (150-mm) diameter fusible pipe with both fused connections and Megalug couplings. The work was undertaken in the Center for Infrastructure, Energy, and Space Testing (CIEST) which is affiliated with the Civil, Architectural, and Environmental Engineering Department at the University of Colorado Boulder.

External and internal loading conditions were imposed on the test specimens. These conditions were representative of the significant deformations possible during earthquake-induced ground deformation such as landsliding, fault rupture, and liquefaction-induced lateral spreading, thus characterizing the pipeline system capacity. As detailed, all tests were designed and performed in accordance with procedures and recommendations provided by Wham et al. (2018 & 2019). In total, seven (7) axial tension tests, two (2) axial compression tests, an axial cyclic test, and three (3) four-point bending tests were performed on various connections, including fused connections, Megalug couplings, and Lokx fittings. All tests were designed to focus on the upper bound performance of a pipe system when faced with various loading conditions due to real-world applications from failure mechanisms listed above.

There are several limitations that are important to note. The primary purpose of this report was to outline the methods and best practices associated with quantifying axial and transverse responses of thermoplastic pipelines. While the test procedures provide valuable results, the report is limited by the number of tests performed. Significant value would be gained from performing identical tests on multiple specimens to assess statistical deviations of results. The testing was performed on new pipe and fittings that had not experienced potential degradation due to long-term operation and other aging effects. Internal pressures were limited in this study to relatively low levels, and it is possible higher pressures may impact transverse performance.

Despite limitations, the methods provided in this study allow for the testing of a wide range of pipeline systems including variable pipe diameter, joint mechanism, and pipe material. Data collected, such as local strain demands at failure and strain thresholds to achieve joint slip and displacement, can be used to validate finite element analysis of pipeline systems to better understand three-dimensional strain demands on pipe segments and perform failure analysis dependent on the parameters described. Once a representative number of tests have been performed, the results will assist in refining fragility functions for risk assessment of pipeline networks.



## Acknowledgements

The authors wish to recognize the excellent effort of University of Colorado students and staff that made these experiments successful. Namely, the contributions of graduate students David Kyle Anderson and Hailey-Rae Rose, and undergraduates David Balcells and Aldrich Valerian are gratefully acknowledged. Great thanks are extended to CIEST staff members Kent Polkinghorne, and John Hindman for their constant support and expertise. Appreciation is extended Aegion for technical and financial support for this study, especially Tom Marti, as well as EBAA for providing materials.

## References

- American Lifelines Alliance (ALA). (2001). *Seismic Fragility Formulations for Water Supply Systems, Part 1- Guideline*. Reston, VA: American Society of Civil Engineers, Federal Emergency Management Agency (FEMA), and the National Institute of Building Sciences (NIBS). Retrieved from [https://www.americanlifelinesalliance.com/pdf/Part\\_1\\_Guideline.pdf](https://www.americanlifelinesalliance.com/pdf/Part_1_Guideline.pdf)
- Davis, C.A., Rajah, S., Wham, B.P., & Heubach, W.F. (2019). "Strain Demands on Buried Pipelines from Earthquake-Induced Ground Movements". *Proceedings: Pipelines 2019* (pp. 357–367). Nashville, TN.
- Ihnotic, C.R. (2019). *Seismic Evaluation of Hazard-Resistant Lifelines: Thermoplastic Pipes and Connections*. M.S. Thesis, Boulder CO: University of Colorado Boulder.
- Wham, B.P., Berger, B.A., O'Rourke, T.D., Pariya-Ekkasut, C., & Stewart, H.E. (2017). *Performance Evaluation of Bionax SR PVC Pipe with Extended Bell Joints under Earthquake-Induced Ground Deformation*. Ithaca, NY: Cornell University. Retrieved from <https://lifelines.cee.cornell.edu/>
- Wham, B.P., Berger, B.A., Pariya-Ekkasut, C., O'Rourke, T.D., Stewart, H.E., Bond, T.K., & Argyrou, C. (2018). "Achieving Resilient Water Networks – Experimental Performance Evaluation". *Proceedings: Eleventh U.S. National Conference on Earthquake Engineering* (p. 11). Los Angeles, CA.
- Wham, B.P., Ihnotic, C.R., Balcells, D., & Anderson, D.K. (2019). "Performance Assessment of Pipeline System Seismic Response". *Proceedings: JWVA/WRF/CTWWA Water System Seismic Conference*. Los Angeles, CA.
- International Organization for Standardization (ISO). (2006). *ISO 16134:2006 Earthquake- and subsidence-resistant design of ductile iron pipelines*. Switzerland: ICS: 23.040.10, TC/SC: ISO/TC 5/SC 2. Retrieved from <https://www.iso.org/standard/40651.html>
- Wham, B.P., Argyrou, C., O'Rourke, T.D., Stewart, H.E., Bond, T.K. (2017a) PVC Pipe Performance Under Large Ground Deformation. *ASME Journal of Pressure Vessel Technology*. Vol.139(1). [10.1115/1.4033939](https://doi.org/10.1115/1.4033939)
- Wham, B.P., Ihnotic, C.R., Anderson, D.K., & Ramos, J. (2020). "Full-scale Testing of Fused PVC Pipe for Externally Applied Loading". *Proceedings: NASTT 2020 No-Dig Show* (pp. 1–10). Denver, CO: North American Society for Trenchless Technology (NASTT).



### Appendix A: Cyclic Tension Test (PS11) Results

The cyclic axial tension test consisted of fused PVC pipe with a Megalug coupling at the midpoint. Figure 8.1 shows photos taken before the test and after specimen failure. Internal pressure for PS11 ranged between 15 – 28 psi (103 – 193 kPa), representing negligible water pressures, as shown by the orange line in Figure 8.2. Figure 8.2 also shows actuator force and displacement relative to time during the test. The internal pressure fluctuation is a function of the increasing/decreasing internal volume during applied tensile/compression loading and the manual adjustments to internal pressure.

Force vs displacement plots of PS11 are provided in Figure 8.3. The difference in displacement between the imposed actuator displacement and measured joint opening represents the stretch in the pipe combined with additional sources of slip and movement at either end restraint.



(a)



(b)

Figure 8.1. Specimen PS11 (a) before and (b) after axial tension test

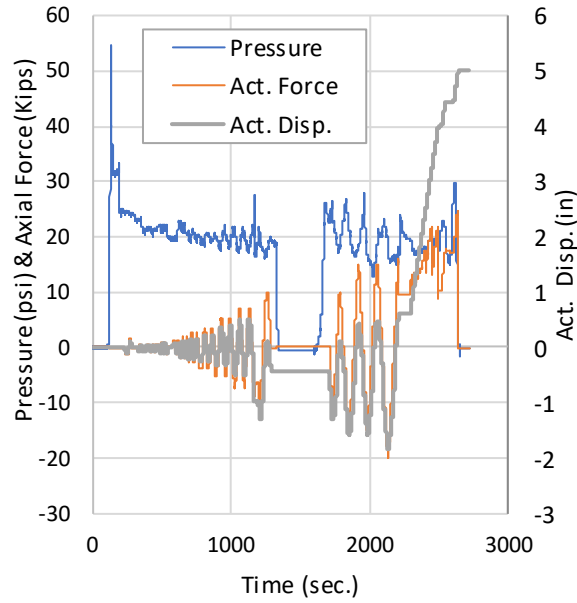


Figure 8.2. PS11 results for internal pressure, actuator displacement and axial force vs time

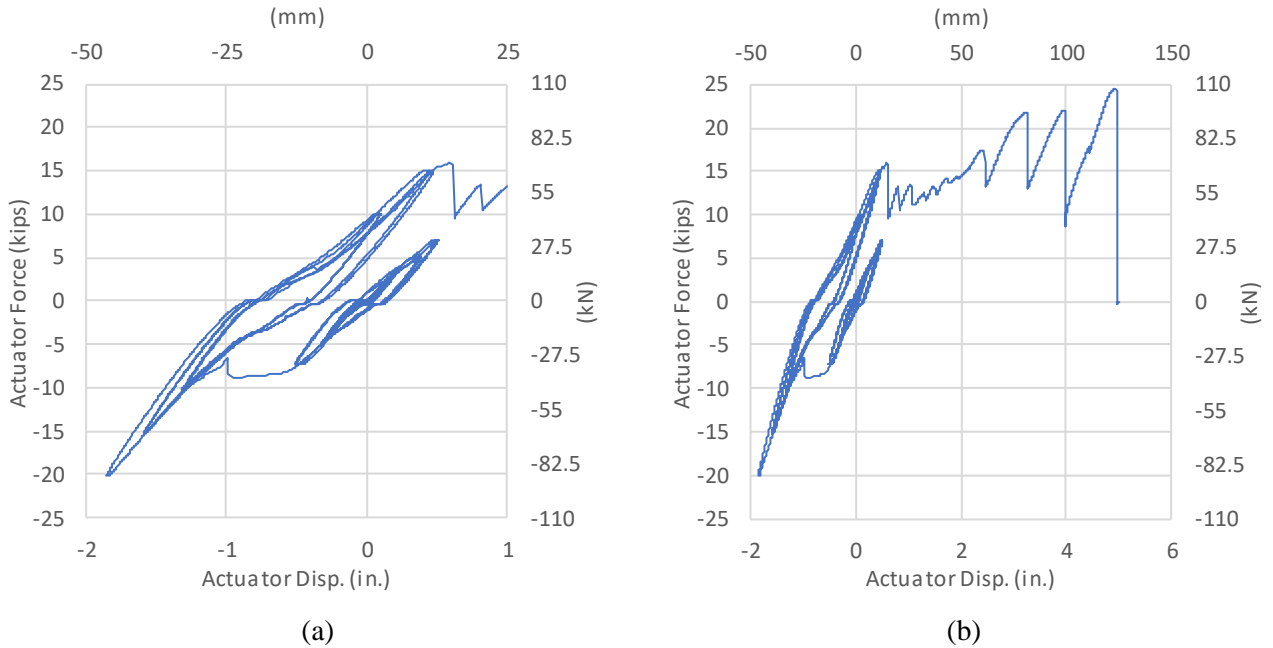


Figure 8.3. Specimen PS11 actuator force vs (a) actuator displacement for cyclic displacements and (b) actuator displacement for entire test

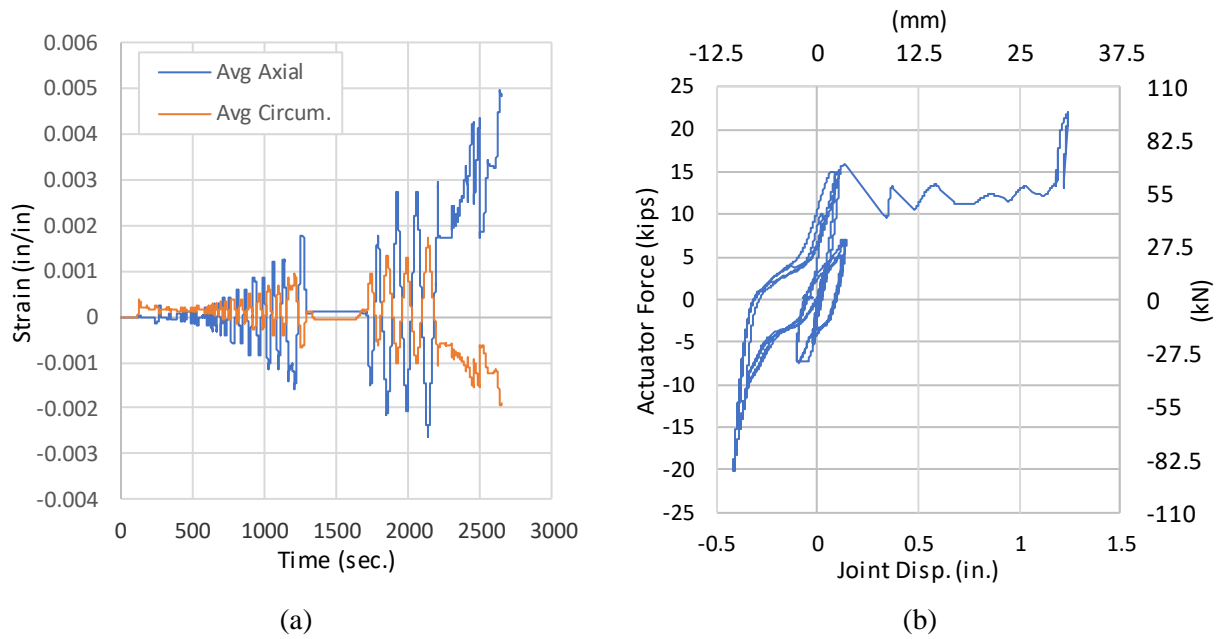


Figure 8.4. Specimen PS11 measured (a) average strains, and (b) joint displacement



(a) Initial position



(b) Initial Slipping, No Leak



(c) Final Slipping Position Without Leak



(d) Initial Leaking Position

Figure 8.5. Progression of cyclic test PS11



(a)



(b)

Figure 8.6. Specimen PS11 after failure: (a) circumferential fracture and (b) test overview



## Appendix B: Field Cut Procedures

### Section 7 Cutting Fusible PVC® Pipe



#### 7.0 Cutting Fusible PVC® Pipe

Recommended practices for working with and handling bell and spigot PVC pipe apply to Fusible PVC® pipe. However, lengths of Fusible PVC® pipe, joined by butt-fusion, are subject to additional stresses during installation. These stresses on assembled pipe lengths may occur as a result of bending, internal pressure, external loading, and/or the method of installation. General guidance for cutting PVC pipe can be found in industry resources, such as the Handbook of PVC Pipe,<sup>(1)</sup> and American Water Works Association documents AWWA C605<sup>(2)</sup> and AWWA M23.<sup>(3)</sup> This section reviews the proper cutting procedure for Fusible PVC® pipe as well as some critical items common to cutting most types of PVC pipe.

#### **The Most Important Items When Cutting Fusible PVC® Pipe:**

1. Follow all safety precautions for lifting and supporting the pipe, operating the cutting equipment, and using personal protection equipment (e.g. safety glasses or face shield, etc.).
2. NEVER USE A CHAINSAW. Use appropriate equipment to cut PVC pipe as detailed in this document.
3. Properly support the pipe during the cutting process to eliminate bending stresses.
4. Always follow Underground Solutions, Inc. recommended cutting procedures.

#### **Safety First!**

Pipe cutting equipment represents a personal injury hazard due to the sharp nature of the tools among other things. Always follow the requirements and recommendations, as well as the caution and warnings, of the manufacturer of the pipe cutting equipment being used.



Fusible PVC® pipe, both as delivered to the project site and when assembled into long lengths represents a large, heavy material that requires attention during handling, movement, and installation on a project site. Moving lengths of pipe improperly creates a hazard that can result in personal injury or even death. Always follow best practice safety procedures as provided by Underground Solutions, Inc., as well as all entities having jurisdiction for the project.

#### 7.1 Cutting Equipment

Serrated bladed saws, such as reciprocating saws are commonly used to cut PVC pipe. Powered 'cut-off' or rotating disc-type saws, as long as they are outfitted with a diamond blade or blades made for use with PVC materials are acceptable as well. Be sure that the rotating blade is properly centered and not off-set when using this type of saw. Wire-type cutters have also been used successfully to cut PVC pipe. See Figure 7.1 for examples of applicable and non-applicable cutting tools for use with Fusible PVC® pipe.

**NEVER USE A CHAIN SAW TO CUT FUSIBLE PVC® PIPE. The crude kerf and ripping action of this type of saw can leave small cracks in the cut face of the PVC pipe. This damage may compromise successful installation and long term performance.**



## Section 7 Cutting Fusible PVC® Pipe



an AEGION<sup>™</sup> company

Fusible C-900® | Fusible C-905® | FPVC®



Figure 7.1. Examples of applicable cutting tools for use with Fusible PVC® pipe. **Never use a chainsaw.**

### 7.2 Pipe Support

To eliminate bending stresses during cutting, it is important that a straight, properly supported pipe alignment on both sides of the cut is provided. If the adjacent pipe alignment cannot be fully straightened, provide support against the outside of the curved pipe section to offset the tensile stress from bending, on both sides of the cut. The pipe must always be fully supported on both sides of the cut and the pipe should be cut on level ground (see Figure 7.2). When the pipe to be cut is cantilevered, such as the end of a pipe string that is supported from only one side; the cantilevered side must be completely supported using a nylon strap or other acceptable arrangement to remove the weight from the cantilevered end (see Figure 7.2). This is particularly important when the cantilevered end of the pipe also has a pull head installed on it. Underground Solutions, Inc. recommends that pull heads be removed in the reverse manner by which they were installed **BEFORE** cutting the pipe. See Section 6 – Pulling Parameters for Fusible PVC® Pipe, for more information related to pull heads, and pipe handling.

## Section 7

### Cutting Fusible PVC® Pipe



#### 7.4 Cutting Procedures

In order to achieve a controlled, perpendicular cut in PVC pipe, the following cutting procedure is recommended. This procedure should be used for ALL cuts made on Fusible PVC<sup>®</sup> pipe.

**ALWAYS MAKE SURE THE PIPE TO BE CUT IS NOT INTERNALLY PRESSURIZED. ALL INTERNAL PRESSURE MUST BE RELIEVED.**



**ALWAYS MAKE SURE THE PIPE IS NOT UNDER TENSILE LOAD FROM PULLING EQUIPMENT OR OTHER SOURCES. RELIEVE ALL LOADING ON THE PIPELINE PRIOR TO MAKING A CUT.**

Internal pressure or tensile loading at the location of the cutting operation can cause sudden and violent movement of the pipe, including shards of pipe that may turn into projectiles that could cause injury or death.

1. Mark a circumferential line around the pipe prior to making the cut. Consider using a “Wrap-A-Round” pipe marking tool or other similar device to align the mark perpendicular to the axis of the pipe and around the full circumference of the pipe. The pipe can be marked effectively with a black “Sharpie” or equivalent marker.
2. Consider the size of the cutting equipment that will be used and position the pipe so that the bottom can be cut cleanly. This may require excavation under the pipe.
3. Score the pipe at a maximum of ¼-inch depth increments. **ONLY SCORE THE PIPE, DO NOT COMPLETELY CUT THROUGH THE PIPE.**

**STEP 1:** Start by making the initial scoring cut from the 9 o’clock position of the pipe to the 6 o’clock position – see Figure 7.4.

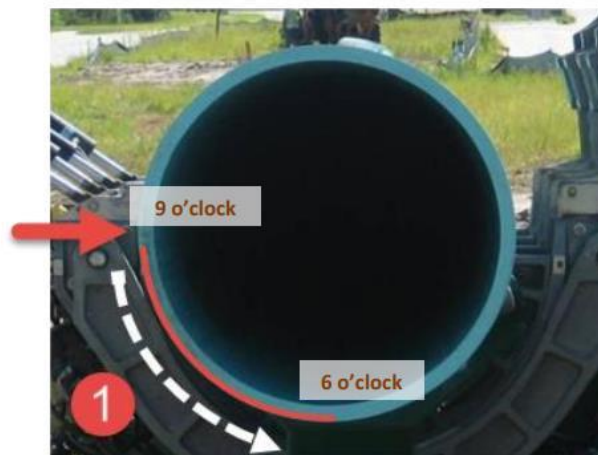


Figure 7.4



## Section 7 Cutting Fusible PVC® Pipe



an AEGION<sup>®</sup> company

Fusible C-900<sup>®</sup> | Fusible C-905<sup>®</sup> | FPVC<sup>®</sup>



Figure 7.2. Two examples of a properly supported pipe alignment on both sides of the cut to be made.

### 7.3 Stress Loading in the Pipe

In addition to the steps taken to relieve the bending stresses, some residual stress may still remain in the Fusible PVC<sup>®</sup> pipe string at the proposed cut location. When the pipe is cut perpendicular to the axial centerline of the pipeline, any unrelieved longitudinal or axial stress may pull the pipe apart. This may result in separation of the pipe at the cut location prior to being cut the entire way through. Always properly support the pipe to minimize problems during the cutting procedure. In cases where axial stresses are present in the pipe, the initial cut may be uneven (see Figure 7.3) and will require that another clean, squared-end cut to be made afterward. Always make sure that enough material is left for this clean-up cut per the requirements of the project.



Figure 7.3. When stress is not relieved in the pipe during the cutting process, the forces in the pipe may cause the cut to be uneven.



## Section 7 Cutting Fusible PVC® Pipe



an AEGION<sup>®</sup> company

Fusible C-900<sup>®</sup> | Fusible C-905<sup>®</sup> | FPVC<sup>®</sup>

**STEP 2:** Continue by making another scoring cut from the 3 o'clock position of the pipe to the 6 o'clock position – see Figure 7.5.



Figure 7.5

**STEP 3:** Continue by making another scoring cut from the 12 o'clock position of the pipe to the 3 o'clock position – see Figure 7.6.

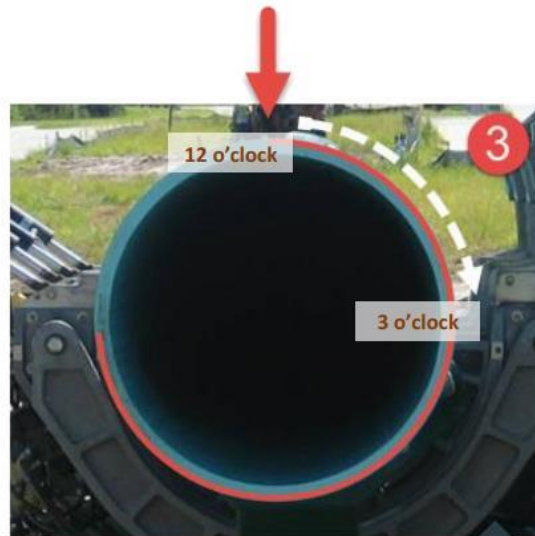


Figure 7.6



## Section 7 Cutting Fusible PVC® Pipe



an AEGION<sup>®</sup> company

Fusible C-900<sup>®</sup> | Fusible C-905<sup>®</sup> | FPVC<sup>®</sup>

**STEP 4:** Complete the first scoring pass by making a final scoring cut from the 12 o'clock position of the pipe to the 9 o'clock position – see Figure 7.7.

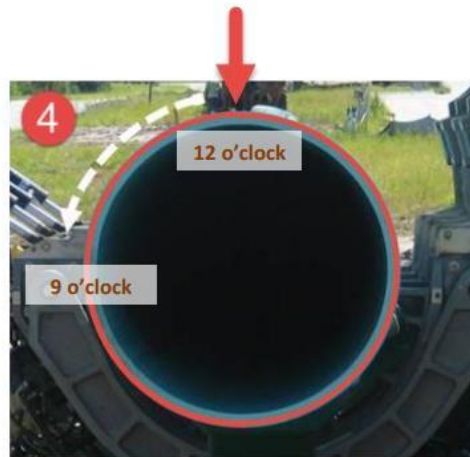


Figure 7.7

**STEP 5:** For smaller diameter (12-inch and less) pipes, make a complete cutting pass for each quarter pipe section in the same order as described in steps 1 through 4 (see Figure 7.8). For larger diameter (14-inch and greater) pipe, continue to make scoring passes, removing approximately ¼-inch increments of the pipe wall for each quarter pipe section in the same order as described in steps 1 through 4. Repeat this scoring cycle until the pipe has been completely cut through (see Figure 7.8).

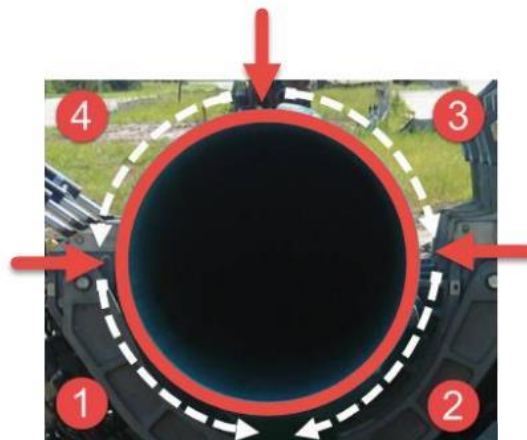


Figure 7.8

## Appendix C: Strain Gauge Application Procedure



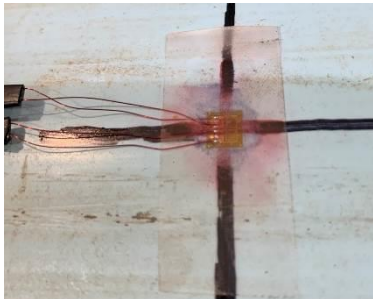
Use both fine and course sand paper to sand the section of pipe the strain gauge will sit on. Sand in several directions for better adhesion.



Place scotch tape over the sanded region, place marks on tape for precision placement.



Open Strain Gauge package, tape wiring onto pipe so that the gauge is easy to work with. Place the gauge onto the tape, lining it up with the marks as close as possible.



Place small amount of super glue on back of gauge, then press it into the pipe. Hold this for at least one minute. Too much super glue will create a poor bond to the pipe.



Remove tape slowly, making sure the gauge is bonded to the pipe. If the gauge lifts from the pipe, continue to press onto the gauge for an additional two minutes.



Use a knife to attempt to lift the corners of the gauge from the pipe. If any part of the gauge is not bonded to the pipe, remove the gauge, and repeat the process.

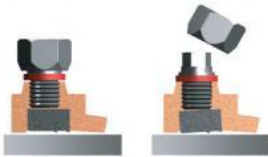


## Appendix D: Megalug Restraint Assembly

### Spacer Instructions (4 in. through 12 in. only)

#### Ductile Iron or C900 PVC O.D. Sized Pipe

For installation on Ductile Iron or C900 PVC sized pipe, use as received and install per instructions.

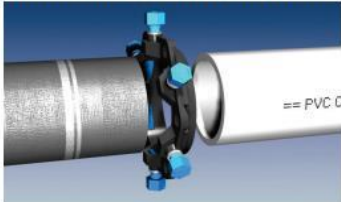


#### Steel or ASTM D2241 O.D. Sized Pipe (IPS O.D.)

For installation on Steel or ASTM D2241 O.D. Sized pipe, remove spacers and replace screws. Install per instructions.



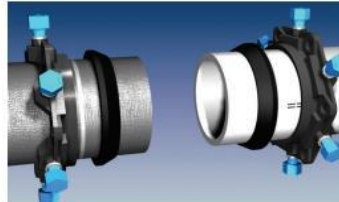
### Installation Instructions All sizes



1. Identify the pipe. The spacers under the actuating screws must be removed for use on ASTM D2241 O.D. sized pipe (4 inch through 12 in. only). The spacers must remain in place for use on Ductile Iron or C900 PVC O.D. sized pipe.

Clean and inspect the pipe ends. Beveling of the ends is not necessary.

**If used on HDPE Pipe**, a pipe wall stiffener insert that encompass the entire bearing length of the restraint devices must be installed prior to step two.



2. Place the end rings on the pipes with the lip extensions toward the pipe ends. For 4 inch through 12 the restraints will be the Series 2000HPV, for 14 inch and above Ductile Iron pipe the restraint ring will be the Series 1100 MEGALUG® and for C900 PVC 14 inch and above the restraint ring will be the Series 2000PV MEGALUG. Lubricate and install the Standard Mechanical Joint Gasket.

(Standard Mechanical Joint Gaskets must be used with Ductile Iron Pipe and C900 PVC pipe 4 inch through 12 inch while the EBAA-SEAL™ Improved Mechanical Joint gasket is used on 14 inch and above. Transition gaskets must be used with Steel or ASTM D2241 pipe).



3. Center the sleeve body over the ends of the pipes while maintaining a 1/2" to 1" gap between the pipe ends. Slide the gaskets and end rings toward the sleeve body.



4. Install the threaded rods and hand tighten the nuts on each end. Gradually tighten the nuts in an alternating manner until the proper torque value has been reached, while maintaining the same distance between the rings and the ends of the body at all points around the rings. For 4 inch through 24 inch torque to 75 - 90 ft.-lbs., for 30 inch and greater torque to 120 - 150 ft.-lbs.



5. Hand tighten the actuating screws until all wedges are touching the pipes. Continue tightening the screws in an alternating manner until the torque limiting heads twist off. The screws may bottom out during this step.



### EBAA IRON Sales, Inc.

P.O. Box 857, Eastland, TX 76448

Tel: (254) 629-1731

Fax: (254) 629-8931

(800) 433-1716 within US and Canada



## Appendix E: Applied Moment Verification

Applied loads on the specimen are considered as either distributed loads or point loads. The equations used in moment contribution can be viewed in Equations 14.1 and 14.2. Self-weight, including the weight of the specimen and internal water, are considered distributed loads and the moment contributions can be viewed in Table 9.1. Point loads on the specimen include the weight of equipment and resisting force developed as the crosshead applies displacement. The moment contributions can be viewed in Table 9.2. As loading saddle locations were held constant throughout all tests completed and cross section properties remained the same, moment contributions are equivalent across tests completed. The total moment that is seen by the specimen can be written as a function of the resisting force,  $P$ , developed and measured by the load cell. The load path from the load cell into the specimen is shown in Figure 9.1. The total moment seen by the specimen can then be written as a function of the force  $P$  and is shown in Equation 14.3.

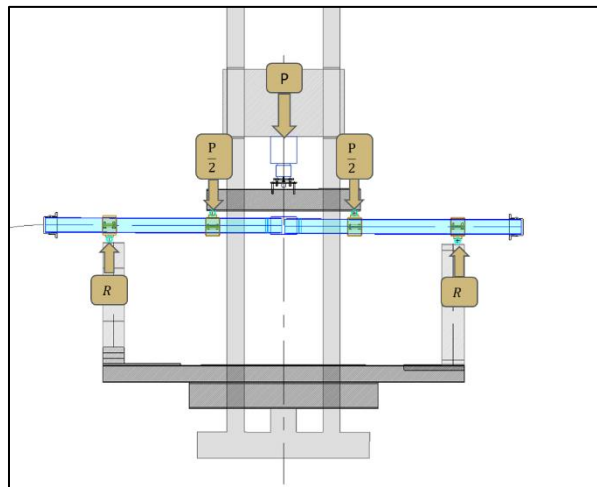


Figure 9.1. Load path of applied force,  $P$

$$M_{max} = \frac{\omega l^2}{8} \quad (14.1)$$

$$M_{max} = \frac{P * L}{4} \quad (14.2)$$



Table 9.1. Distributed Load Moment Contributions

<b>Distributed Moment Contribution</b>	<b>Loading (lbs/in)</b>	<b>Length of Loading (in)</b>	<b>Moment Contribution (k-in.)</b>
<b>Internal Water</b>	1.04	162	3.40
<b>Self-weight</b>	25	162	0.820

Table 9.2. Point Load Moment Contributions

<b>Point Loads Moment Contribution (kip)</b>	<b>Loading (lbs)</b>	<b>Moment Arm (in)</b>	<b>Moment Contribution (k-in.)</b>
<b>Equipment Weight</b>	50	48	0.6
<b>Applied load</b>	P/2000	48	8P

$$M_{max} = 4.82 + 8P \quad (14.3)$$

Moment contributions from all static loads were applied linearly over the initial 2 in. (50 mm) of displacement of the test. This displacement is considered to be due to the sag of the pipe from level placement in the frame once support structures are removed. From this point, increasing moment contributions occur only from the increased resisting load developed through crosshead displacement. The applied moment can then be compared to the theoretical stress developed by the moment through beam theory compatibility equations. Cross sectional properties of the specimen tested can be viewed in Table 9.3 in which the moment of inertia is calculated through Equation 14.4. Equations of beam theory compatibility can be viewed in Equations 14.4-14.7.



Table 9.3. Cross Section Properties of 6 in. Diameter PVC Pipe

	<b>Outside Radius (in.)</b>	<b>Inside Radius (in.)</b>	<b>Moment of inertia (in<sup>4</sup>)</b>	<b>Modulus of Elasticity (ksi)</b>
<b>Fused PVC</b>	3.45	3.02	45.9	446
<b>C900 (iPVC)</b>	3.44	2.93	53.6	450

\*Note: values for Fused PVC used in this Appendix for sample calculation

$$I_x = \frac{\pi}{4} (r_{outside}^4 - r_{inside}^4) \quad (14.4)$$

$$\sigma_{b,applied} = M * y / I_x \quad (14.5)$$

$$\varepsilon_{bending} = \frac{\varepsilon_{tension} - \varepsilon_{compression}}{2} \quad (14.6)$$

$$\sigma_{b,strain} = E * \varepsilon_{bending} \quad (14.7)$$

By combining Equations 14.6 and 14.7, the bending stress can be determined through strain data recorded within the area of maximum moment. This bending stress can then be compared to the theoretical bending stress corresponding to the applied maximum moment through Equation 14.5. A comparison of these values can be viewed in Figure 9.2 up to the yield stress of the material. Stress from moment calculations are higher within the elastic strain region which could be due to an underestimation of strain.

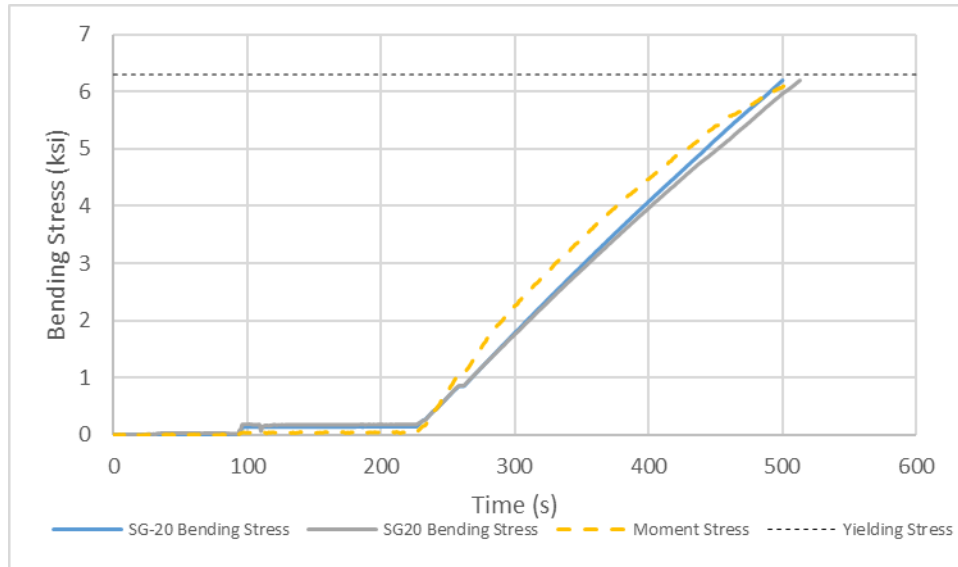


Figure 9.2. Comparison of BT03 Bending Stress

Variations in response were noted in the strain plots of Figure 7.17 in comparison to compression response and tension response, showing a material hardening while the specimen is under compressive loads. This material hardening effect would therefore increase the Young's Modulus of Elasticity and improve the accuracy of the stress calculated from bending moment. As moment calculations agree with strain measurements throughout the elastic response, moment calculations are accurate and the assumption that no axial force has been introduced holds within the elastic region. To verify the response of the plastic region of the test, a full plastic analysis with material properties of fusible PVC in both tension and compression is needed. At present time, only tensile response of the material is available with a defined yield strength and Modulus of Elasticity.



## Appendix F: Radius of Curvature (RoC) Calculation

When looking at the measure of curvature of the pipeline, there are two main measurements of curvature available for measure: the imposed curvature depicted by the red arc in Figure 9.3 and the localized curvature within the inner third of the test frame as shown by the green arc. As discussed in Appendix E, the bending strain is directly related to the resisting moment developed within the pipe. Moment is only constant within the inner third region of a four-point bending test and varies linearly to zero from the third-points to both end points. Due to this moment distribution, the area of highest curvature will be found within the inner third and calculations that include data from outside of the inner third region will under-value to the highest curvature achieved by the pipe system. As the information important to quantifying failure within a system is dependent on extreme values at failure, radius of curvature is calculated with information collected within the inner-third region.

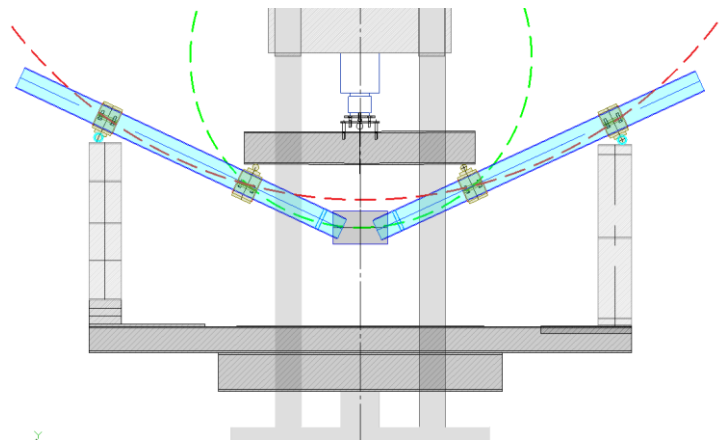


Figure 9.3. Circles of curvature shown for imposed displacement in red and region of maximum moment in green

Global radii of curvature calculations are based on knowing the geospatial coordinates of several locations throughout the duration of the test. It is assumed that there is no horizontal translation of the specimen, resulting in fixed horizontal positions along the specimen used in calculation. By recording the displacement from the original position of the specimen, the vertical locations can be calculated. Then, using three points, the radius of the circle encompassing the known points can be calculated. Four combinations of geospatial coordinates are shown in Table 9.4 that are used in calculating four separate radii of curvature.

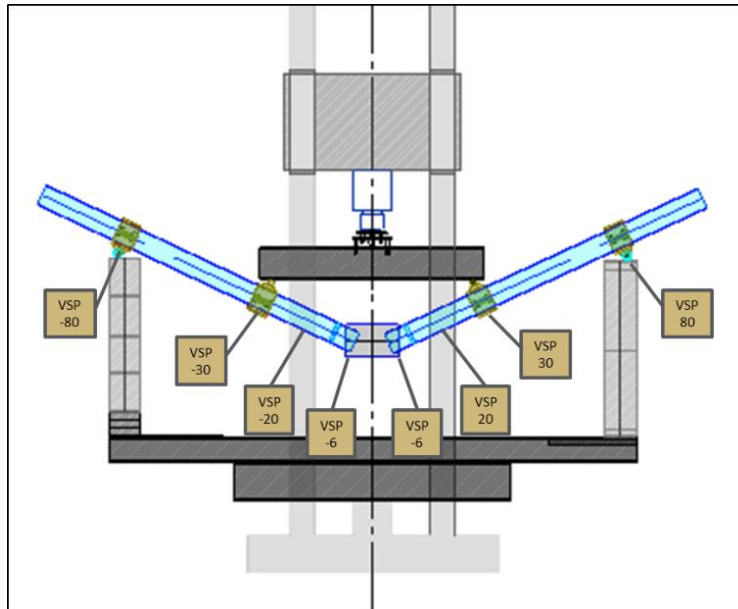


Figure 9.4. RoC coordinate locations for representative deflected shape

Table 9.4. Coordinates of Radius of Curvature Locations

	$x_1$	$y_1$	$x_2$	$y_2$	$x_3$	$y_3$
<b>RoC_A</b>	-33	VSP-30	-18.25	VSP-20	33	VSP30
<b>RoC_B</b>	-33	VSP-30	-6	VSP-6	33	VSP30
<b>RoC_C</b>	-33	VSP-30	6	VSP6	33	VSP30
<b>RoC_D</b>	-84	0	-6	VSP-6	84	0

\*Note: For this analysis each VSP measure represents the pipe displacement relative to its initial position

The algorithm to locate the centroidal coordinates of the encompassing circle is based on solving the system of equations shown as matrices in Equations 8.1-8.3 through the relationships shown in Equations 8.4 and 8.5. These are used to identify the coordinates of the centroid of the encompassing circle shown in Figure 9.5. Then the radius,  $\rho$ , of the circle can be determined through Equation 8.6 that shows the relationship between the length of a line segment given the end coordinates. This process is repeated for the triplets of locations shown in Table 9.4.

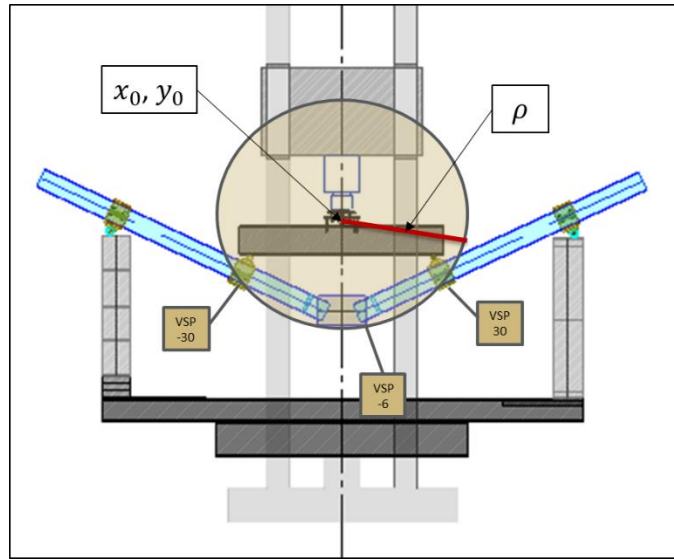


Figure 9.5. Image showing the theurgical circle from which the radius of curvature is determined

$$A = \begin{bmatrix} x & y & 1 \\ x_1 & y_1 & 1 \\ x_2 & y_2 & 1 \\ x_3 & y_3 & 1 \end{bmatrix} \quad (15.1)$$

$$B = \begin{bmatrix} x^2 + y^2 & x & 1 \\ x_1^2 + y_1^2 & x_1 & 1 \\ x_2^2 + y_2^2 & x_2 & 1 \\ x_3^2 + y_3^2 & x_3 & 1 \end{bmatrix} \quad (15.2)$$

$$C = \begin{bmatrix} x^2 + y^2 & y & 1 \\ x_1^2 + y_1^2 & y_1 & 1 \\ x_2^2 + y_2^2 & y_2 & 1 \\ x_3^2 + y_3^2 & y_3 & 1 \end{bmatrix} \quad (15.3)$$

$$x_0 = \frac{|B|}{2|A|} \quad (15.4)$$

$$y_0 = \frac{|C|}{2|A|} \quad (15.5)$$

$$R = \sqrt{(x_2 - x_0)^2 + (y_2 - y_0)^2} \quad (15.6)$$



Once the global radius of curvature ( $R=\rho$  in the figure) has been determined, the curvature can then be calculated through the relationship shown in Equation 8.7. From the geometric relationship shown in Figure 9.6, strain induced by the curvature can then be calculated. A plot of the comparison between recorded strain measurements and calculated values based on global curvature can be seen in Figure 9.7.

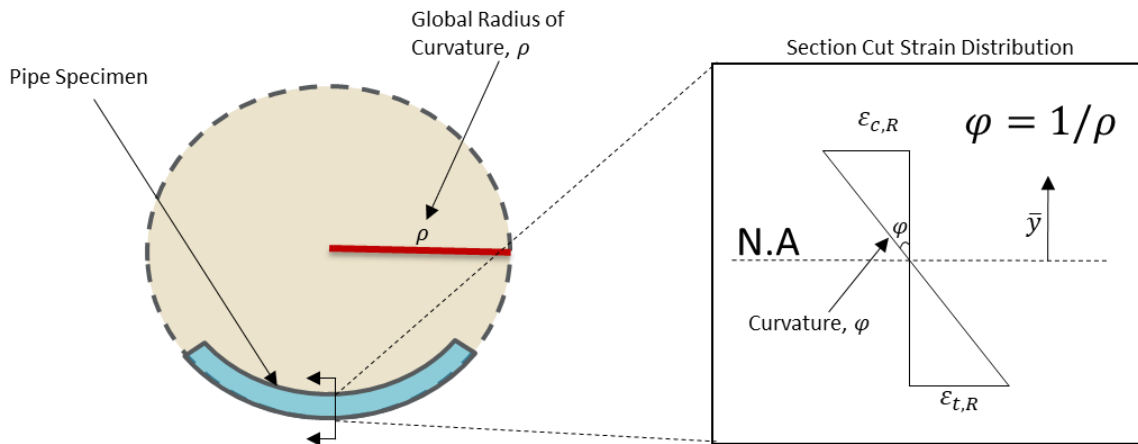


Figure 9.6. Strain-Curvature relationship

$$\varphi = 1/\rho \quad (15.7)$$

The comparison of calculated strain values to measured strain values shows that the calculated values are consistently higher than measured. This could be due to several factors. Any error in strain gauge placement could reduce the measured axial strain, so measured strain values could be recording below the actual strain values. Vertical data recorded was assumed to be fixed horizontally when horizontal movement did occur, this assumption would reduce the vertical displacement further from the centerline in comparison to measurements taken at the centerline, creating the effect of more curvature. This would be offset by assuming the specimen did not move horizontally inward, reducing curvature. Another possible explanation is that the horizontal locations are too close and should be adjusted away from the centerline. As depicted in Figure 9.3, the imposed curvature derived from the four loading saddle positions will undervalue the actual maximum curvature achieved. This can be seen in the data when looking at Figure 9.7 as the strain calculated from this data, shown as RoC\_D, does not align with measured strain values and undervalues the achieved curvature.

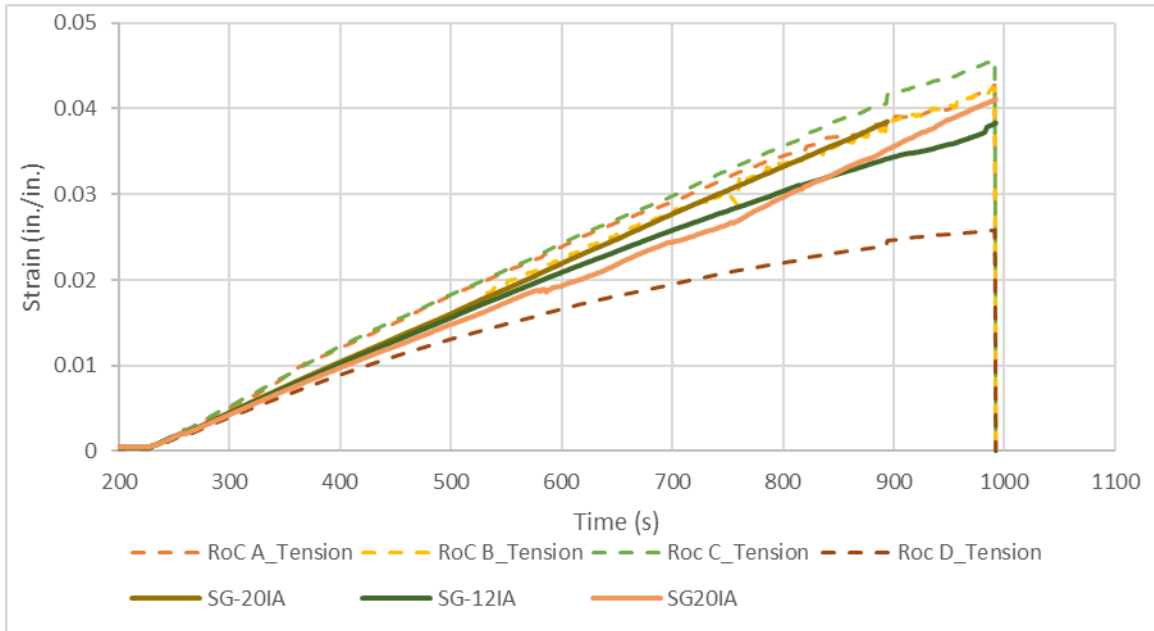


Figure 9.7. Comparison of calculated strain versus measured strain at pipe invert

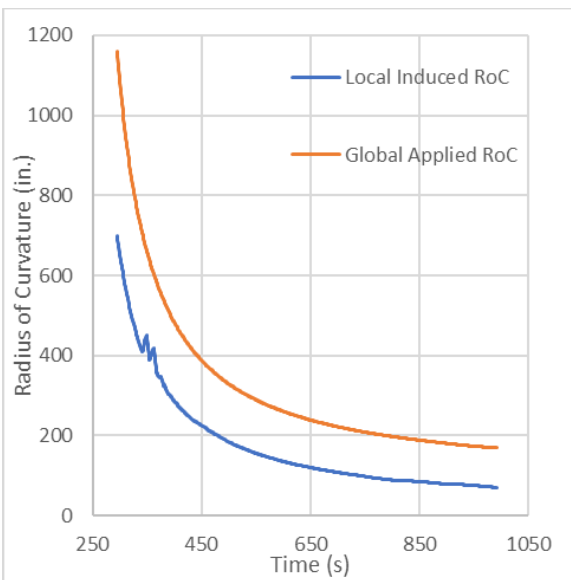
For reference, Table 9.5 provides the basic relationship between radius of curvature and curvature, joint rotation angle, and the applied crosshead displacement that is specific to the CIEST test frame. Joint rotation angle is considered as the angle between the outer and inner loading saddle on the west side of the test frame. This would be an equivalent joint rotation angle seen by a segmented pipe response. As radius of curvature is the inverse of curvature, both can be used interchangeably as a measure of geometrical bending capacity.

Table 9.5. Relationship Between Crosshead Displacement and Global Applied Curvature

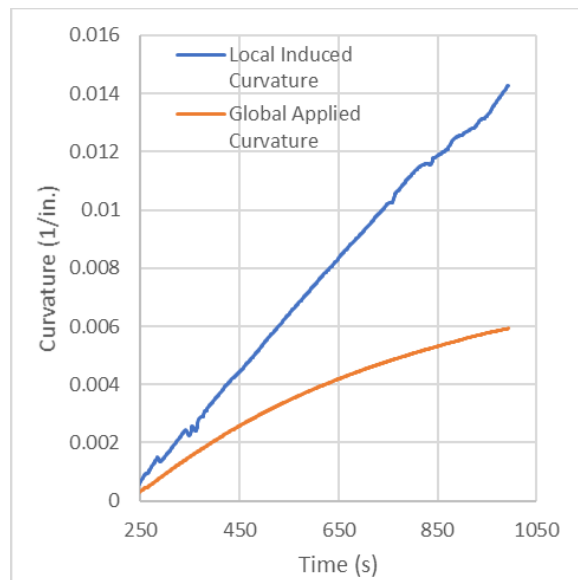
Crosshead Displacement (in.)	Global Applied Radius of Curvature (in.)	Global Curvature (1/in.)	Joint Rotation Angle (degrees)
1	2730	3.66E-04	1.2
2	1370	7.32E-04	4.8
5	541	1.85E-03	11.8
7.5	355	2.81E-03	17.7
10	260.8	3.83E-03	23.3



As radius of curvature is already used within the pipeline industry to measure bending capacity, it makes sense to use the same variable for pipeline system bending response. The selection of radius of curvature as the main variable also prevents confusion as to the information that is conveyed. Because curvature is directly related to the strain found within a specimen, as described in appendix A, the use of this metric to describe a response that is not directly related to strain occurs because the ability for the joint to slip seems improper. Due to the nature of bending tests to start out straight, the initial radius of curvature would be infinite and, as a result, curvature provides a better measure to plot and compare data as the curvature of a straight pipe is zero. A comparison of test data as functions of both radius of curvature and curvature is shown in Figure 9.8 as a function of time and Figure 9.9 as a function of crosshead displacement. In both comparisons, the difference in local and global data are shown better as plots of curvature compared to radius of curvature. This graphical relationship holds true for comparison between joint types as well.



(a)



(b)

Figure 9.8. Comparison of Radius of Curvature and Curvature calculations as a function of time

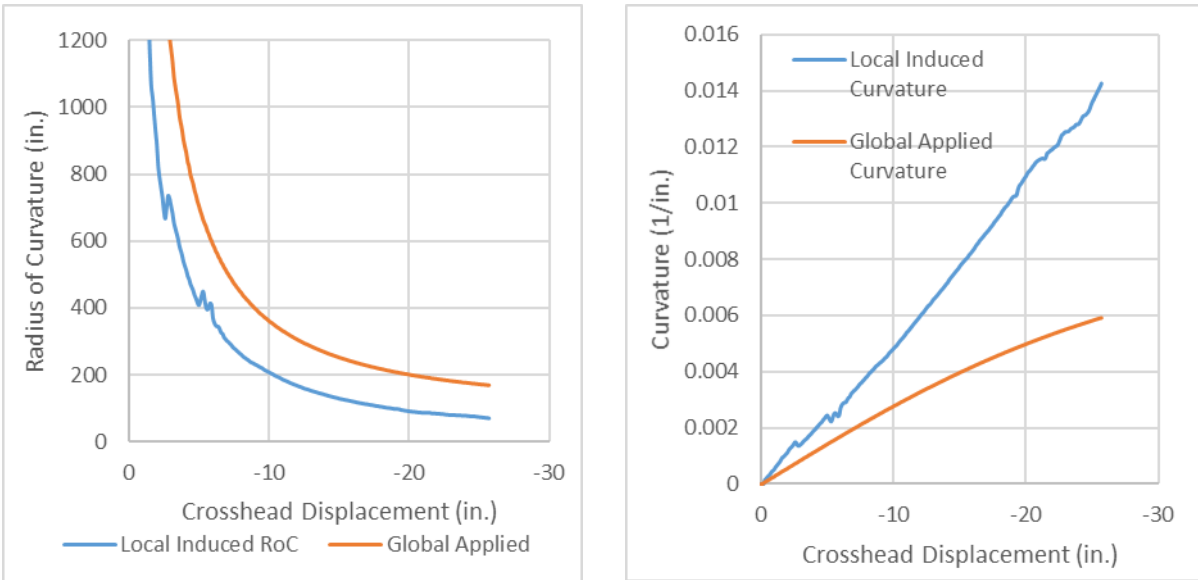


Figure 9.9. Comparison of Radius of Curvature and Curvature calculations as a function of crosshead displacement